OPTIMIZATION OF PROCESS PARAMETERS FOR RESIDUAL STRESS ANALYSIS IN TURNING ALLOY STEEL UNDER HIGH-PRESSURE COOLANT JET CONDITION

By
Shanta Saha

A Thesis
Submitted to the
Department of Industrial & Production Engineering
in Partial Fulfillment of the
Requirements for the Degree
of
M.Sc. in Industrial and Production Engineering

**DEPARTMENT OF INDUSTRIAL & PRODUCTION ENGINEERING
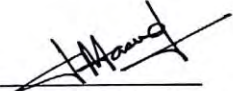BANGLADESH UNIVERSITY OF ENGINEERING & TECHNOLOGY
DHAKA, BANGLADESH**

May, 2018

The thesis entitled as **Optimization of Process Parameters for Residual Stress Analysis in Turning Alloy Steel under High-Pressure Coolant Jet Condition** submitted by Shanta Saha, Student No. 0413082007, Session-April 2013, has been accepted as satisfactory in partial fulfillment of the requirement for the degree of M. Sc. in Industrial and Production Engineering on May 30, 2018.

BOARD OF EXAMINERS

1. _____

   Dr. Nikhil Ranjan Dhar   Chairman

   Professor
   Department of Industrial & Production Engineering
   BUET, Dhaka

2. _____

   Dr. Kais Bin Zaman   Member

   Professor and Head   (Ex-officio)
   Department of Industrial & Production Engineering
   BUET, Dhaka.

3. _____

   Dr. A.K.M. Masud   Member

   Professor
   Department of Industrial & Production Engineering
   BUET, Dhaka.

4. _____

   Dr. Md. Ariful Islam   Member

   Professor   (External)
   Department of Industrial and Production Engineering
   Shahjalal University of Science and Technology (SUST)
   Sylhet

ii

Declaration

It is hereby declared that this thesis or any part of it has not been submitted elsewhere for the award of any degree or diploma.

Shanta Saha

This work is dedicated to my

Loving Parents

ACKNOWLEDGEMENT

ABSTRACT

Machining induced residual stress is an important aspect of study on controlling machining parameters to get desired product quality as the functional behavior of machined component can be enhanced or impaired by it. Besides, high pressure coolant (HPC) supply during machining is considered as favorable cutting environment to get better machinability indices over dry condition. In the purpose of gaining superior product quality it would be beneficial to study the effect of residual stress under HPC condition along with rational setting of machining parameters.

This study aims at finding the optimum cutting conditions and monitoring the residual stress in turning of 42CrMo4 alloy steel by HPC lubrication. On the basis of experimental results this paper develops empirical models for predicting cutting temperature, surface roughness and tool wear in terms of workpiece hardness, cutting speed and feed rate using multiple regressions modeling method.The results of ANOVA prove that the models could adequately describe the performance indicators within the limits of the statistical factors. Then, multi-objective optimization approach based on genetic algorithm has been employed to get the optimal setting of process parameters that simultaneously minimize cutting temperature, surface roughness and tool wear.It was found that the optimum results provide consistent results compared to experimental measurements. The optimum results was then used in finite element method based simulation of residual stress. This paper presents a 2D finite element model based on Arbitrary-Lagrangian-Eulerian formulation using ABAQUS software. The Johnson-Cook material and damage model have been used for chip formation. Based on this model the effects of coolant application on temperature variation were investigated in simulations. The temperature distribution of chip-tool interface in simulation shows a good agreement with the measured cutting temperature. Simulation results offer an insight into workpiece hardness and cutting parameters influence on the induced residual stresses. Based on the simulation results, cutting speed and workpiece hardness show trend for machining induced residual stress. However, more investigation is needed in determining a trend for the feed rate influence.

Table of Contents

List of Figures

List of Tables

Chapter-1

INTRODUCTION

1.1   Introduction

Turning, milling and drilling are the most commonly used machining operations in the world of manufacturing. Though the names are different, the physics of metal cutting is the same, i.e. it is the process when the edge of the tool engages with the workpiece and removes the material by chip formation and generates the newly machined surface. Throughout the manufacturing industry, interest in the turning operation is increasing as the technology replaces more grinding and finishing operations due to the benefits of cost reduction and raise productivity [**Bogdan and Gavrila, 2017**]. On the contrary, there exist some machining complexities due to the plastic deformation, thermal stresses,and phase transformation during metal cutting. Complexities in the machining process alter the quality and performance of the machined component which is directly relatedto surface integrity. So, understanding metal cutting process and achieving the ability to predict the outcomes will essentially improve productivity, reduce cost and obtain the desired surface quality of the products. Here, surface integrity includes the topological parameters like surface roughness, surface topographic features; mechanical properties like residual stresses, hardness, etc. and metallurgical states of the work material during processing like phase transformation, microstructure, related property variations, etc. [**Kaya and Akyüz, 2007**]. This relation is not only at the surface level but also to certain depths.

Nearly every component in use undergoes a machining process at some point inits manufacturing cycle. During such processes, engineering components are subjected to stresses and strains of variable magnitudes and nature. The stresses produced as a result of machining processes and locked into the material are called residual stresses (RS). The

significance of RS comes from its significant effect on the fatigue life of machined components. RS are by-products of machining processes which cannot be ignored. When a component's surface integrity is evaluated, RS are often considered to be one of the most critical parameters to assess the quality of the machined surface, in the purpose of reaching high-reliability levels. In the vicinity of the machined surface, tensile RS have negative effects on fracture resistance and stress corrosion. This can lead to a substantial reduction in the component's life [**Miguélez et al. 2009**]. Thus, the task of developing a methodology capable of predicting RS induced by machining is of great value. Huge amounts of efforts have been made by researchers to develop analytical, experimental and numerical models in order to predict the post process induced residual stresses in a workpiece. However, all methodologies come in shy to express the cutting process parameters as functions to determine the machined RS profile; in order to manage the process to achieve the desired RS profile. Nonetheless, questions still arise concerning the effect of cutting environment on generating RS in machining. Most applied methods for measuring RS are destructive measurement techniques involving a layer removal or hole-drilling. The X-ray technique is the most highly developed and costly non-destructive measurement technique available today. So, there is a necessity to develop an alternative reliable method for measuring and predicting RS in the simple and cost-effective way.

There are several causes those are directly and indirectly related to the development of this detrimental RS and poor surface finish of the product. RS in the machined surface layers are affected by the cutting tool, workmaterial, cutting parameters (for example: cutting speed, depth of cut and feed) andcontact conditions at the tool-chip and tool-workpiece interfaces. A huge amount of heat generation at the chip-tool interface during hard turning is the most prominent reason to occur this bad effect. This heat is concentrated at the chip-tool interface and distributed around this contact point. In practice, the magnitude of the heat rises in the high production machining with high cutting velocity, feed, and depth of cut. The elevated temperature softens and weakens the tool, the tool tipbecomes blunt and in the result, produce a poor surface finish, dimensional deviation, surface and sub-surface defects including micro-cracks and shorten the tool life. So, the combination of optimum machining parameters along with tool-work material and application of effective cutting fluid can trim down the heat generation. Use of proper lubrication is one of the ways of reducing the amount of heat generation at the tool-chip

interface. Over the past few decades, the lubrication technology has been significantly changed because of a combination of environmental, health, economic, and performance challenges. Researchers have been initiated to address these challenges by developing the effective lubrication processes namely cryogenic machining, high-pressure coolant (HPC) jet assisted machining and minimum quantity lubricant (MQL) machining.

This chapter provides the background information relevant to the present study. The consequences of machining induced residual stress on the job, problems of high temperaturerise in dry machining, machining with conventional cutting fluids and another alternative lubrication system- HPC jet system with its positive effects on the finished products are explained thoroughly in this chapter with researchers remarks. Literature about the necessity of modeling of different process parameters, different researchers' study about temperature and residual stress modeling are alsodescribed.

1.2   Effects of Residual Stress on Machined Component

The residual stress state in a component is one of the most important parameters influencing its service behavior. RS are generated in structural components during the manufacturingprocessessuch as grinding, cutting, milling, turning and processes similar to shot peening and blasting. This stress is always a consequence of inhomogeneous plastic deformations due to the removal of chips, thermochemical treatments due to heating during machining, and/or phase transformations if the temperature is sufficiently high. The RS can be compressive or tensile. The presence of RS can be distinguished as [**Totten et al. 2002**]:

> ➢ *Plastic deformation involving a smearing of the material in the plane of the surface tends to give compressive RS.*

> ➢ *Temperature increase that momentarily causes an expansion, which is constrained by the bulk material. The resulting thermal stresses may exceed the yield stress at the actual temperature and, therefore, the surface material will be upset. During the subsequent cooling, tensile RS are created.*

> ➢ *If the workpiece is hardened steel, martensite may form due to the rapid heating and cooling, causing compressive residual stresses.The martensitic transformation of the carburized surface of a steel component puts the surface*

under compression. It is argued that this is because of the expansion at the surface due to the formation of the lower-density martensite from austenite.

Therefore, the final RS state is the algebraic sum of the three components: mechanical, thermal and metallurgical effect. The first two components are always present in machining and occur simultaneously, while the third one depends on the cutting temperature and cooling rate [**Nasr, 2008**]. During machining, the mechanical deformation in the near-surface region of the workpiece, the material undergoes compressive plastic deformation near the cutting edge and tensile plastic deformation behind it. If the tensile deformation is greater than the compressive one, the net result will be tensile plastic deformation. This would induce surface compressive RS on relaxation as the near-surface layer is restricted by the underlying bulk material. The opposite would happen if the net plastic deformation was compressive [**Wiesner, 1992**].Fig.1.1 shows how tensile plastic deformation results in compressive RS. Unlike mechanically induced RS, thermally induced RS are always tensile in the near-surface layer. During cutting, the surface layer is heated more than the underlying material, and since cooling occurs mainly from the inside by conduction, the surface layer stays hotter than the bulk material after cutting and tends to expand experiencing compressive stresses. If these compressive stresses exceed the yield strength, the material will be plastically deformed under compression resulting in tensile RS after cooling**.**
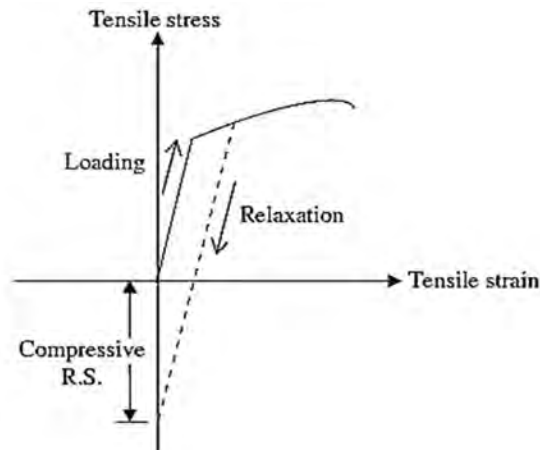
Fig.1.1 Tensile plastic deformation resulting in compressive RS [**Matsumoto et al. 1984**]

The machining-induced stress can be either beneficial or detrimental to component behavior in service. The stressed layer has multiple depths, depending upon the

cutting conditions, working material and cutting tool geometry and contact conditions at the tool-chip and tool-workpiece interfaces. The primary concern regarding RSis the effect on the mechanical properties,in particular, fatigue, contact fatigue, wear, and stress-corrosion cracking. In the medium- and high-strength steels tensile macro RS must strictly be avoided since they always promote crack initiation and propagation. Moreover, RS are considered a key factor in the surface integrity of machined parts due to their critical role in component life and corrosion resistance, as discussed by Schwach and Guo [**2006**].

Compressive macro RS in the surface region of materials increase the fatigue limit at cyclic loading compared to materials states that are free of residual stresses. This improvement is caused by an increased resistance to crack initiation and, to a certain extent, against crack propagation if the RSare sufficiently stable in the highest loading areas. Moreover, compressive macro RS can increase the resistance of materials against crack propagation and promote working tensile stress [**Outerio et. al. 2006**]. On the other hand, tensile RS tend to increase working stresses which lead to premature failure of components. These stresses may affect dramatically the performance of the machined part causing its premature failure, excessive wear, corrosion, part distortion etc. [**El-Axir, 2002, Outerio et.al 2006, Ulutan 2007**].

1.3 Machining with High-Pressure Coolant Jet

Heat generation and high cutting temperature is inherent characteristics of machining due to shearing of work material, friction between the flowing chips and rake face of the tool as well as the friction of auxiliary flank with the finished surface. At elevated temperature, the cutting tool edge deforms plastically and wears rapidly, which lead to dimensional inaccuracy, increased cutting forces and premature tool failure [**List et al. 2005**]. The use ofHPC supply during machining is one of the many ways to dissipate extensive heat generation in the cutting zone **[Ezugwu, 2005].** The integrity of HPC assisted machining had been thoroughly investigated over the years [**Machado et al. 1998; Senthil et al. 2002; Ezugwu, 2005; Globočki – Lakić et al. 2016; Mia et al. 2017**].

The most common way to reduce the cutting temperature is the application of various cutting fluids. Such cutting fluids cool the tool and job, provide lubrication and remove the chip from the cutting tool tip. But the conventional fluid types and methods of

application do not always assist in controlling the cutting temperature,especially under high speedmachining. In this case, the coolant is heated beyond its boiling point and creates a blanket of vapor that insulates the cutting zone from the coolant. That reduces the coolant's ability to remove heat. With HPC, the coolant effectively removes heat generated by the cutting process before it can accumulate and increase temperatures to the point at which tooling and workpiece surfaces are damaged. HPC can provide the following benefits:

> **Consistent machining process:** A fixed nozzle helpsin ensuring optimal performance of a HPC system and helpsin elimination of inconsistency from the process. The design and quality of the nozzles and delivery through the cutting tools also play a crucial role in getting the most out of the system.

> **Better chip control:** The proper application of HPCjet facilitates on-chip breaking. The jet can penetrate to the tool's cutting edge to provide a short shear zone that leads to the creation of thin chips that readily break into small pieces and also cools it, makes it more brittle and easy to break. Broken chips that fall away from the tool and workpiece, or are blown away by the force of the coolant, prevent the chip-related problems.

> **Better component quality:** In terms of machining heat, the coolant forced into the cutting zone has a significant impact on transporting heat away from the job and tool. The coolant flow can help stabilize component temperature, but it does not penetrate the barrier. At high pressure, the coolant becomes much more effective in removing heat. This results inthe better surface finish of job, increases tool life and allows for the use of higher cutting parameters.

The application principle of HPC is that the area reduction in the convergent fluid outlet (nozzle) produces an increase in the fluid velocity coming out of the nozzle. Larger the nozzle the higher the flow rate of the fluid. The larger the nozzle outlet diameter, the greater the flow rate requirement needed to deliver a certain pressure [**Li, 1996**]. As the fluid passes from a larger diameter tube to a smaller diameter tube, the flow rate requirements are smaller to achieve a high velocity jet. Compared to the conventional cooling, the idea of HPC is to inject a high-pressure jet of the emulsion in the cutting zone. The jet is injected directly in between the rake face and the chip or can be directed to the gap between the flank face and the workpiece.

Machining with HPC supply enables the coolant flow to pass through the machined surface faster, significantly increasing heat transfer of the coolant, penetrating deep into the cutting area and achieving high chip breakability through increased chip curl [**Machado et al. 1998**]. This consequently reduces the tool-chip contact area, minimizes friction at the tool-chip interface, removes more heat from the cutting region and consequently improves tool performance during machining. HPC injection technique not only provided a reduction in cutting force and temperature but also reduced the consumption of cutting fluid by two to four times [**Wrethim et al. 1992; Umbrella and Filice, 2009; Kramar and Kopac, 2009**].Globočki-Lakić et al. [**2016**] reported that the cutting performance of HPC machining is better than that of conventional flooding because HPC provides the benefits by giving the superior machinability. Their analysis of the results revealed that in the case of HPC the cutting forces were about 10% lower and tool life was approximately five times longer than when MQL was applied.

The application of HPC over conventional fluid in hard turning may be beneficial in terms of surface finish, tool wear, RS development, tool life, cutting zone temperature etc. In this regard, the present research work is carried out to experimentally investigate the role of HPC jet in respect of average chip-tool interface temperature, chip reduction coefficient and surface roughness and model RS profile in machining alloy steel by coated carbide insertsat a different speed and feed rate combinations.

1.4   Literature Review

RS generation in the machined surface layer is affected by various variables, such as workpiece material, machining parameter, and tool parameter. The knowledge of how these variables influence residual stress is very significant for controlling machining RS distribution, which is very useful to improve the service life of parts. However, previous efforts have been made to study metal cutting processes and understand the physical phenomenon of the formation of residual stresses by experimental investigation and theoretical modeling. In this study, cutting temperature and residual stress distribution is predicted by Finite Element Method (FEM) incorporating the optimized turning parameters under HPC machining.

The reviews on literatures are carried out on three areas related to the ability to create numerical simulations that accurately predict the RS induced by the turning process in the machined workpiece. The first section will address research related to the optimization of machining parameters in orthogonal cutting. The second section will focus on research studies about the HPC application to control cutting temperature. Finally, the third section will discuss research related to the approaches to predicting theRS profile.

1.4.1 Modeling and Optimization of Process Parameters

Cutting is one of the most important and common manufacturing processes in the industry. Beside the experimental investigation and theoretical analysis, the approaches such as empirical modeling, artificial intelligence (AI), numerical modeling are adopted to get a useful insight into the mechanics of cutting. Different techniques like statistical, artificial neural network (ANN), genetic algorithm (GA), FEM etc.areemployedto optimize the cutting process parameters.

Kaladhar et al. [**2013**] investigated the effects and the optimal setting process of parameters on surface finish and tool flank wear in turning AISI 304 with CVD coated (TiCN-Al2O3). Taguchi approach and Analysis of Variance (ANOVA) were employed to achieve the optimal result. The result reveals that cutting speed most significantly influences both surface roughness (46.05%) and tool wear (49.52%).

Das et al. [**2012**] presented an experimental study to investigate the effect of cutting parameters on tool wear, surface roughness and material removal rate during dry turning of EN-31 steel. The authors performed ANOVA to identify the effect of the cutting parameters on the response variables. The results revealed that cutting speed is only the significant parameter on tool wear and surface roughness. However, depth of cut (78.8%) only showed significant parameters for material removal rate.

Makadia and Nanavati [**2013**] presented the application of response surface methodology (RSM) for output optimization of AISI 410 turning by the ceramic insert. The machining parameters (cutting speed, feed, depth of cut and nose radius) were optimized with consideration of surface roughness. Total 81 cutting experiments were carried out. The results indicate that middle level of speed, low level of feed and depth of cut and high level of nose radius yield the optimal result. The feed rate was found the

dominant factor on surface roughness followed by nose radius, cutting speed and depth of cut. Verified experiments showed the error is within 6% for the developed model.

The study of Patil et al. [2011] revealed the effect of dry, wet and MQL environment on turning of AISI 4340 steel using CBN insert. Cutting speed, feed and environment were the process parameters and the machining responses were cutting force, surface roughness and tool wear. The experiment was based on Taguchi method. From ANOVA analysis it was found that the cutting speed and environment are the important factors in effecting the surface roughness value. The best surface finish (0.9 μm) was found in MQL machining at high speed (220 m/min). The resulting cutting force and tool wear were found in smallest amount least (24%) under MQL compared to dry (44%) and wet (32%) environment.

Considering minimum production cost as the objective function, Manna and Soladkar [2008] proposed a methodology for turning E0300 alloy steel. Taguchi method based parametric optimization was employed here for evaluation of surface roughness. The study found that cutting speed having highest effect on surface roughness as compared to the depth of cut and feed rate.

Ozel and Karpat [2005] developed the neural network and regression models for the prediction of surface roughness and tool flank wear in finish turning of AISI 52100 steel using cubic boron nitride (CBN) inserts. They compared the neural network models with regression models and they found that the neural network models were capable of better prediction for surface roughness and tool flank wear.

Ozel et al. [2007] developed a model using regression analysis and ANN for the prediction of surface finish and flank wear in finish turning of AISI D2 steels (60 HRC). They also compared the neural network based prediction of surface roughness and tool flank wear with a non-training experimental data. It was found that the neural network models are suitable to predict tool wear and surface roughness for a range of cutting conditions.

RSM and ANN were employed by Mia and Dhar [2016] to predict the average tool-workpiece interface temperature in hard turning of AISI 1060 considering cutting

speed (58, 81, 115 m/min), feed rate (0.10, 0.12, 0.14 mm/rev) and material hardness (40 HRC, 48 HRC an 56 HRC). The experiment was conducted both in dry and HPC environment. They found both prediction models were acceptable whereas the ANN model demonstrated a higher accuracy over RSM. Considering the environment, for HPC condition, the ANN model shows higher accuracy than dry. But with respect to RSM, this higher accuracy appears in dry cutting.

Metelski et al. **[2015]** applied the dynamic programming approach in the context of process parameter optimization of Duplex stainless steel turning with a coated carbide insert. In order to optimal values modified Dijkstra's optimization algorithm was used along with ANOVA analysis. The analysis indicates that cutting speed has the higher effect on tool life than feed rate. Predicted maximal tool life is around 48 min was found.

Addona and Teti[**2013**] developed a GA optimization model to find the optimal cutting parameters (speed, feed, and depth of cut). Process optimization yields minimum production time while considering the constraint of tool life, cutting force, power and surface roughness. The machining process was associated with cast steel blank using HSS.

The continuous development of more and more powerful computers and numerical methods and their ever-widening application in manufacturing, phenomena in metal machining, such as cutting force, temperature, and even tool wear are gradually studied using numerical methods including Finite Differential Method (FDM) and FEM.

Till the late 1990s, the majority of researchers generated their own FEM codes to use in their studies. Due to the long computational hours of simulations and high memory capacity needed, the use of FEM was limited and if used, 2D simulations were dominant. However, over the last 20 years, developments in technology dramatically increased, overcoming to an extent the limitations faced in modeling and computational difficulties. Commercially available software packages became more in use. These packages include NIKE-2D, DEFORM, FORGE2D, ABAQUS/standard and/Explicit, ANSYS/LS-DYNA, ALGOR and FLUENT.

Yen et al. **[2004]** analyzed the cutting process by considering the effect of tool edge preparation using the FEM simulation. It was aimed to provide a fundamental

understanding of the process variables and mechanics, necessary for the optimization of tool edge designs.

Attanasio et al. **[2008]** focused on the 3D numerical prediction of tool wear in metal cutting operations. In particular, an analytical model capable of considering the diffusive wear mechanism was implemented through a specific subroutine. Furthermore, an advanced approach to model heat transfer phenomena at the tool-chip interface was included in the numerical simulation. The adopted simulation strategy gave the possibility to properly evaluate the tool wear. The 3D FEM results were compared with some experimental data obtained turning AISI 1045 steel using uncoated WC tool; a good agreement was found.

Ozel [**2009**] presented a finite element model using DEFORM in turning of AISI 4340 alloy steel to predict the chip formation, forces, stresses, temperatures, and tool wear on uniform and variable edge design tools of PCBN inserts. The workpiece wasmodelled as rigid-perfectly plastic material where the material constitutive model is represented with Johnson-cook material model. They stated that the variable micro-geometry insert edge design reduces the heat generation and stress concentration along the tool cutting edge significantly and induced less plastic strain on the machined workpiece.

Swamy et al. **[2012]** analyzed the turning process of AISI 1045 by PCBN tool with FEM model by means of DEFORM 3D. The authors investigated the effect of cutting speed on effective stress, strain, and temperature where cutting speed was varied from 100 m/min to 200 m/min while feed and depth of cut were kept constant (0.05mm and 0.5mm respectively). The study reveals that cutting speed has an inverse effect on effective stress whereas temperature increases (743°C to 1120°C) with cutting speed.

In general, the mechanical process energy is converted to heat flows into the workpiece, tool, chip and the environment. Due to the complex phenomena which are related to the analytical methods, mostly exclude local effects of the chip formation process and are limited to the dry environment in the majority of cases. However, the FE based chip formation simulation is able to calculate the local heat generation caused by plastic deformation and friction.

1.4.2   Effect of HPC Jet on Cutting Temperature

The effect of cutting temperature, particularly when it is high, is mostly detrimental to both the tool and the job. Due to the high shear and friction energy generation in machining operation the temperature in the primary and secondary shear zones are usually very high, hence affect the shear deformation and tool wearresults in poor surface quality. Therefore, it is desirable to control the temperatures of the tool and chip interface. Cooling with high pressures in turning operations is an effective method for providing higher productivity, reducing the temperature in the cutting zone and improving chip control depending on the pressure and flow rate of the fluid jet.

Kaminski and Alvelid [**2000**] investigate the effects of a high and ultra-high pressure water jet directed into the tool-chip interface on tool temperature, cutting forces, chip shape and surface roughness in regular turning operations. The results show that a significant reduction of edge temperature, by 40-45%, is possible. It has been reported that the use of HPC is capable of increasing productivity when compared to the conventional methods of coolant delivery [**Ezugwu, 2005**]. Reduction of temperature in the cutting zone, lower cutting forces, lower vibration levels, better surface integrity and closer tolerances of the machined components are other major benefits reported by these studies.

Senthil et al. [**2002**] performed an experimental investigation of ASSAB-718 steel material during the milling operation. They showed the effectiveness of HPC in terms of improved surface finish, reduced tool wear and cutting forces, and control of chip shape. The tool wear with HPC was found significantly better than that of dry cut and conventional coolant. The effect of the coolant in relation to chip formation, cutting forces and thermal generation was modelled by Hadzley et al. [**2013**]. The result showed that increasing coolant pressure significantly reduces the friction at the tool-chip interface, which significantly reduced the cutting force and temperature. Ezugwu and Bonney [**2004**] reported that machining Inconel-718 with coated carbide inserts under HPC improve tool life by up to seven folds, especially at high-speed conditions. Tool life tends to improve with increasing coolant pressure.

Mia and Dhar [**2015**] investigated the performance of HPC technique during turning HRC 48 steel. It was found from the study that the application of HPC provides a

substantial reduction in average chip-tool interface temperature up to 12% and improves tool life and surface quality. A significant temperature reduction in the cutting zone and surface roughness due to the use of HPC is reported in [**Dahlman and Escursell, 2004; Kaminski et al. 2000**].

1.4.3   Residual Stress Prediction

The deformation of the workpiece material during the machining process results in stress in the workpiece surface. Typically these stresses are large in magnitude near the surface and decrease with distance from the machined surface. A qualitative RS profile is shown in the Fig.1.2. Profiles like this have been reported by a number of researchers, to name only a few [**Valiorgue et al. 2007; Lazoglu et al. 2008; Huang and Yang, 2016**]. Common to all of the publications, is the fact that the magnitude, as well as stress profile, greatly depends on the process parameters.
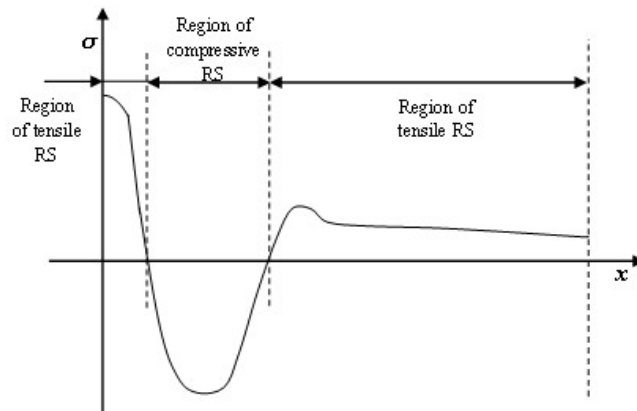
Fig.1.2   Typical residual stress profile induced after machining

In hard turning very high compressive stresses are achieved in the cutting zone. The theory of hydrostatic pressure gives an explanation for a crack-free chip formation process of this zone. Cutting tools used for hard turning typically have a negative rake angle on the major first which carries out of most of the cutting action. Large compressive stress with a high proportion of hydrostatic pressure occurs in the chip forming zone due to the low undeformed chip thickness and at the same time strong negative rake angle. The critical flow shear stress is reached without material cracks. They also have a cutting edge radius which is only two or three times smaller than the depth of cut and leads to what are

effectively even more strongly negative rake angles. As a result of the small undeformed chip thickness, the chip formation takes place entirely in the region of the cutting edge radius. These strong negative rake angles create very high stresses in the workpiece and in particular in the region of the primary shear zone. So that, the cutting edge geometry has a direct impact on the stress levels generated in finish hard turning because the increased edge radius and strong negative rake angle on the insert generate higher cutting forces. A higher passive force tangential to the surface generates higher compressive RS. With this consideration, brittle materials are plastically deformable. Additionally, hardened steel typically consists of a martensitic structure and temperatures during hard turning typically reach 700-800°C. After machining, subsequent cooling generates tensile RS.

Umbrello et al.[**2011**] presented an innovative experimental and numerical approach to predict stresses induced during machining of AISI 52100 steel. It was found that the microstructural phenomena associated with metallic and dark layers formation influence the residual stress profile. Considering the effect of workpiece hardness on residual stress under otherwise constant machining conditions was also reported. AISI 52100 steel in hardness ranging from HRC 55-HRC 63 were tested. By using the same cutting parameters larger compressive residual stresses are generated for the higher hardness work material [**Hua et al. 2005**]**.** Again, it was found that materials with higher initial yield strength or lower strain hardening effects experience lower surface tensile RS. In addition, lower surface tensileRSwas induced in materials with higher hardness [**Matsumoto et al. 1984; Thiele and Melkote, 2000; Capello, 2005**].

Shet and Deng [**2003**] investigated the frictional interaction along the tool-chip interface and a range of rake angles. They concluded that the tool-chip friction and tool rake angle have nonlinear effects on residual stresses and strains. Outeiro et al. [**2006**] investigated the influence of the tool geometry and cutting parameters on the RS induced in turning of AISI 316L steel. The study showed that the uncut chip thickness had the strongest influence on RS and that stresses increase with most of the cutting parameters and cutting tool edge radius. Matsumoto et al. [**1999**] examined the effect of machining parameters and the cutting edge geometry on RS profiles in hard turned steel. The research concluded that the tool edge geometry is the dominant factor affecting the residual stress profile. Wang et al. [**1997**] studied the effects of machining parameters on the variations of

RS in the machined surface layer. The results showed that high cutting speed is the main factor affecting the RS. Again, Coto et al. [2011] found in their study that with the increase of feed, residual stress increases whereas high cutting speed results in less tensile stress. The same result was obtained by Sharman et al. [2015] in turning Inconel 718. Capello [2005] verified once again that the influencing process parameters on RS are feed rate and tool nose radius. The depth of cut, on the contrary, does not influence RS. Dahlman et al. [2004] also showed that the depth of cut doesn't have a big impact onRS formation. In this investigation, the RS profiles are almost the same for the various depths of cut in the machining of AISI 52100 using solid CBN inserts.

Wu and Matsumoto [1990] showed that shear angle effects dominate the stress patterns in facing of AISI 4340 steelof different hardness values.Matsumoto et al. [1986] also reported similar observations when examining the effect of workpiece hardness on residual stress produced in facing of AISI 4340 steel. They have studied total seven level of hardness ranging from HRC 29 to HRC 56 and showed that, in the absence of phase transformations, residual stresses become more compressive as workpiece hardness increased.Thieleand Melkote [2000] investigated the subsurface residual stresses inorthogonal machining of through hardened AISI 52100 steelwith different tool edge preparations and two levels of hardness,keeping the cutting parameters fixed. By using X-ray measurements,they found that the hone edge preparation produces morecompressive residual stresses than the chamfer edge geometryafter machining a workpiece hardened to HRC 41 and HRC 57. Furthermore, they observed that more compressive residual stress was induced in the subsurface when a harder material was used.

Thus, several studies on RS induced by machining have been performed. However, all of these studies remain experimental in nature. Experiments are done by measuring RS using the X-ray diffraction technique. Analytical modeling based on RS prediction was also performed by some authors such as Ulutan et al.[2007], Liang and Su[2007],Lazoglu et al. [2008],Huang and Yang,[2016]. Numerical modeling was also adopted by Valiorgue et al. [2007] Another investigation way of RS is getting popularity is FEM. Due to the availability of FE coded software considering large complexities that come upon metal cutting (i.e. large deformation, strain rate effect, tool-chip contact and friction, local heating and temperature effect, different boundary and loading conditions)

the use of FEM is increasing. Many studies on FE modeling of the orthogonal cutting process have been published which shows the results obtained are in good agreement with experimental one. Review of some FEM based research works associated with RS evaluation in metal cutting is put on following.

Liu and Guo [**2000**] studied the effect of sequential cuts and tool-chip friction on RS, using the explicit finite element code; ABAQUS. It was observed that by optimizing the second cut, tensile RS from the first cut can be turned into compressive. Miguélez et al. [**2009**] investigated the generation of residual stresses in orthogonal metal cutting using an Arbitrary-Lagrangian-Eulerian (ALE) finite element approach. The study concluded that tensile stresses are the result of both thermal and mechanical effects. Considering the cutting parameters of machining Outerio et al. [**2006**] found that residual stresses increase with most of the cutting parameters including cutting speed, uncut chip thickness and tool cutting edge radius. The authors designed a Lagrangian implicit code utilizing FEA software DEFORM-2D, for the orthogonal cutting process of AISI 316L. In the later study of Outerio [**2008**] presents new knowledge on surface integrity in terms of residual stresses generated in turning of Inconel 718 and AISI 316L. The author developed 2D model of turning operation for both materials which shows the appearance of high tensile residual stresses at the machined surface and compressive RS in the sub-surface below 10–25 mm. Higher RS values were obtained on the transient surface than on the machined surface. Mohammadpour et al. [**2010**] investigated the effect of machining parameters on RS in orthogonal cutting. The study concluded that the maximum tensile RS increased with increasing the cutting speed and feed rate. The study of Ozel and Ulutan [**2012**] also shows the more compressive RS with increased edge radius in turning of Ti–6Al–4V and IN100 alloys. The authors developed a 3D FEM based model where DEFORM software was utilized.

So muchstudieswere performed in the area of residual stress all which are found examined under dry condition. A numerical model was developed by Courbon et al. [**2011**] for the purpose of machining performance evaluation in high-pressure jet assisted turning of Inconel 718.Hadzley et al. **[2013]**presented a finite element model for high-pressure jet assisted machining of the Ti-6Al-4V alloy. Very recent the same Ti alloy was analyzed by Klocke et al. [**2017**] and Imbrogno et al. [**2017**] in turning operation considering cutting

fluid. The former one was done only for investigating the effects of HPC application on chip formation. Whereas the latter was related to predicting cutting forces, temperature, and machining-induced microstructural alterations under cryogenic conditions. But none of the studies was for RS evaluation. Concerning FE modeling residual stresses under HPC in alloy steels, the available studies are even more restricted.

The aforementioned studies stated, have provided a good insight of the turning process, RS formation and FEM used in RS projecting. As research takes more interest in predicting the residual stress induced in the workpiece surface, there will be opportunities to advance these predictive methods. Generated finite element codes can be said generally achieves its purpose in estimating residual stresses to an extent, but its main drawback is in its simulation time requirement which is not adaptable for process optimization. This limits the ability to generalize the application of the results and models reached by FE codes. The research is limited to the materials investigated in the papers published and in order to apply the model, further experimentation and estimation of parameters are needed.

1.5   Summary of the Review

The prediction of different cutting responses in turning operation for various material like AISI 304, AISI 410, AISI 1040, AISI 1045, AISI 4340, E0300, EN24, Al-6082-T6, Al 2024 T351alloy, 42CD4 Ti6Al4V alloys, Ductile cast iron, Duplex stainless steel, Inconel 718TM etc. was attempted by various researchers. Analytical, Numerical and Empirical models were developed for the prediction and measurement of surface roughness, cutting force, cutting temperature and tool wear by several researchers. The researchers investigated the process parameter for turning operation that influences the responses are cutting tool properties (tool material, tool geometry), machining parameters (cutting speed, cutting feed, depth of cut, cooling fluid), workpiece material (workpiece dimension, workpiece hardness) and cutting phenomena (cutting force variation, chip formation, friction) in the cutting zone. Summarizing the literature survey it is revealed that, cutting speed and feed are the two most influential process parameters for machining responses.Considering the optimization of process parameters artificial intelligence based techniques like GA, simulated annealing, andANN was applied by researchers to get the desired surface roughness, cutting temperature and cutting force. Statistical techniques like

the factorial design, Taguchi technique,and RSM were employed by a number of researchers for developing empirical models and to study the effect of process parameters on surface roughness, cutting force, cutting temperature and tool wear for various materials.

Controlling the cutting temperature is considered the most important task to increase production quality. In this regard, almost all of the researchers found fluid application methods such as MQL, HPC, and cryogenic as a viable alternative to dry cutting. Among these techniques HPC is found the most favored technology in high speedmachining, which economically addresses the machining processes, environmental and health concerns.

It is revealed from the literature that RS has become a vital analyzing field in the machining processes. Summarizing, RSwere analyzed in the axial and circumferential directions. The determination of the influence of machining parameters on the RS was addressed as well. Beside the experimental investigation by X-ray diffraction method, the FEM based approaches are adopted to get a useful insight into the residual stress profile. The application of FEM is beneficial to gain a better understanding of chip formation mechanism, stress and strain distribution, the effect of cutting parameters, analysis of heat generation and observation of contact conditions. Thus, FE software makes it somewhat easy to model this stress profile. However, the studies regarding the residual stress concerning FEM models to represent the machining with HPC are still limited. Moreover, there is a lack of RSmodeling for machining alloy steel. So there is the necessity of thorough investigation to explore RS circumstance for alloy steel machining under HPC jet.

1.6   Scope of the Study

The application of HPC jet in machining assist in reducing the cutting temperature at tool-chip interface. This results inthe good surface finish of the job. On the other hand, the service life of the product depends on the metal cutting condition as the machining-inducedRS is responsible for the product's fatigue life. However, only a few works have been conducted to model the cutting process under consideration of the lubricant, while modeling of the interaction between fluid and chip formation is still a challenge. A lot of

study on dry machining considering the effect of RS were performed. Keeping all this in view, the present study will be carried out to predict the RS under HPC condition in turning alloy steels by coated carbide tool under different process parameters conditions. The study will focus on finding optimum processes parameters considering the effect of cutting temperature, surface roughness and tool wear as well.

1.7   Objectives of the Study

The objectives of the present work are as follows:

(i)   Investigate the role of high-pressure coolant jet in machining alloy steel at different process parameters and workpiece hardness in terms of temperature and tool wear

(ii)   Ascertain the optimal process parameters by minimizing the cutting temperature and tool wear

(iii)   Develop a model for temperature distribution using Finite Element Method

(iv)   Use the optimal process parameters to determine the minimal residual stress developed in the workpiece during machining

1.8   Organization of the Thesis Paper

Chapter 1 presents the assessment of previous work regarding the effect of machining induces residual stress after machining, the influence of cutting temperature and controlling way of it with the effective application of HPC jet. Reviews of different kinds of literature have been given here based on the process parameters optimization, HPC jet utilization, and RS prediction. This chapter also contains the objective of the present work along with a brief methodology of the whole study.

Chapter 2 provides experimental conditions and procedure of the machining carried out with the measurement of quality characteristics. This chapter also includes the experimental results on the effects of HPC relative to dry machining on chip formation, chip-reduction coefficient, cutting zone temperature, surface roughness and tool wear in turning alloy steel by coated carbide SNMM inserts under different speed-feed combinations and at different hardeness level of workpice.

Chapter 3 is comprised of the empirical model development and validation of the developed model of cutting temperature, surface roughness and tool wear.

Chapter 4 explains the principle of GA based optimization including multi-objective optimization method. Then the optimization problem formulation for the present work has been carried and placed in this chapter. The results of the optimization have been included here as well.

Chapter 5 focuses on the finite element modeling of RS which has been developed by the ABAQUS software. This chapter contains the basic of FE modeling of metal cutting and different features of the finite element used in this research. The model development procedure adopted for both of the dry and HPC cutting conditions has been thoroughly described in this chapter.

Chapter 6 contains the detailed discussions on the experimental results, possible interpretations on the results obtained from experiments, empirical modeling and optimization of cutting temperature and surface roughness, FEM of RS distribution.

Finally,conclusion and recommendations for future work are given in **Chapter 7**.

1.9   Methodology of the Study

The methodology of the study was as follows:

(i)   A HPC delivery system has been utilized for supplying coolant at high pressure from the coolant tank and impinged at high speed through the nozzle into the chip-tool interface. A specially designed nozzle was used to supply high-pressure oil.

(ii)   A series of experiments in turning alloy steel of different hardness level have been performed under dry and HPC condition at different combination of cutting speed and feed rate. Chip shape, chip color and chip thickness ratio under both environmental conditions have been studied. The average cutting temperature, surface roughness and tool wear have been measured by specific instruments.

(iii)   The experimental results have been used to developmathematical model for cutting temperature, surface roughness and tool wear by RSM. The adequacy of the model has been verified by analysis of variance technique. Validity test was also done for the developed models.

(iv)   By utilizing the developed empirical models three different objectives - cutting temperature, surface roughness and tool wear minimization have been carried out by multi-objective optimization method based on GA to find the optimal hardness values and process parameters in turning process. Confirmation experiments were then carried out to check the consistency of the generated optimized results.

(v)   The FEM-based simulation has been run based on the optimum results obtained from GA solver.The ALE boundary condition has been utilized for the chip formation process. Temperature distribution on chip-tool interface has been modeled and using the simulated temperature values necessary verification has been carried out to justify the reliability of the finite element model. The simulation was then performed for predicting the machininginduced RS profile under coolant effect. Finally, the simulation was conducted for RS prediction through the relaxation procedure, and the stress profile was studied.

Chapter-2

EXPERIMENTAL INVESTIGATION

2.1 Introduction

Increasing the productivity and the quality of the machined parts are the main challenges of the metal-based industry. In this regard, there has been increased interest in monitoring and understanding the behavior of machining. In this research experimental investigations were carried out by turning 42CrMo4 steel (42 HRC, 48 HRC, 56 HRC) in a lathe with coated carbide inserts at variable cutting speed and feed combination under dry and HPC condition. The influence of cutting speed, feed and environment were examined on cutting temperature, tool wear and machined surface roughness. Chips morphology was also studied in order to examine and relate the effect of cutting temperature on chip's color. Chip formation and machining temperature are two of the main challenges while machining hardened materials. Moreover, cutting temperature is the crucial response which directly effects the residual stress accumulation in the machined job. Even when performance already have been optimized with tooling and insert technology, adoption of HPC machining can make the machining more raise the ceiling for further improvement through localized cooling at the point of contact.

2.2 Experimental Procedure and Conditions

In this research work,HPC jet has been applied in machining in order to have better experimental results. The proper application of a jet of HPC has a positive effect on both chip breaking and heat. A HPC system can enlarge the chip-breaking area for an insert geometry and break previously unbreakable chips. During machining with traditional flood cooling, the coolant is heated beyond its boiling point and generates a blanket of vapor. That insulates the cutting zone from the coolant. Thus, reduces the coolant's ability to remove heat. High-pressure, high velocity coolant eliminates this vapor barrier so the

generated heat is removed effectively at a high rate. The purpose of the experimental investigation in this present work is to investigate the behavior of cutting temperature and chips morphology experimentally under dry and HPC which is a pre-requisite in order to predict different machining phenomenon.

Table 2.1 Experimental Conditions

Machine Tool	: Lathe (China), 7.5 kW
Work Materials	: 42CrMo4 Steel
Hardness, H	: 42 HRC, 48 HRC, 56 HRC
Size	: Length= 200mm, Diameter = 98 mm
Cutting Tool	: SNMM 120408, Widia
Coating	: TiCN, WC, Co
Geometry	: -6°,-6°,6°,6°,15°,75°,0.8 (mm)
Tool Holder	: PSBNR 2525 M12 (ISO specification), Widia
Process Parameters	
Cutting Velocity, V	: 54, 82, 118 and 165 m/min
Feed Rate, f	: 0.12, 0.14 and 0.16 mm/rev
Depth of Cut, t	: 1.5 mm
Environment	: Dry and High-pressure coolant (HPC) condition
Pressure	: 80 bar
Flow Rate	: Coolant: 6.0 l/min through the external nozzle
Coolant Type	: VG-68 (ISO grade)

The present experimental study involves machining of hardened alloy steel with of different hardness (42 HRC, 48 HRC, 56 HRC) with coated carbide insert under dry and HPC environment. The process utilized was straight turning operation performed on reasonably rigid and powered center lathe (7.5 kW, China). The experiments plan has two variables of cutting parameter, named as cutting speed and feed rate. Keeping in view the less significant role of depth of cut on cutting temperature and RS, ithas kept fixed. The recommended range of depth of cut value for finishing operation for the studied tool-workpiece combination is 0.3mm to 2mm [**Widia^TM Value**]. On the other hand, the depth of cut should be greater than the nose radius of insert. So considering all of these the constant value was set to 1.5 mm which is greater than the nose radius of 0.8 mm and approximate medium value of suggested range.A tool holder with a general specification PSBNR 2525M12 was used in this experiment. Theinsert with a general specification of SNMM 120408 was used as the cutting tool. The experimental details are given in Table 2.1.

Getting the positioning just right is one of the keys to the effectiveness of this coolantdelivery technology. The pressurized coolant was directed towards the rake and flank surfaces of the tool using specially designed nozzle system developed by Khan [**2015**]. The diameter of the nozzle channels was 0.5 mm each and the flow rate was 6 l/min per channel. The pictorial view of the HPC nozzle is shown in Fig.2.1. The final arrangement used is shown in Fig.2.2.

The chip samples were collected during short run machining for all the *V-f* combinations under both dry and HPC conditions. Chips were visually examined and categorized with respect to their shape and colour. The thicknesses of the chips were repeatedly measured by a digital slide caliper (Mitutoyo Digimeter) to determine the value of chip reduction coefficient (ratio of chip thickness after and before cut). The cutting temperature was measured using tool-work thermocouple while the emf generated by this was recorded by a digital multimeter (Rish Multi, India). The calibration curve for this tool-work pair determined by Kamruzzaman [**2009**] was used for converting emf (mV) to temperature (°C). Measurement of surface roughness was performed by a Talysurf (Surtronic 3+) surface roughness tester with a 0.8 mm sampling length. The measurements are repeated three times at different locations and the average value is used in research work. During machining under each condition, the cutting insert was withdrawn at regular intervals and average flank wearwere measured under an optical microscope (Carl Zeiss, Germany) fitted with a precision micrometer.
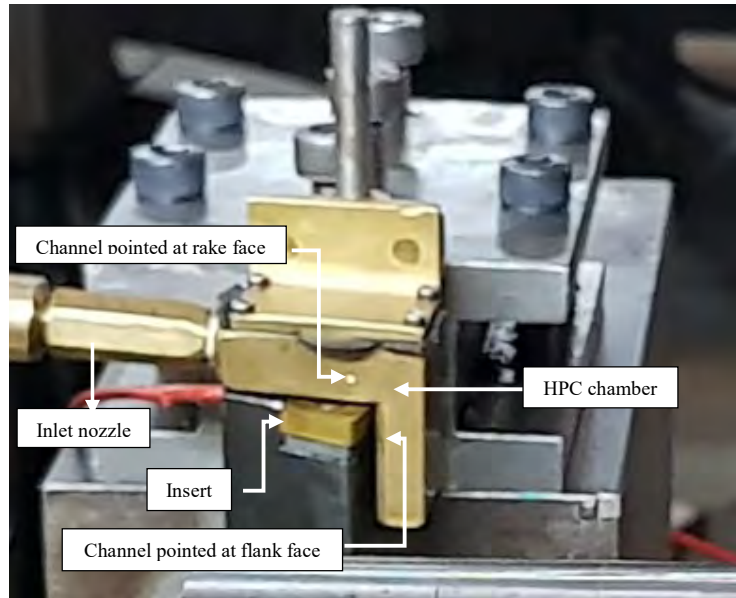
Fig. 2.1 Pictorial view of HPC nozzle
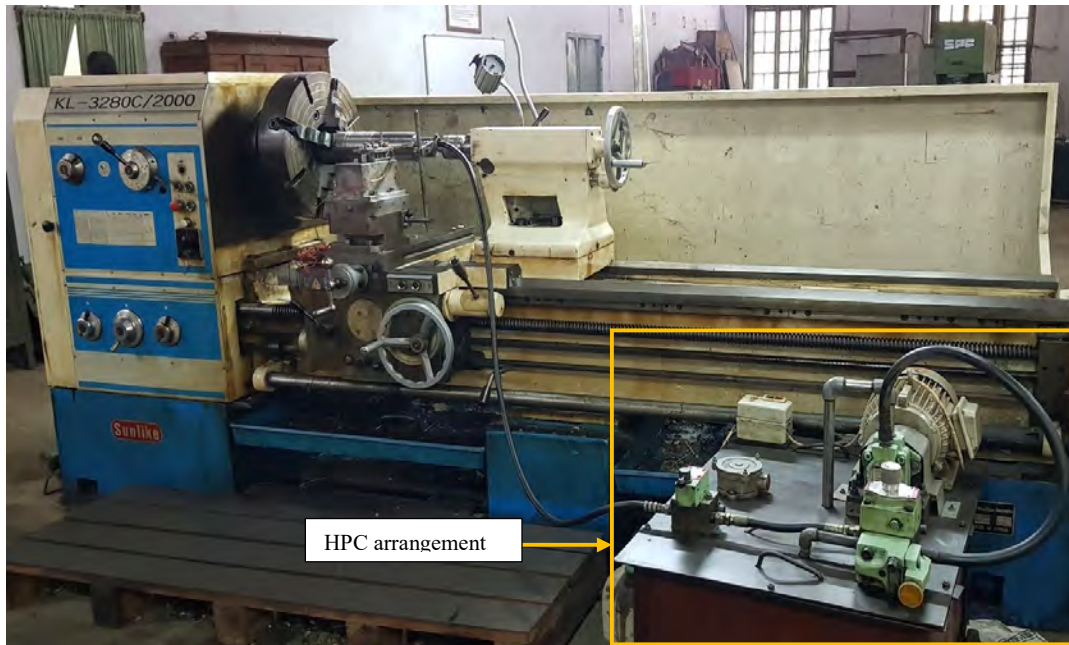
Fig. 2.2 Photographic view of the experimental set-up

2.3 Experimental Results

2.3.1 Machining Chips

When a cutting edge performs its metal cutting function properly, it deforms some of the workpiece material plastically and then pushes it off. Chips separate in either of three ways- break by themselves, break against the tool, or break against the workpiece. The chips were collected during all the machining run for studying their shape and color. Chip shape and colourfordifferent steel are incorporated in Table 2.2, Table 2.3 and Table 2.4. These tables show that machining under HPC condition the colour of the chips was also become much lighter (metallic from blue) compared to the dry cut.This indicates that the application of HPC jet reduces the chip-tool interface temperature. Under HPC Again, looking to the morphologies of the chips, washer-type long helical chips was generated at HPC condition while ribbon-type snarled chips result at dry. Considering cutting speed and feed, long and stringy chips was generated at low speed and feed while short and thicker chips result at high speed and feed.

Table 2.2 Chip Shape and colour during turning 42CrMo4 steel of 42 HRC
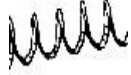
V (m/min)	f (mm/rev)	Environment			
		Dry		HPC	
		Shape	Color	Shape	Color
54	0.12	■	Blue	●	Metallic
	0.14	■	Blue	◉	Metallic
	0.16	■	Blue	◉	Metallic
82	0.12	■	Blue	◉	Metallic
	0.14	■	Blue	◉	Metallic
	0.16	■	Blue	●	Metallic
118	0.12	■	Blue	●	Metallic
	0.14	■	Blue	◉	Metallic
	0.16	■	Blue	◉	Metallic
165	0.12	■	Blue	◉	Metallic
	0.14	■	Blue	◉	Metallic
	0.16	■	Blue	◉	Metallic
Chip Shape	Ribbon type (Snarled) ■			Tubular ▲	
	Arc-Loose ●			Washer-Long Helical ◉	

Table 2.3 Chip Shape and colour during turning 42CrMo4 steel of 48 HRC

V (m/min)	f (mm/rev)	Environment			
		Dry		HPC	
		Shape	Color	Shape	Color
54	0.12	■	Blue	◉	Metallic
	0.14	■	Blue	◉	Metallic
	0.16	■	Blue	◉	Metallic
82	0.12	■	Blue	◉	Metallic
	0.14	▲	Blue	◉	Metallic
	0.16	▲	Blue	●	Metallic
118	0.12	■	Blue	◉	Metallic
	0.14	■	Blue	◉	Metallic
	0.16	■	Blue	◉	Metallic
165	0.12	■	Blue	◉	Metallic
	0.14	■	Blue	◉	Metallic
	0.16	■	Blue	◉	Metallic

Table 2.4 Chip Shape and colour during turning 42CrMo4 steel of 56 HRC

V (m/min)	f (mm/rev)	Environment			
		Dry		HPC	
		Shape	Color	Shape	Color
54	0.12	■	Blue	◉	Metallic
	0.14	■	Blue	◉	Metallic
	0.16	■	Blue	◉	Metallic
82	0.12	▲	Blue	◉	Metallic
	0.14	●	Blue	◉	Metallic
	0.16	●	Blue	◉	Metallic
118	0.12	●	Blue	◉	Metallic
	0.14	■	Blue	◉	Metallic
	0.16	●	Blue	◉	Golden
165	0.12	●	Blue	◉	Metallic
	0.14	■	Blue	◉	Golden
	0.16	■	Blue	◉	Golden
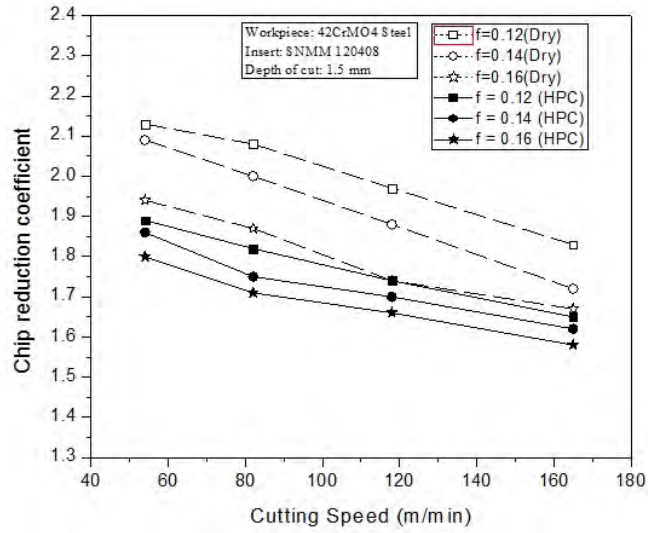
(a) 42 HRC
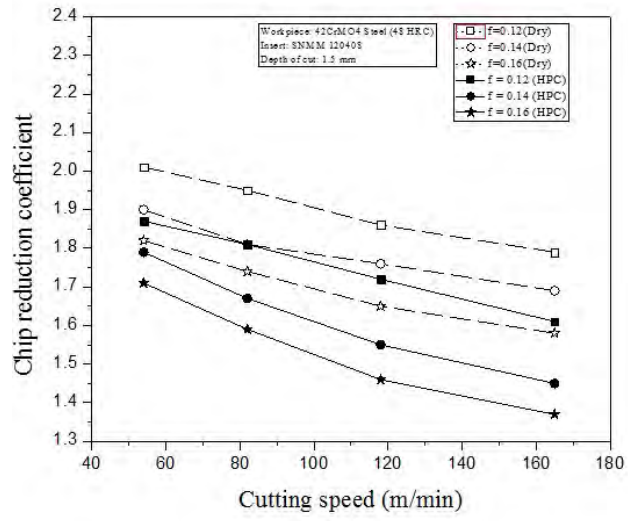
(b) 48 HRC
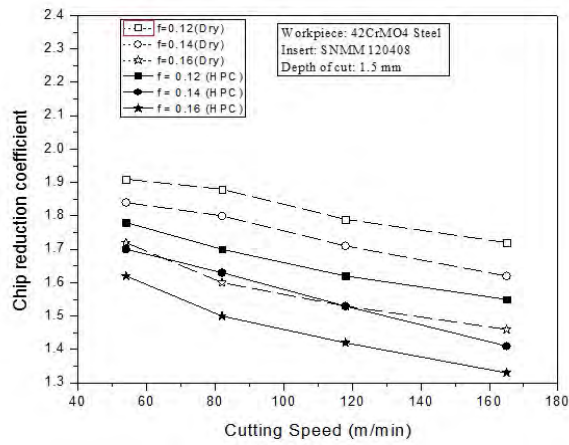
(c) 56 HRC

Fig.2.3 Variation of ξ with V and funder dry and HPC conditions

The chip reduction coefficient, ξ is an important machining performance index of chip formation and power consumption for a given tool-work combination. It is primarily influenced by cutting speed, feed, and depth of cut and form of the chips expected to be influenced by the high-pressure coolant. Decreasing chip reduction coefficient indicates improvement in cutting tool life, surface finish and the energy required for machining. Larger of ξ means larger cutting forces and friction and is hence undesirable.

Chip reduction coefficient was measured for each of the experiment conducted. The chip thickness has been computed as the average of three measurements done to evaluate the chip thickness after each machining operation. The chip reduction coefficient has been obtained by taking the ratio of the chip thickness to uncut chip thickness. The variation in the value of chip reduction coefficient, ξ with a change in cutting speeds and feed rate as well as machining environment evaluated for 42CrMo4 steel of different hardness level have been plotted and shown in Fig.2.3.

2.3.2 Cutting Temperature

Energy consumption increases with the increase in cutting velocity, feed, and depth of cut as well as strength and hardness of work material. The greater the energy consumption, the greater is the temperature at the tool-chip interface and consequently the higher is the dimensional inaccuracy and tool wear. The effective application of high-pressure coolant is expected to be a possible solution for high speed machining in achieving intimate chip-tool interaction and low cutting temperature.

In the present work, the average chip-tool interface temperature (T) has been determined by using tool-work thermocouple technique under all the machining conditions. The evaluated role of HPC on average chip-tool interface temperature in turning different hardened steel at different speed-feed combinations in compare to dry condition have been shown in Fig.2.4. The increasing trend of temperature with the increase of cutting speed-feed is found common for both machining environment due to increase in energy input. But in magnitude, the temperature is extensively found lower in HPC machining compared to dry condition machining for all the speed-feed combination. Such apparent reduction in the cutting temperature is expected to have some favorable influence on other machinability indices.
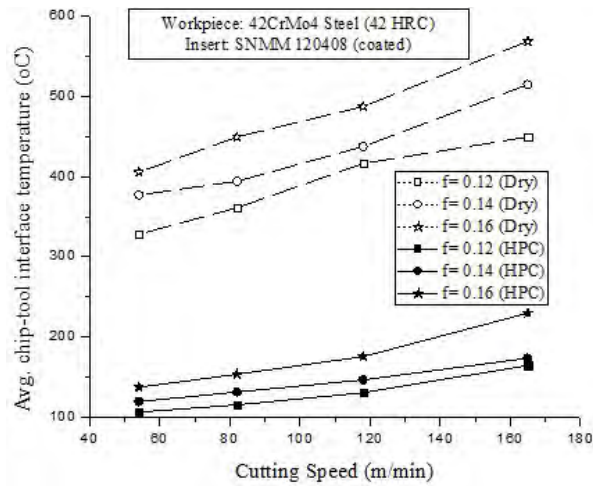
(a) 42 HRC
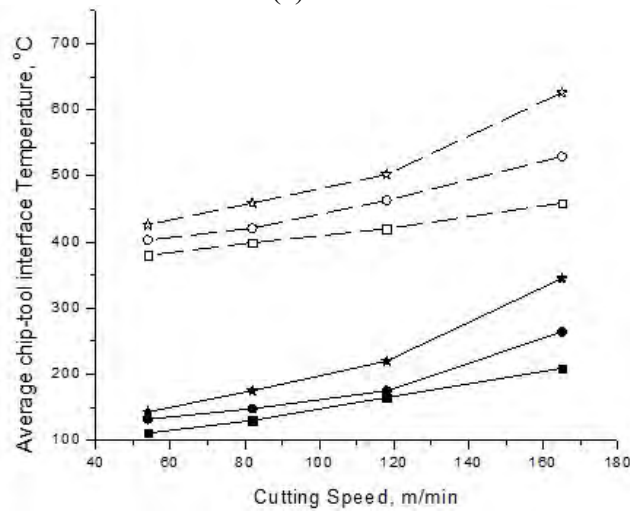
(b) 48 HRC
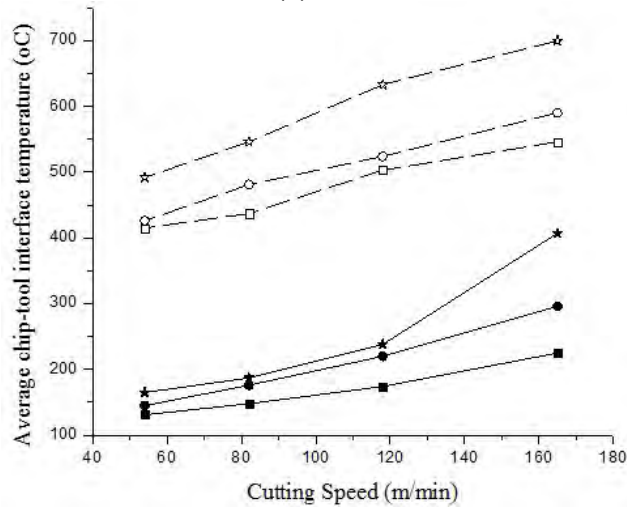
(c) 56 HRC

Fig.2.4 Variation of T with V and f under different cutting condition at depth of cut 1.5 mm

2.3.3   Surface Roughness

Surface finish is an important parameter in manufacturing engineering. It is a characteristic that could influence the performance of mechanical parts and the production costs. Surface roughness is substantially influenced by the machining environment for given tool-work pair and speed-feed conditions. In the present work, surface roughness has been investigated to evaluate the relative role of HPC on those two major aspects.
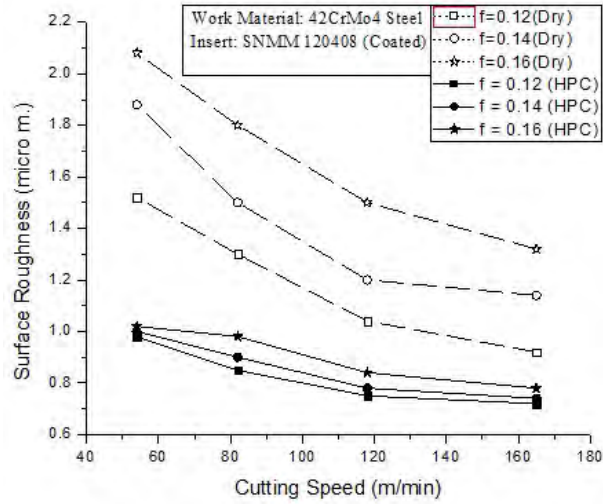
(a) 42 HRC
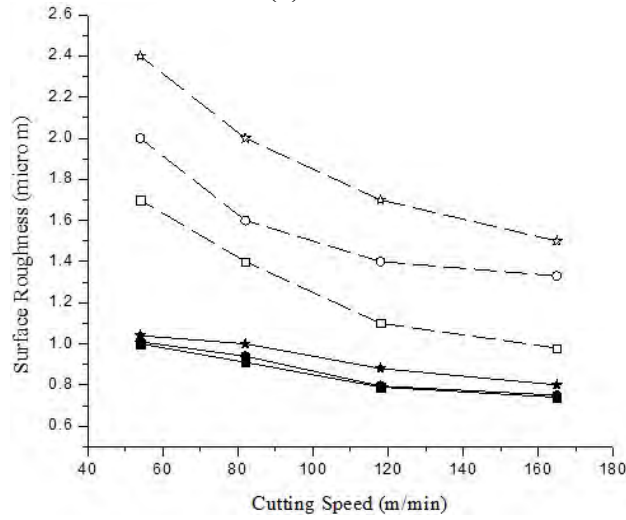
(b) 48 HRC

(c) 56 HRC
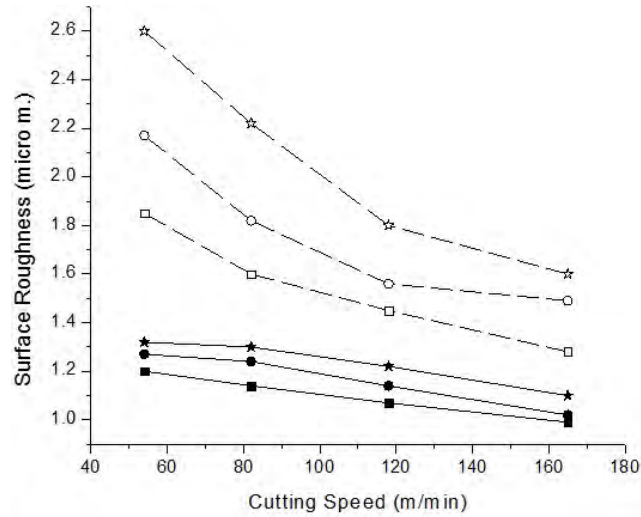
Fig.2.5 Variation of R with V and f under different cutting conditions at depth of cut 1.5 mm

The surface roughness attained after machining of the alloy steel of different hardness by the sharp inserts at stated speed-feed combinations under dry and HPC conditions are shown in Fig.2.5. Here, it is seen that there is a substantial reduction of surface roughness at all cutting speed-feed combination for HPC compared to the dry cutting condition.

2.3.4 Tool Wear

Tool wear describes the gradual failure of cutting tools due to machining. Cutting tools often fail prematurely, randomly and catastrophically by mechanical breakage and plastic deformation under adverse machining conditions caused by intensive pressure and temperature and/or dynamic loading at the tool tips particularly if the tool material lacks strength and fracture toughness. Tool wear on the cutting edges is an important issue affecting process outputs such as tool deflections and surface roughness.

The growth of average flank wear (V_B) with progress of machining recorded while turning alloy steel of different hardness under both dry and HPC conditions is shown in Fig.2.6. Fig. 2.7 shows the variation of tool wear with the change of cutting speed at different feed rate under HPC condition for different hardness level. In this case the tool wear was measured after 0.30 min of machining.
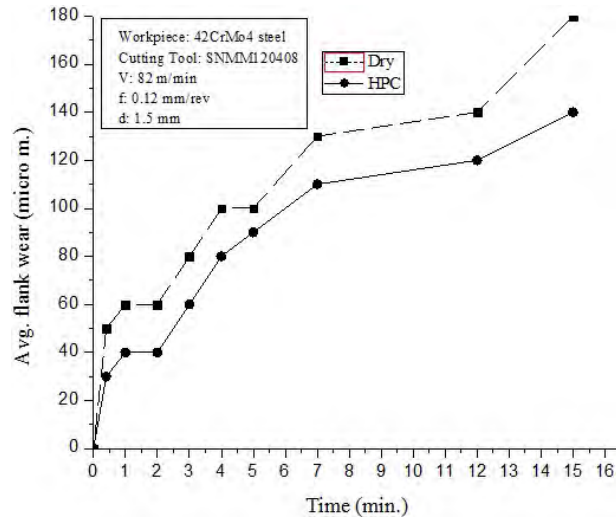
(a) 42 HRC
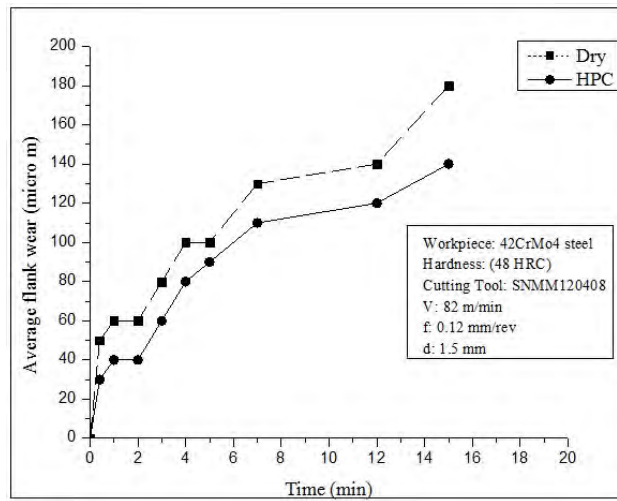
(b) 48 HRC
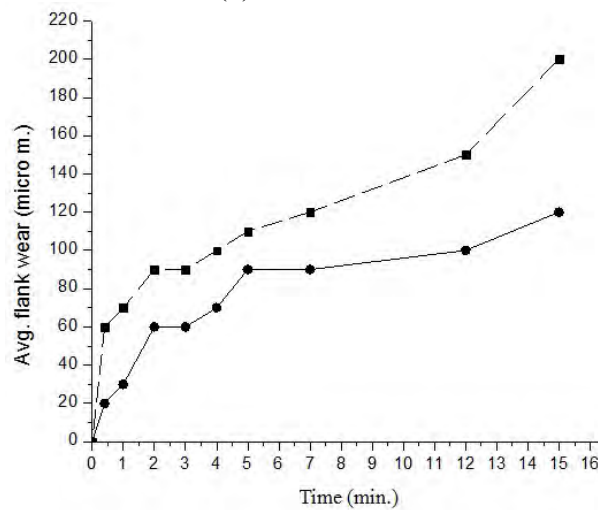
(c)56 HRC

Fig. 2.6 Growth of V_B under dry and HPC condition at different hardness
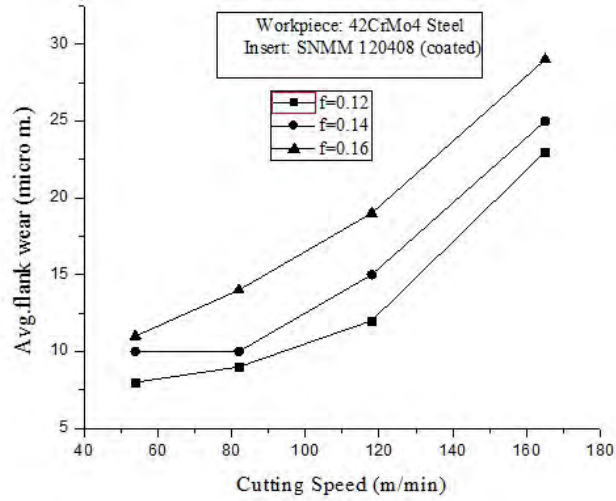
(a) 42 HRC
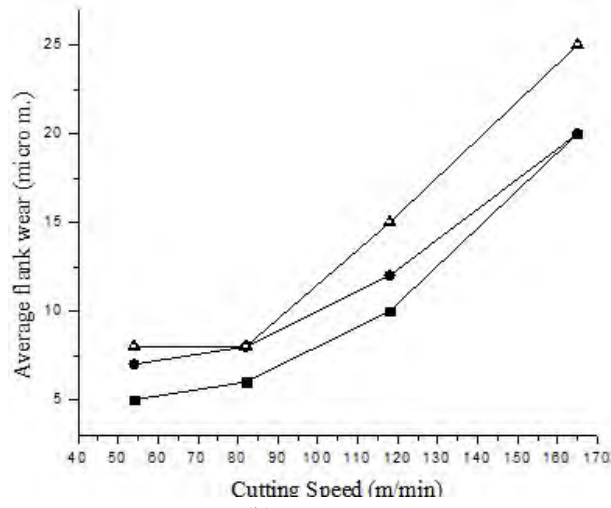
(b) 48 HRC
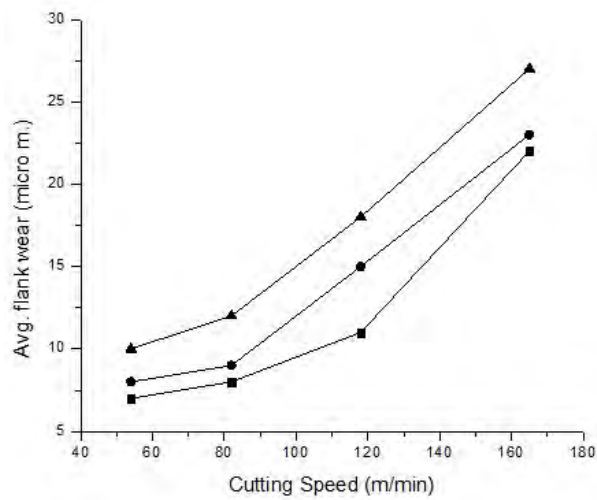
(c) 56 HRC

Fig. 2.7 Variation of V_B with V and f under HPC conditions at different hardness level

Chapter-3

EMPIRICAL MODELING OF MACHINING RESPONSES

3.1 Introduction

Choice of the process parameters that would produce an excellent surface quality with ensuring low tooling cost is the main challenges for today's manufacturers. Thus, there is a requirement of selection of the best combination of input parameters to generate the desired responses. Various empirical methods are available to define the output variables. Among these many types of research have been motivated to apply RSM for its capability of reducing a great number of experimental trials as compared to other approaches and developing the logical-mathematicalrelationship between input and output machining parameters. RSM was applied to the experimental data using the Design-Expert Software V7.0 to develop mathematical models relating the selected turning parameters-cutting speed and feed to each of the two output responses – cutting temperature, surface roughness and tool wear for HPC cutting condition. The adequacies of the models developed and their significant terms were measured by analyzing variance and other adequacy measures. Finally, these mathematical models were used to determine the optimal setting of turning parameters is discussed in the next chapter.

RSM is a collection of mathematical and statistical techniques that are useful for modeling and analyzing engineering problems [**Montgomery, 2005**]. In this technique, the main objective is to optimize a response (output variable) which is influenced by several independent variables (input variables). An experiment is a series of tests, called runs, in which changes are made in the input variables in order to identify the reasons for changes in the output response.The method was introduced by George E. P. Box and K. B. Wilson in 1951 [**Wikipidea, 2017**]. The main idea of RSM is to use a sequence of designed

experiments to obtain an optimal response. Box and Wilson suggest using a second-degree polynomial model to do this. Originally, RSM was developed to model experimental responses and then migrated into the modeling of numerical experiments. The difference is in the type of error generated by the response. The mathematical model of response surface can be expressed by,

$$Y = f(\psi_1, \psi_2, \ldots\ldots\ldots, \psi_k) + \varepsilon \tag{3.1}$$

where Y is the response of the system, f is the true response function whose form is unknown, ψ is the variable of action called factor, k is the number of independent variables and ε is the error which is normally distributed about the dependent variables. In order to optimize the response Y, it is therefore essential to find a suitable approximation for the true functional relationship between the independent variables and the response surface.

The mathematical model used in RSM is typically a first or second order polynomial model. The first-order model is likely to be appropriate when the experimenter is interested in approximating the true response surface over a relatively small region of the independent variable space in a location where there is little curvature in function. It includes only the main effects of the variables. The form of the first-order model is Eq. 3.2. If there is an interaction between these variables, it can be added to the model as Eq. 3.3.

$$Y = b_0 + \sum_{i=1}^{k} b_i x_i + \varepsilon \tag{3.2}$$

$$Y = b_0 + \sum_{i=1}^{k} b_i x_i + \sum_{i<j} \sum_{j=2}^{k} b_{ii} x_i x_j + \varepsilon \tag{3.3}$$

Often the curvature in the true response surface is strong enough that the first-order model (including the interaction) is inadequate. A second-order model will likely be required in these situations. The general second-order model is as Eq. 3.4.

$$Y = b_0 + \sum_{i=1}^{k} b_i x_i + \sum_{i=1}^{k} b_{ii} x_i^2 + \sum_{i<j} \sum_{j=2}^{k} b_{ii} x_i x_j + \varepsilon \tag{3.4}$$

where, $b_{ij} = 0, 1, \ldots\ldots k$ are called the regression coefficients.

3.2 Mathematical Model Development

RSM was applied to the experimental data using the Design-Expert Software V7.0. Experiments were performed considering two-factor three-level design matrix. The selected turning input variables are cutting speed (A), feed (B), and workpiece hardness (C) for HPC cutting environment. The measured results of cutting temperature (T), surface roughness (R) and tool wear (V_B) from each run were inserted into the Design-Expert Software.

At this stage, the fit summary is used to select the models that best describe the response factors. The fit summary includes the sequential model sum of squares to select the highest order polynomials and the model is not aliased. In addition model summary statistics of the fit summary focuses on the model that maximizes adjusted R^2 and predicted R^2 values. The ANOVA for both response model is carried out using the same software package to check if the regression model is significant and to find out the significant model terms of the developed models as well.

Model fit summary output of the measured responses shown in Table 3.1,Table 3.2 and Table 3.3. The quadratic model is the recommended for all of the responses as Prob > F is less than 0.05 and RSM selects the highest order polynomial where the additional terms are significant and the model is not aliased.Therefore, it is evident that quadratic model is shown in Eq. 3.4 is statistically fitted to the experimental data to obtain the regression equations for all responses and can be used for further analysis.

Table 3.1 Sequential model sum of squares for cutting temperature

Source	Sum of Squares	df	Mean Square	F Value	p-value > F	Remark
Mean vs Total	1.180E+006	1	1.180E+006			
Linear vs Mean	1.239E+005	3	41310.57	50.91	< 0.0001	
2FI vs Linear	15677.61	3	5225.87	14.73	< 0.0001	
Quadratic vs 2FI	3845.92	3	1281.97	5.17	0.0062	Suggested
Cubic vs Quadratic	5316.74	8	664.59	10.62	< 0.0001	Aliased
Residual	1126.77	18	62.60			
Total	1.330E+006	36	36955.03			

Table 3.2 Sequential model sum of squares for surface roughness

Source	Sum of Squares	df	Mean Square	F Value	p-value > F	Remark
Mean vs Total	34.04	1	34.04			
Linear vs Mean	0.97	3	0.32	91.10	< 0.0001	
2FI vs Linear	4.034E-003	3	1.345E-003	0.35	0.7860	
Quadratic vs 2FI	0.093	3	0.031	46.65	< 0.0001	Suggested
Cubic vs Quadratic	0.014	8	1.791E-003	11.14	< 0.0001	Aliased
Residual	2.892E-003	18	1.607E-004			
Total	35.12	36	0.98			

Table 3.3 Sequential model sum of squares for tool wear

Source	Sum of Squares	df	Mean Square	F Value	p-value > F	Remark
Mean vs Total	6916.69	1	6916.69			
Linear vs Mean	1410.36	3	470.12	88.52	< 0.0001	
2FI vs Linear	6.41	3	2.14	0.38	0.7689	
Quadratic vs 2FI	145.12	3	48.37	68.31	< 0.0001	Suggested
Cubic vs Quadratic	9.46	8	1.18	2.38	0.0605	Aliased
Residual	8.95	18	0.50			
Total	8497.00	36	236.03			

The ANOVA of each response surface models is tabulated in the table. Model terms were evaluated by the F probability value with 95% confidence level. The P values were used to check the significance of each coefficient. The Tables 3.4, 3.5and 3.6demonstrates that calculated Fisher's "Model F" and "Model P" values, are, respectively 64.32 and <0.0001 for temperature model, 179.50 and <0.0001 for surface roughness model and 245.07 and <0.0001 for tool wear respectively. These F and P values of all models imply that the selected models are highly significant and there is only 0.01% chance these F values could occur due to noise. The associated P values of less than 0.05 for the models indicate that the models are statistically significant.

The same ANOVA tables show the other adequacy measures e.g., R^2, adjusted R^2 and predicted R^2 values. All these are in logical agreement and indicate significant relationships. The R^2 value is high, close to 1, which is desirable for all models (0.9570, 0.9842 and 0.9883). This gives the proportion of the total deviation in the predicted response. Considering the determination coefficient adj. R^2 is 94.21% for cutting

temperature, 97.87% for surface roughness and 98.43% for tool wear which demonstrate that the modelsare well fitted. Moreover, adequate precision compares a range of predicted values at the design points to average prediction error. Ratios greater than 4 are desirable. In case of cutting temperature the value is 31.963, for roughness, it is 48.296and for tool wear this value is 54.004which are well above 4. This indicates adequate signals to use the models to navigate the design space.

Table 3.4ANOVA table for cutting temperature quadratic model

Source	Sum of Squares	df	Mean Square	F Value	p-value > F	Remark
Model	1.435E+005	9	15939.47	64.32	< 0.0001	significant
A (m/min)	82986.52	1	82986.52	334.86	< 0.0001	
B (mm/rev)	28446.53	1	28446.53	114.78	< 0.0001	
C (HRC)	17221.07	1	17221.07	69.49	< 0.0001	
AB	7441.45	1	7441.45	30.03	< 0.0001	
AC	7050.69	1	7050.69	28.45	< 0.0001	
BC	1185.47	1	1185.47	4.78	0.0379	
A^2	2841.16	1	2841.16	11.46	0.0023	
B^2	242.00	1	242.00	0.98	0.3322	
C^2	762.76	1	762.76	3.08	0.0911	
Residual	6443.50	26	247.83			
Cor Total	1.499E+005	35				
$R^2 = 0.9570$ Adjusted $R^2= 0.9421$ Predicted $R^2=0.8974$ Adequate Precision= 31.963						

Table 3.5ANOVA table for surface roughness quadratic model

Source	Sum of Squares	df	Mean Square	F Value	p-value > F	Remark
Model	1.07	9	0.12	179.50	< 0.0001	Significant
A (m/min)	0.30	1	0.30	449.22	< 0.0001	
B (mm/rev)	0.057	1	0.057	85.60	< 0.0001	
C (HRC)	0.69	1	0.69	1034.83	< 0.0001	
AB	7.712E-006	1	7.712E-006	0.012	0.9149	
AC	6.190E-004	1	6.190E-004	0.93	0.3425	
BC	3.407E-003	1	3.407E-003	5.15	0.0318	
A^2	4.508E-003	1	4.508E-003	6.81	0.0149	
B^2	8.681E-004	1	8.681E-004	1.31	0.2627	
C^2	0.087	1	0.087	131.84	< 0.0001	
Residual	0.017	26	6.622E-004			
Cor Total	1.09	35				
$R^2 = 0.9842$Adjusted $R^2= 0.9787$ Predicted $R^2=0.9693$Adequate Precision= 48.296						

Table 3.6ANOVA table for the tool wear quadratic model

Source	Sum of Squares	df	Mean Square	F Value	p-value > F	Remark
Model	1561.89	9	173.54	245.07	< 0.0001	Significant
A (m/min)	1173.33	1	1173.33	1656.91	< 0.0001	
B (mm/rev)	122.31	1	122.31	172.72	< 0.0001	
C (HRC)	0.92	1	0.92	1.29	0.2660	
AB	6.25	1	6.25	8.83	0.0063	
AC	0.012	1	0.012	0.017	0.8969	
BC	0.14	1	0.14	0.20	0.6556	
A^2	76.82	1	76.82	108.48	< 0.0001	
B^2	2.35	1	2.35	3.31	0.0802	
C^2	65.95	1	65.95	93.13	< 0.0001	
Residual	18.41	26	0.71			
Cor Total	1580.31	35				
$R^2 = 0.9883$ Adjusted $R^2 = 0.9843$ Predicted $R^2 = 0.9793$ Adequate Precision= 54.004						

Now, considering the main effects of variables, from the ANOVA Table 3.4 it is clear that, the influence of cutting speed (A), feed (B), hardness (C) and the interactions AB, AC, BC and quadratic effect of A are the significant model terms associated with cutting temperature. The effect of A, B, and C, interaction of B and C and the quadratic effect A^2 and C^2 are important term for surface roughness (Table 3.5). On the other hand, A, B, AB, A^2, and C^2 are found as the significant terms for tool wear model (Table 3.6). The developed models are determined by Design-Expert software are given in the Eq. 3.5, 3.6 and 3.7.

a) Cutting temperature

$T = 509.89712 - 6.15569\ V - 7456.94323\ f + 9.56739H + 21.20010\ Vf + 0.058760\ VH + 61.27534\ fH + 0.00656844V^2 + 13750\ f^2 - 0.20412\ H^2$ (3.5)

b) Surface roughness

$R = 6.36089 - 0.00483776\ V - 9.90092\ f - 0.20853\ H - 0.000682491\ Vf + 0.00174104\ VH + 0.10389\ fH + 0.00000827377V^2 + 26.04167\ f^2 + 0.00218378\ H^2$ (3.6)

c) Tool wear

$V_B = 170.73322 - 0.17736\ V - 296.0739\ f - 5.86856\ H + 0.61454\ Vf - 0.0000770475VH - 0.67568\ fH + 0.00108008\ V^2 + 1354.16667\ f^2 + 0.06002\ H^2$ (3.7)

3.3   Statistical Validation of Developed Model

Normality of residual data, the pattern of error variance, the presence of outliers and amount of residuals in prediction are checked to ensure statistical validation of the developed models. The normality data is verified by plotting the normal probability plot of residuals. The residual is the difference between observed and predicted value obtained from the regression model. The data set is normally distributed if the points on the plot fall fairly close to the straight line. The normal probability plots of residual values for cutting temperature, surface roughness and tool wear are illustrated in Fig.3.1. The experimental points are reasonably aligned with predicted points suggesting the normality of data.

Fig.3.2 demonstrate studentized residuals versus predicted values for cutting temperature, surface roughness and tool wear. The residuals are found to be scattered randomly about zero. This indicates that errors have a constant variance for all response variables. The plot of studentized residuals versus predicted values also shows the possible existence of outliers. If a point lies far from the majority of points, it may be an outlier. It is important to identify the outlier as these can significantly influence the model and provide potentially misleading results. As shown in the Fig.3.2 all the points are within $\pm 3\sigma$ limits for each of the response models and confirm no existence of such outliers.

Fig.3.3 showing the relationships between the actual and predicted values of the three machining responses. These figures indicate that the developed models are adequate and predicted results are in good agreement with the measured data as the residuals are close to the diagonal line.

(a) Cutting temperature

(b) Surface roughness

(c) Tool wear

53
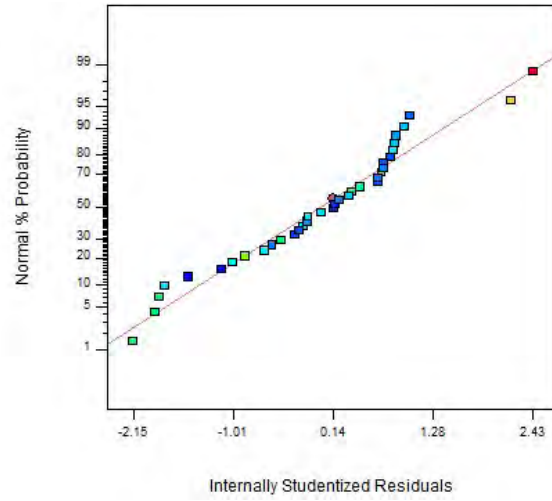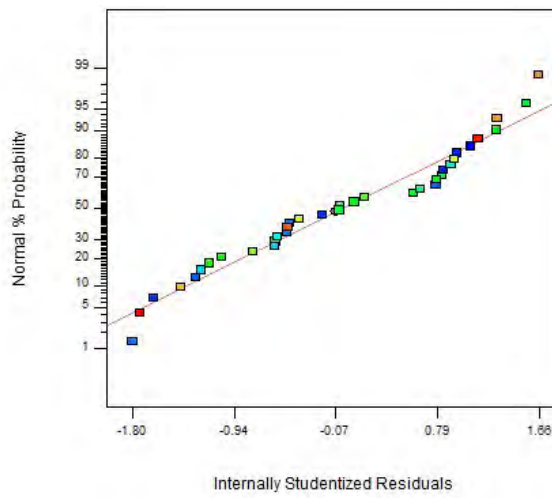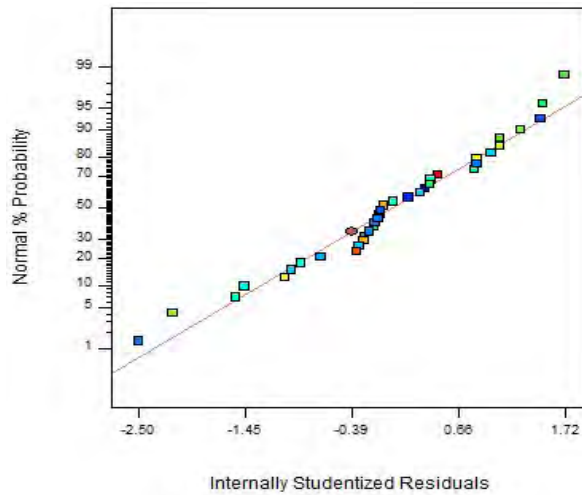
Fig. 3.1 Normal probability plot
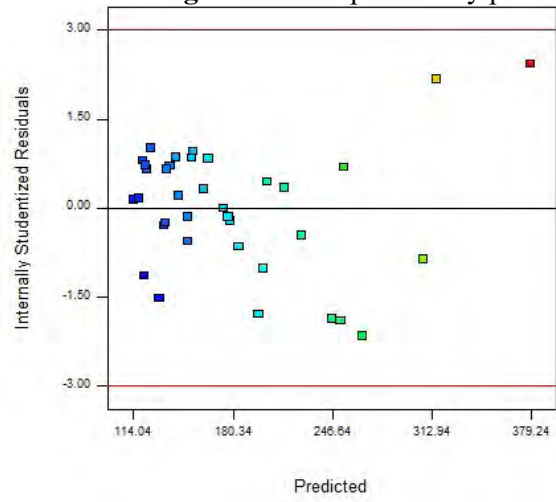
(a) Cutting temperature
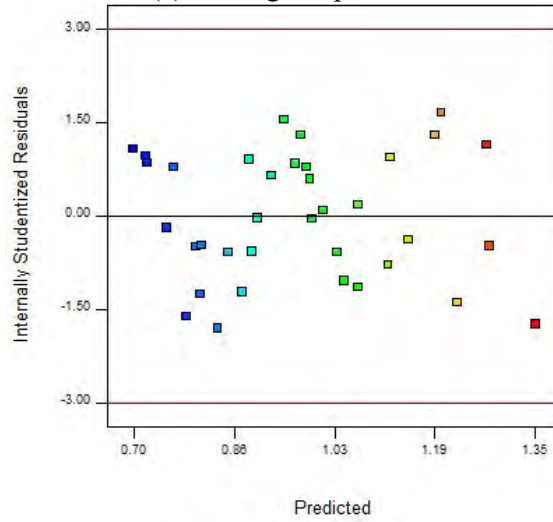
(b) Surface roughness
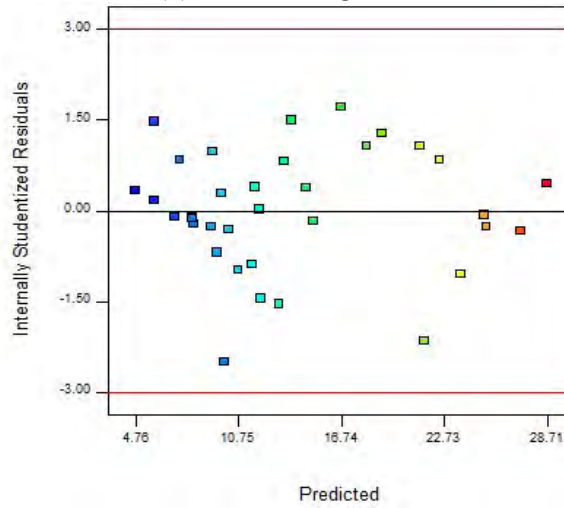
(c) Tool wear

Fig.3.2 Standardized residual vs. predicted plot
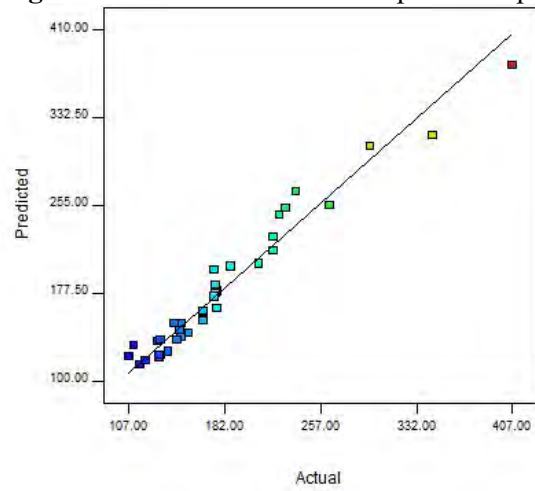
(a) Cutting temperature
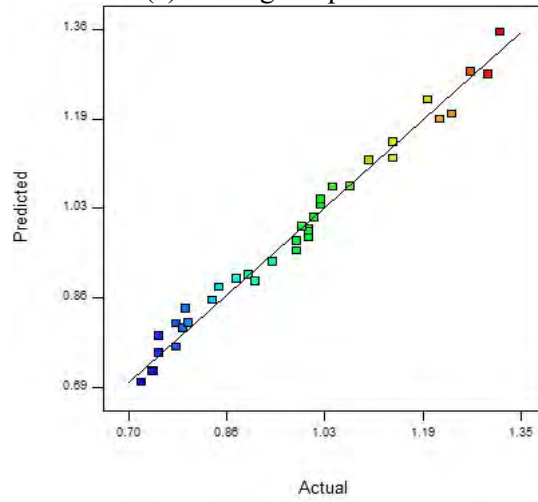
(b) Surface roughness
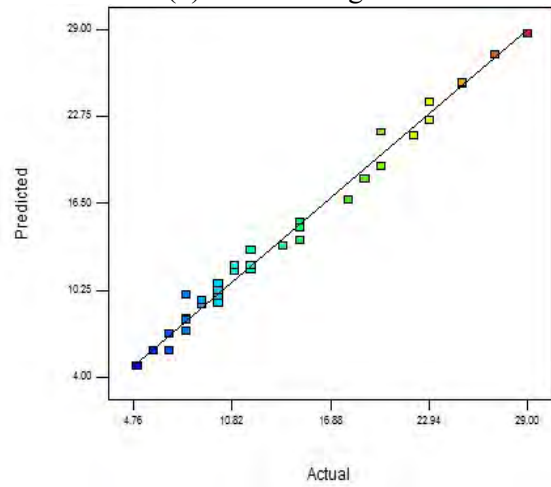
(c) Tool wear

Fig.3.3 Predicted vs. actual plot

Chapter-4

OPTIMIZATION OF MACHINING PARAMETERS

4.1   Introduction

Machining parameters have a major effect on the quantity and quality of the produced part and cost of production. The selected machining parameters should yield desired need while utilizing the machining resources such as machine tool and cutting tool to the fullest extent with considering the associated constraints on these resources. Hence, the optimization of the parameters is essential. The aim of the optimization is to improve an existing process that meets the given requirements and satisfies all the constraints placed on it. As one of the objectives of this study is to get optimum values of cutting speed and feed while minimizing cutting temperature, surface roughness and tool wear; it requires multiple objective optimization method. GA is a popular meta-heuristic algorithm that is particularly well-suited for this class of problems [**Konak et al., 2006**]. GAs are customized to adapt multi-objective problems by using specialized fitness functions and introducing methods to promote solution diversity. In addition, the behavior of GA is suitable for machining optimization problem that requires a robust search method which runs well in complex situations. Goldberg [**2001**] described that GAs are search algorithms based on the mechanics of natural selection and natural genetics. GA exploits the idea of the 'survival of the fittest' technique to produce a new generation of solutions which are hopefully better approximations to the ideal solution.

GAs are naturally suitable for solving maximization problems according to its 'survival-of-the-fittest' nature. However, minimization problems are also resolved by transforming into maximization problems through some suitable transformation. In

general, a fitness function $F(x)$ is first derived from the objective function $f(x)$ and used in successive genetic operations. For maximization problems, the fitness function can be considered to be the same as the objective function or $F(x) = f(x)$. While for a minimizationproblem, the fitness function is an equivalent maximization problem chosen such that optimum point remains unchanged. A number of such transformations are possible.The following function (Eq. 4.1) is often used for that purpose.This transformation does not alter the location of the maximum but converts a minimization problem to an equivalent maximization problem.

$$(4.1)$$

$$F(x) = \frac{1}{1 + f(x)}$$

The operation of GAs begins with an initial set of random string called 'initial population' which is made of a group of chromosomes. These chromosomes are evolved through a number of successive iterations to get an optimized solution. Each string is evaluated to find the fitness value. The population is then operated by three main operators- selection, crossover, and mutation. Individuals are selected according to their fitness for the production of offspring (selection operator). Parents are then recombined to produce offspring (crossover operator). All of these offspring are mutated with a certain probability (mutation operator). After that, the fitness of the offspring is then computed. The offspring are then inserted into the population replacing the parents, producing a new generation. The new population is further evaluated and tested for termination. This cycle is performed until the optimization criteria are met. The cycle is called generation. The general procedure GA is presented in Fig.4.1 [**Malhotra et al., 2011**].
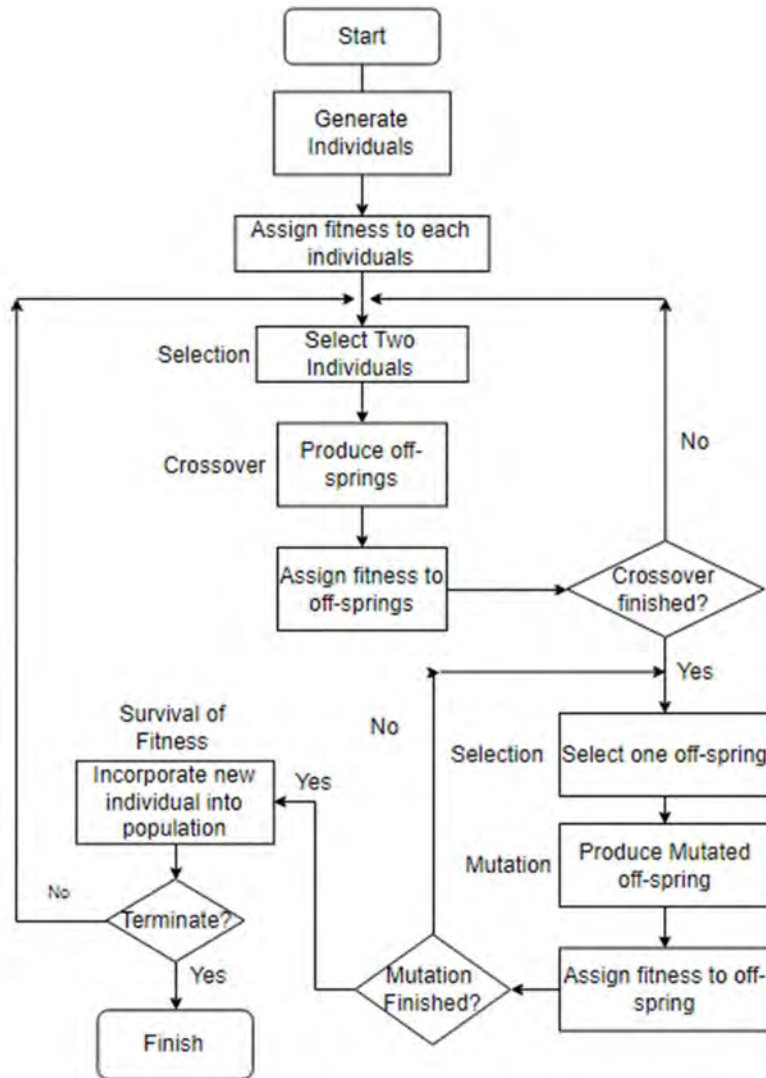
Fig.4.1 The general procedure of GA

Selection operator: Selection is the first operator in GA. It selects good strings in a population and forms a mating pool with a probability proportional to the fitness (F_i).Since the population size is usually kept fixed in a simple GA, the sum of the probability of the strings being selected for the mating pool must be 1. The probability for selecting the ith string is given in Eq. 4.2.

$$p_i = \frac{F_i}{\sum F_j} \tag{4.2}$$

where, i and $j$vary from 1 to n, n being the population size.

There are many selection mechanisms that have been proposed in the literature. Among thee, roulette wheel selection (RWS) and tournament selection (TS) are favorable to many researchers. One way to implement RWS is to imagine a roulette-wheel with its circumference marked for each string proportionate to the string's fitness. The wheel is spun n times, each time selecting an instance of the string chosen by the pointer. The higher fitness value with a bigger area of the roulette wheel has more chances of being chosen. The advantage of RWS is that it gives no bias with the unlimited spread. However, it cannot handle negative fitness values and a minimization problem directly [**Pencheva et al. 2009**]. On the other hand, TS has the ability to handle either minimization or maximization problems and minimize the early convergence of the algorithm. In addition, the negative value is allowed without any restriction [**Wahde, 2008**]. TS involves running several tournaments among a few individuals at random. In each tournament, the winner (one with the best fitness) is selected for crossover. If the tournament size is larger, weak individuals have a smaller chance to be selected because if a weak individual is selected to be in a tournament, there is a higher probability that a stronger individual is also in that tournament.

Crossover operator: In the crossover operator, new strings are created by exchanging information among strings of the mating pool. In most of the crossover operators, two strings are picked from the mating pool at random and some portions of the strings are exchanged between the strings. The crossover operator is divided in many ways such as single point, two-point, uniform, arithmetic etc. Due to the ability to operate on any chromosome representation, single-point and two-point crossover are commonly used. The crossover process is shown as following:
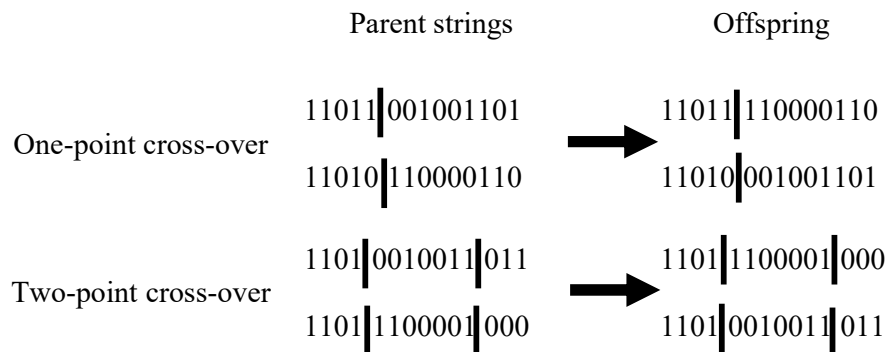
The vertical line indicates the chosen crossover point. If good strings are created by crossover there will be more copy of them in the next mating pool generated by reproduction operator. But if good strings are not created by crossover, they will not survive too long. Thus, crossover operator is not applied to all parents but it is applied with probability (p_c) which is normally set equal to 0.6 to 0.95 [**Cao and Wu, 1999**].

Mutation operator: Mutation is a genetic operator used to maintain genetic diversity from one generation of a population of genetic algorithm chromosomes to the next. Mutation provides diversity in the population and enables the genetic algorithm to search a broader space. The mutation operator randomly changes 1 to 0 and vise-versa with a small mutation probability (pm). The probability of applying the mutation operator is low, normally 0.001 and 0.01 [**Cao and Wu, 1999**]. With non-binary representations, mutation is achieved by either perturbing the gene values or random selection of new values within the allowed range. For the constrained associated problem, the 'adaptive feasible' type of mutation is used. In case of this function, randomly generates directions that are adaptive with respect to the last successful or unsuccessful generation. The mutation chooses a direction and steps length that satisfies bounds and linear constraints.

The multiobjective GA (MOGA) works on a population using a set of operators. A general multi-objective design problem could be expressed by Eq. 4.3.

$$\min F(x) = (f_1(x), f_2(x), \ldots\ldots, f_k(x))$$
$$s.t. x \epsilon S \quad \quad (4.3)$$
$$x = (x_1, x_2, \ldots, x_n)$$

where, $f_1(x), f_2(x), \ldots, f_k(x)$ are the k objectives functions, $x_1, x_2, \ldots, x_n$ are the n optimization parameters, and $S \epsilon R^n$ is the solution or parameter space.

A Pareto optimal set is a set of solutions that are non-dominated with respect to each other. While moving from one Pareto solution to another, there is always a certain amount of sacrifice in one objective to achieve a certain amount of gain in the other. The ultimate goal of a multi-objective optimization algorithm is to identify solutions in the Pareto optimal set. The space in R^k formed by the objective vectors of Pareto optimal solutions is known as the Pareto optimal front. The non-dominated rank (fitness value) is

used to compute the next generation from the randomly generated initial population. A non-dominated rank is assigned to each individual using the relative fitness. Considering a minimization problem and two solution vectors x, yϵS. x is said dominates y, ('x' has a lower rank than 'y') if 'x' is strictly better than 'y' in at least one objective and 'x' is no worse than 'y' in all objectives. This is same as saying 'y' is dominated by 'x'. 'x' and 'y' are considered to have equal ranks if neither dominates the other. The distance measure of an individual is used to compare individuals with equal rank. It is a measure of how far an individual is from the other individuals with the same rank.

The MOGA function uses a controlled elitist genetic algorithm. An elitist GA always favors individuals with better fitness value whereas, a controlled elitist GA also favors individuals that can help increase the diversity of the population even if they have a lower fitness value. It is very important to maintain the diversity of population for convergence to an optimal Pareto front. This is done by controlling the elite members of the population as the algorithm progresses. Two options 'ParetoFraction' and 'DistanceFcn' are used to control the elitism. The Pareto fraction option limits the number of individuals on the Pareto front and the distance function helps to maintain diversity on a front by favoring individuals that are relatively far away on the front.

Various performance metrics are reported for MOGA. In this work, two different measures such as average distance or spacing (S) and spread (Δ) are used for numerical comparison of the non-dominated fronts. S and Δ are used to evaluate the spread of the obtained non-dominated solutions. An algorithm finding a set of solutions having smaller spacing S and Δ is able to find a better diverse set of non-dominated solutions.

4.2   Formulation of the Optimization Problem

The optimization was performed with an objective of minimization. In the constructed optimization problem, two decision variables are considered: cutting speed, X(1) and feed, X(2) and workpiece hardness, X(3). The problem of the optimization of cutting parameters are formulated by defining the goal function as the minimum cutting temperature f(1), minimum surface roughness f(2) and minimum tool wear f(3). The empirical models obtained for cutting temperature, surface roughness and tool wear are considered in the formulation of the objective function given in the following.

Min f(1) = 509.89712 - 6.15569 $X(1)$ - 7456.94323 $X(2)$+ 9.56739$X(3)$+ 21.20010
$X(1)X(2)$+ 0.058760 $X(1)X(3)$+ 61.27534 $X(2)X(3)$ + 0.00656844 $X(1)^2$+
13750 $X(2)^2$- 0.20412 $X(3)^2$

(4.4)

Min f(2) =6.36089 - 0.00483776$X(1)$ - 9.90092$X(2)$- 0.20853 $X(3)$ - 0.000682491
$X(1)X(2)$+ 0.00174104 $X(1)X(3)$+ 0.10389 $X(2)X(3)$ + 0.00000827377$X(1)^2$+
26.04167 $X(2)^2$+ 0.00218378 $X(3)^2$ (4.5)

Min f(3) = 170.73322 - 0.17736 $X(1)$ - 296.0739 $X(2)$- 5.86856 $X(3)$+ 0.61454 $X(1)X(2)$-
0.0000770475$X(1)X(3)$ - 0.67568 $X(2)X(3)$+ 0.00108008 $X(1)^2$+ 1354.16667
$X(2)^2$+ 0.06002 $X(3)^2$ (4.6)

The following speed, feed, andworkpiece hardness limitations are considered as physical constraints in the formulation of the objective model. Due to the limitations of the machine and cutting tool and due to the safety of machining, the cutting parameters are limited to the upper and lower allowable limit. The allowable range of cutting conditions are:

$$V_{min} \leq V \leq V_{max}$$

$$f_{min} \leq f \leq f_{max}$$

$$H_{min} \leq H \leq H_{max}$$

A lower bound [54, 0.12, 42] and an upper bound [165, 0.16, 56] was used for three variables respectively cutting speed, feed and workpiece hardness. To optimize the multi-objectives of Eq. 4.4, 4.5 and 4.6 GA toolbox of MATLAB was utilized. The MOGA function 'gamultiobj' was used from the toolbox. Table 4.1 exhibits the GA parameters selected in the toolbox for optimization.

Double vector type population was selected for this problem as this the mixed integer program. The 'two-point' crossover was chosen for reproduction of the next generation. The type of mutation chosen for the GA algorithm implementation was 'adaptive feasible' mutation. Crossover or mutation was performed to the parent individuals, with the chosen crossover rate of 0.8. The selection of individuals for mating was done using the tournament selection. For other parameters, the suggested default

values of the software were used. The default distance measure function 'distancecrowding'provided in the toolbox takes an optional argument to calculate distance either in function space or design space whereas the default choice is diversity will be happened based on the function space. The Pareto fraction has a default value of 0.35 i.e., the solver will try to limit the number of individuals in the current population that are on the Pareto front to 35% of the population size.'gamultiobj' uses three different criteria to determine when to stop the solver. The solver stops when any one of the stopping criteria is met. It stops when the maximum number of generations is reached; by default, the number is '100*numberOfVariables'.'gamultiobj' also stops if the average change in the spread of the Pareto front over the 'MaxStallGenerations' generations (default is 100) is less than tolerance specified in options 'FunctionTolerance'(default is 1e-4). The third criterion is the maximum time limit in seconds (default is Infinite).

Table 4.1 Selected GA parameters for multi-objective optimization

GA parameters	Selected option
Population Type	Double Vector
Population Size	50
Selection Function	Tournament
Tournament Size	10
Crossover Function	Two-point
Crossover Fraction	0.8
Mutation Function	Adaptive feasible
Distance measure Function	'distancecrowding'
Pareto front Population Fraction	0.35

4.3   Optimization Results

Optimal results were obtained after 204 iterations. The necessary time for solving was approximately 40 seconds. Population size, tournament size, and crossover function have been changed several time but, the same or much-closed results have been obtained. Table 4.2 presents the final 15 generations obtained with the end of the optimization process ranked by X(1) values from lowest to the highest order.

In Fig.4.2, the obtained non-dominated points were plotted to form the Pareto front, which is subject to minimization.Fig.4.3 indicates the average distance measure of each individual from its neighbors. It shows that the solutions are nearly spaced and the

corresponding distance measure is 0.02 which is small as desired. Fig.4.4 displays the average Pareto spread plot showing the change in distance measure level of individuals with respect to the previous. The average value of spread is 0.07413 which is small as well ensures the diversity of searching results.

Table 4.2 GA optimal cutting parameters resulted after optimization process

No. of generation	X(1)	X(2)	X(3)	f(1)	f(2)	f(3)
1.	54	0.12	50	131.65	1.00	4.61
2.	55	0.12	51	130.93	1.04	4.79
3.	56	0.12	42	120.18	0.96	8.10
4.	56	0.13	42	117.34	0.97	8.90
5.	68	0.12	45	126.76	0.91	5.99
6.	91	0.12	43	117.43	0.85	9.34
7.	118	0.12	44	133.30	0.77	11.52
8.	118	0.12	43	124.73	0.78	12.56
9.	127	0.12	49	165.39	0.81	10.97
10.	146	0.12	49	183.19	0.76	14.57
11.	147	0.12	47	176.29	0.74	15.02
12.	150	0.12	45	164.63	0.71	16.81
13.	150	0.12	43	149.57	0.71	18.12
14.	151	0.12	44	159.48	0.71	17.37
15.	152	0.12	42	144.95	0.72	19.06
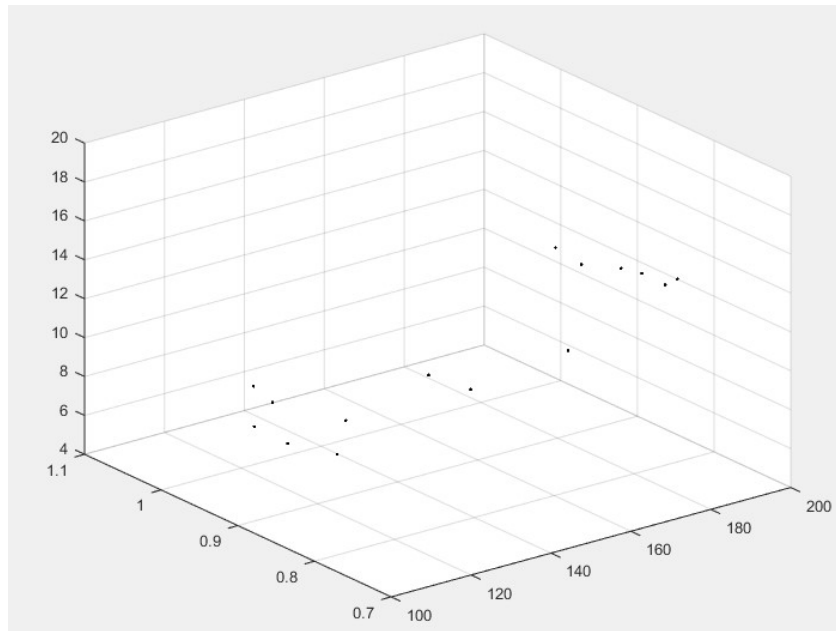
Fig.4.2 Pareto Front
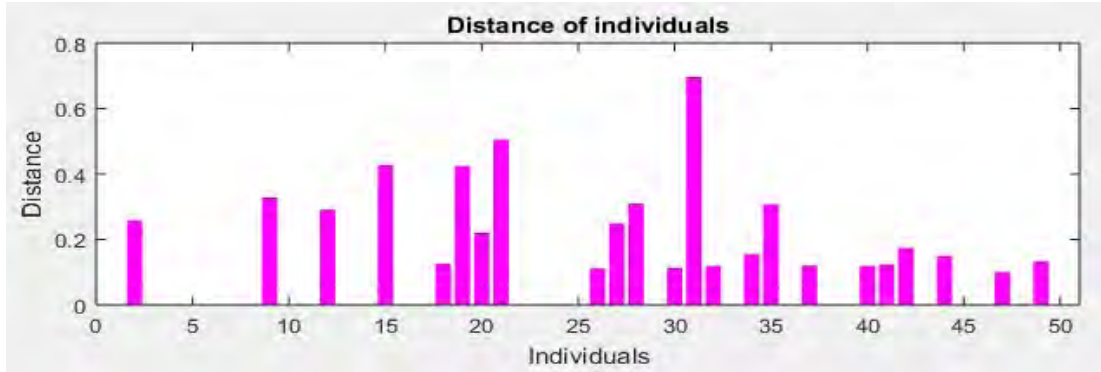
Fig.4.3 Average Pareto distance plot
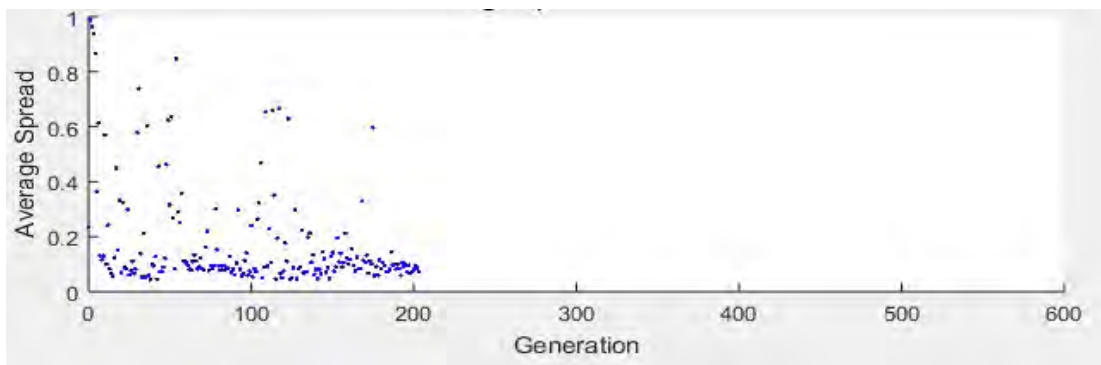
Fig.4.4 Average Pareto spread plot

4.4 Validation Experiments

From the Pareto-optimal solution set, three runs were chosen randomly to verify the prediction of response variables. Validation experiments revealed a superior agreement with the predicted values of responses with an error less than 10% (Table 4.3).

Table 4.3 Validation experiment result based on optimization

Optimal Values	Predicted			Measured			Error (%)		
	T (°C)	R (μm)	V_B (μm)	T (°C)	R (μm)	V_B (μm)	T	R	V_B
56 m/min, 0.13 mm/rev, 42 HRC	117.34	0.97	8.90	113	1	9	3.84	3.0	1.11
56 m/min, 0.12mm/rev, 42 HRC	120.18	0.96	8.10	111	0.96	8	8.27	0.0	1.25
152 m/min, 0.12 mm/rev, 42 HRC	144.95	0.72	19.06	148	0.74	20	2.06	2.7	4.7

Chapter-5

FINITE ELEMENT MODELING OF RESIDUAL STRESS

5.1   Introduction

Finite element analysis is a powerful numerical modeling approach that can provide valuable insight into the behavior of metal cutting processes. In recent years, finite element analysis has become the main tool for simulating of metal cutting processes and a lot of research activities were done in simulating both the cutting process and the machine tool. Various outputs and characteristics of the metal cutting processes such as cutting forces, stresses, temperatures, chip shape, etc. can be predicted by using FEM without any experimental investigation.The choice of finite element software for machining analysis is an important factor in determining the quality and scope of analysis that can be performed. Three of the most common software for FEM analysis machining are presented and well described by Gardner et al.[2005]: DEFORM, ABAQUS, and AdventEdge.

If a quick, easy to setup machining simulation is needed, then the preferable software packages are DEFORM and AdventEdge. These packages allow quick setup of simulations and have built in modules to specify material properties, tool and workpiece geometries and process parameters. Between these two packages, DEFORM offers more control over the simulation process while AdventEdge is easier to setup. However, in order to perform detailed simulations where different solver mechanisms need to be used and precise control is needed over the mesh and the boundary conditions, then the favored software package is ABAQUS. Though, ABAQUS does not have any material models but materials can be defined in with a lot of detail. Hence, the user has to define the tool and the workpiece, the process parameters and the simulation controls. Simulations are

structured in ABAQUS by using keywords that define the functioning of the simulation. The user is free to model the machining operation, thus providing a good deal of control over the simulation. The user also has very fine control over the meshing and the element types used in the model. As for disadvantages, it takes a lot of time to arrange the simulations as the user has to manually set many of the simulation parameters.
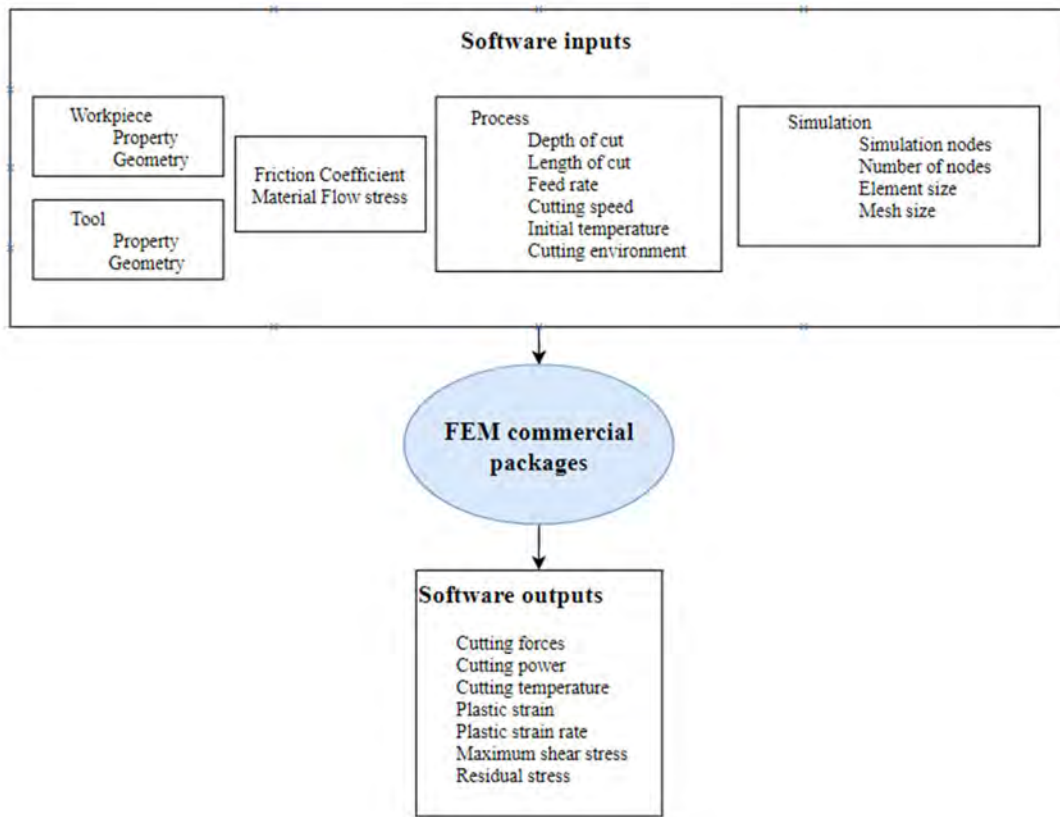
Fig.5.1 Typical FEM machining software inputs and outputs

FEM software demands several input values to predict the thermo-mechanical behavior of the machining operation. The inputs can be geometric like tool rake angle, cutting edge radius, etc. Cutting parameters like cutting speed, feed rate or depth of cut are also crucial as an input in the software. The number of nodes and the mesh also have weight in the FEM results in Abaqus. Typical FEM machining software inputs and outputs are showed in Fig.5.1.

The FE model formulations are based on either implicit or explicit schemes. When the dependent variables are defined by coupled sets of equations, and matrix or iterative

technique is required, the numerical method is said to be implicit. Even though this scheme provides better accuracy, this encounters a higher level of complexity in metal cutting while dealing with discontinuous chip formation and critical conditions. On the other hand, explicit scheme solves uncoupled equation system based on known quantities from previous steps. This type of scheme is able to handle the problems involving high non-linearity complex friction-contact metal cutting conditions.

There are two common classical approaches for numerical modeling used in FEM; namely Lagrangian and Eulerian. In addition, there are two more formulations based on the former methods combining the basic advantages of the classical approaches; the updated Lagrangian formulation and theALE formulation.

> **Lagrangian formulation:** In the Lagrangian formulation the mesh moves with the material which allows simulating chip formation without defining initial chip shape from incipient to the steady state. It gives more realistic results as a prediction of chip geometry, compute the stress and strain incrementally, and update the nodal coordinates at the end of each step increment. Although many advantages are related to the use of Lagrangian method, by this method the severe plastic deformation taking in the material cause extreme element distortion.

> **Eulerian Formulation:** In the Eulerian formulation the mesh is fixed in space and the material moves with respect to the grid. Allowing steady state machining to be simulated, it requires fewer element for the analysis, and thereby computing time is reduced. The model does not need to define chip separation criterion but it is required to define the chip geometry, chip thickness and the chip-tool contact length prior to the simulation. This requirement limits the investigation of machining chip formation.

> **Updated Lagrangian Formulation:** In the attempt of overcoming the drawbacks of the classical Lagrangian formulation, an updated Lagrangian formulation was developed. In this approach, the element distortion problem is solved by the mesh adaptivity and automatic remeshing technique. The element local coordinates of the FE mesh and local reference frame are continuously updated. It is therefore suitable when large deformations are

employed. The main shortcomings of this formulation are the limited benefit from continuous remeshing and mesh adaption and at alot of expense in computation time.

➢ **ALE Formulation:** The ALE method is more suitable than the updated Lagrangian method in the context of stability and accuracy. In the attempt of combining the best features of the Lagrangian and the Eulerian description an approach known as ALE is first adopted by Donea etal. [**1977**] in finiteelement context. In this approach, the mesh is allowed to move in an arbitrarily specified way. For an explanatory demonstration of the differences between Eulerian, Lagrangian and ALE descriptions are shown in Fig.5.2.

(a) $t = t_0$

(b) $t > t_0$
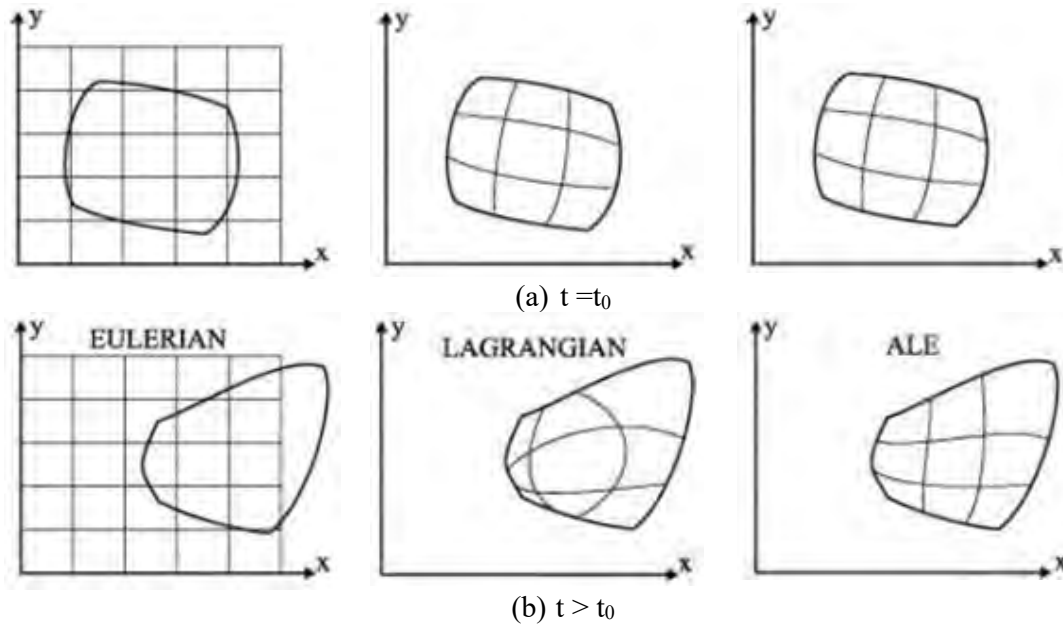
Fig.5.2 Demonstration of the Eulerian, Lagrangian and ALE formulations [**Proudian, 2012**]

ALE relocates the positions of the nodes according to the applied mesh smoothing method. One of the most common element smoothing method is referred to volume smoothing (supported where every node is surrounded by four elements in 2D). The new position of a node is determined by a volume weighted average of the centers of the elements adjacent to the node of interest. For example, in Fig.5.3 the new position of node M is determined by a volume-weighted average of the positions of the element centers, C of the four surrounding elements. The volume weighting will tend to push the node away

from element center C1 and toward element center C3, thus reducing element distortion. Due to this method of ALE, the material is free to flow underneath the mesh. This unique characteristic of ALE differs itself from traditional remeshing and makes it very suitable for simulating problems with metal cutting. The frequency of adaptive meshing is the parameter that mostly affects the mesh quality and the computational efficiency of adaptive meshing. In an adaptive meshing increment, thesoftware creates a new smoother mesh by sweeping iteratively over the adaptive mesh domain. During each sweep, nodes are adjusted slightly to reduce element distortion.
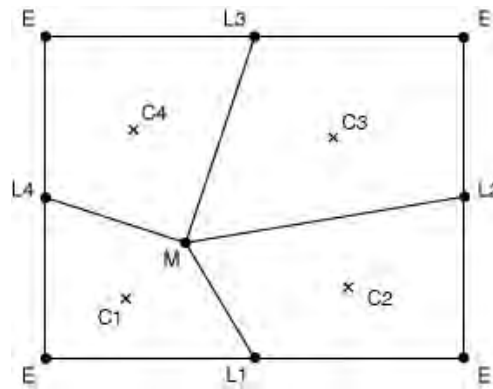
Fig.5.3 Volume smoothing method [**ABAQUS Analysis User's Manual, 2014**]

A fully coupled thermal stress analysis is used in the present study. This analysis is necessary when the stress is dependent on the temperature distribution and temperature distribution depends on stress solution. In Abaqus/Explicit heat transfer equation are integrated using the explicit forward difference time integration rule expressed by Eq. 5.1.

$$\theta^N_{(i+1)} = \theta^N_{(i)} + \Delta t_{(i+1)} \dot{\theta}^N_{(i)} \tag{5.1}$$

where, θ^N is the temperature at node N and the subscript i refers to the increment number in an explicit step. The values of $\dot{\theta}^N_{(i)}$ are computed at the beginning of the increment by Eq. 5.2.

$$\dot{\theta}^N_{(i)} = (C^{NJ})^{-1}(P^J_i - F^j_i) \tag{5.2}$$

where, C^{NJ} is the lumped capacitance matrix, P^J is the applied nodal source vector, and F^J is the internal flux vector. The forward-difference integration is explicit in the

sense that no equations need to be solved when a lumped capacitance matrix is used. The current temperatures are obtained using known values of $\dot{\theta}_{(i)}^N$ from the previous increment.

The mechanical problem is formulated in terms of nodal accelerations and explicitly advances the kinematic state of the system from the previous time step without iteration. The motion for the body is integrated using the explicit central-difference integration ruleexpressed by the following Eq. 5.3.

$$
\left.
\begin{aligned}
\dot{U}_{(i+1/2)}^N &= \dot{U}_{(i-1/2)}^N + \frac{\Delta t_{(i+1)} + \Delta t_{(i)}}{2} \ddot{U}_{(i)}^N \\
U_{(i+1)}^N &= U_{(i)}^N + \Delta t_{(i+1)} \dot{U}_{(i+1/2)}^N
\end{aligned}
\right\}
\tag{5.3}
$$

where, U^N is a degree of freedom (a displacement) and the subscript i refers to the increment number in an explicit dynamics step. The central-difference integration operator is explicit in the sense that the kinematic state is advanced using known values of $\dot{U}_{(i-1/2)}^N$ and $\ddot{U}_{(i)}^N$ from the previous increment by Eq. 5.4.

$$
\ddot{U}_{(i)}^N = (M^{NJ})^{-1}(P_i^J - I_i^j)
\tag{5.4}
$$

where, M^{NJ} is the mass matrix, P^J is the applied load vector, andI^J is the internal force vector.

In the case of explicit time integration, the time increment will be smaller than by choosing the stability limit for both central-difference and forward-difference operators stated by Eq. 5.5.

$$
\Delta t \leq \min\left(\frac{2}{\omega_{max}}, \frac{2}{\lambda_{max}}\right)
\tag{5.5}
$$

where ω_{max} is the highest frequency in the system of equations of the mechanical solution response and λ_{max} is the largest eigenvalue in the system of equations of the thermal solution response. An approximation to the stability limit for mechanical and thermal solution response is given by Eq. 5.6 and Eq. 5.7 respectively,

$$
\Delta t \approx \frac{L_{min}}{C_d}
\tag{5.6}
$$

$$
\Delta t \approx \frac{L_{min}^2}{2\alpha}
\tag{5.7}
$$

where L_{min} is the smallest element dimension in the mesh, C_d is the dilatational wave speed depends on material's Young's modulus and poison's ratio; and $\alpha = {k}/{\rho C_p}$ is the thermal diffusivity of the material. This estimate for Δt is only approximate and in most cases is not a safe estimate. In general, the actual stable time increment chosen by Abaqus/Explicit will be less than this estimate by a factor between $1/\sqrt{2}$ and 1 in a 2D model. The time incrementation can be automatic or fixed where global or element by element stability limit is applied. The concept of the stable time increment is the time required to propagate a dilatational wave across the smallest element dimension when element-by-element is used.

5.2   Failure Theories and Work Material Constitutive Model

In ductile material, yielding occurs due to sliding of atoms (movement of dislocations). Hence, in a ductile material, the maximum shear stress causes yielding of the material. For ductile materials, the two well-established phenomenological failure theories are the Distortion Energy Theory (von Mises) and the Maximum Shear Stress Theory (Tresca). Between these Von Mises is the most favored theory for describing the failure of ductile materials.

The work done by the applied force is stored in the solid as potential energy, is called strain energy. The strain energy density, U_0 in a body can be obtained by integration as follows:

$$U = \iiint_V U_0(x, y, z)dV \tag{5.8}$$

where the integration is performed over the volume V of the solid. In the case of uniaxial stress state stain energy density is equal to the area under the stress-strain curve (Fig.5.4). Thus, it can be written as Eq. 5.9.

$$U_0 = \frac{1}{2}\sigma\epsilon \tag{5.9}$$
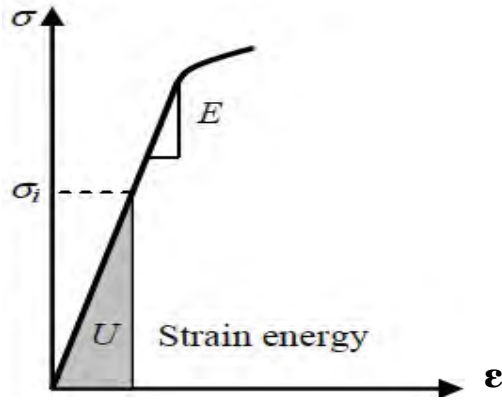
Fig.5.4 The stress-strain curve and the strain energy

Considering a coordinate system that is parallel to the principal stress directions; there is no shear components exist. Extending Eq. (5.9) to this stress states yield Eq. 5.10.

$$U_0 = \frac{1}{2}(\sigma_1\epsilon_1 + \sigma_2\epsilon_2 + \sigma_3\epsilon_3) \tag{5.10}$$

The strain energy density in terms of principal stresses can be written as

$$U_0 = \frac{1}{2E}[\sigma_1^2 + \sigma_2^2 + \sigma_3^2 - 2v(\sigma_1\sigma_2 + \sigma_2\sigma_3 + \sigma_1\sigma_3)] \tag{5.11}$$

The strain energy density at a point in a solid can be divided into two parts: dilatational strain energy density, U_h that is due to change in volume, and distortional strain energy density, U_d that is responsible for chathe nge in shape. In order to compute these components, the stress matrix can be divided into similar components, dilatational stress matrix, σ_h and deviatoric stress matrix, σ_d . The dilatational component σ_h is defined as

$$\sigma_h = \frac{\sigma_1 + \sigma_2 + \sigma_3}{3} \tag{5.12}$$

which is also called the volumetric stress whichis a state of hydrostatic stress and hence the subscript h denotes the dilatational stress component as well as dilatational energy density. The dilatational energy density can be obtained by substituting the stress components of the hydrostatic stress state in Eq. (5.12) into the expression for strain energy density in Eq. (5.11),

$$U_h = \frac{3}{2}\frac{(1-2v)}{E}\sigma_h^2 \tag{5.13}$$

73

The distortion part of the strain energy is now found by subtracting U_h from U_0 and expressed as the following Eq. 5.14,

$$U_d = \frac{1+\vartheta}{3E} \frac{(\sigma_1-\sigma_2)^2+(\sigma_2-\sigma_3)^2+(\sigma_3-\sigma_1)^2}{2} \tag{5.14}$$

To write U_d in terms of equivalent stress called von Mises stress σ_{VM} can be written as

$$U_d = \frac{1+\vartheta}{3E}\sigma_{VM}^2 \tag{5.15}$$

The von Mises stress is defined in terms of principal stresses as

$$\sigma_{VM} = \sqrt{\frac{(\sigma_1-\sigma_2)^2+(\sigma_2-\sigma_3)^2+(\sigma_3-\sigma_1)^2}{2}} \tag{5.16}$$

According to the von Mises's theory, a ductile solid will yield when the distortion energy density reaches a critical value for that material. Since this should be true for uniaxial stress state also, at the instance of yielding in a uniaxial tensile test, the state of stress in terms of principal stress is given by: $\sigma_1=\sigma_Y$(yield stress) and $\sigma_2=\sigma_3=0$. The distortion energy density associated with yielding is-

$$U_d = \frac{1+\vartheta}{3E}\sigma_Y^2 \tag{5.17}$$

Then according to von Mises's failure criterion, the material under multi-axial loading will yield when the distortion energy is equal to or greater than the critical value for the material. The von Mises stress can be rewritten in terms of stress components as

$$\sigma_{VM} = \sqrt{\frac{(\sigma_{xx}-\sigma_{yy})^2+(\sigma_{yy}-\sigma_{xx})^2+(\sigma_{zz}-\sigma_{xx})^2+6(\tau_{xy}^2+\tau_{yz}^2+\tau_{zx}^2)}{2}} \tag{5.18}$$

For a 2D plane stress state, $\sigma_3=0$, the von Mises stress can be defined in terms of principal stresses as Eq. (5.19)

$$\sigma_{VM} = \sqrt{\sigma_1^2 - \sigma_1\sigma_2 + \sigma_2^2} \tag{5.19}$$

In the case of pure shear stress, the 2D distortion energy describes an ellipse which is plotted on σ_1- σ_2 plane as shown in Fig. 5.5. The interior of this ellipse defines the region of combined bi-axial stress where the material is safe against yielding under static loading. Considering any shear stress, such that, $\sigma_x = \sigma_y = 0$ and $\tau_{xy} = \tau$. For this,

principal stresses are $\sigma_1 = -\sigma_2 = \tau$. On the $\sigma_1 - \sigma_2$ plane the pure stress state is represented as line AB through the origin at (-45°) as shown in Fig.5.5. The magnitude of σ_1 and σ_2 at the point A and B can be found from following Eq. 5.20. Thus, in a pure shear stress state, the material yields when the shear stress reaches $1/\sqrt{3}$ of σ_Y.

$$\sigma_Y^2 = \sigma_1^2 + \sigma_1\sigma_1 + \sigma_1^2 = 3\sigma_1^2 = 3\tau_{max}^2$$
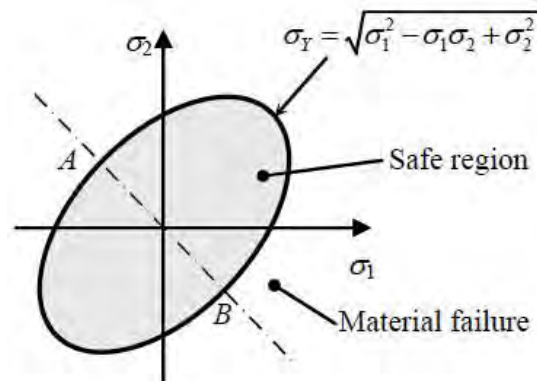
Fig.5.5 Failure envelop of the distortion energy theory

The flow stress is the instantaneous value of yield stress and is represented mathematically by constitutive equations depending on the strain, strain-rate, and temperature. The most widely used constitutive material models are Oxley, J-C, and Zerilli – Armstrong. In the literature review, studies have favored the use of the J-C constitutive material model for FEM used by authors Marbouki, [**2008**], Nasr et al. [**2008**], Courbon et al. [**2011**] etc.

The von Mises criterion describes the yield surface beyond which the material goes under failure. If there is strain hardening or thermal softening the size of yield surface can change through achieving larger stress. The material may be rate dependent, in which case the surface has a different size at different strain rates. The J-C model gives a way of finding what the size of the yield surface is under different loading condition. J-C is a constitutive material model used to describe material behavior in the plastic regime over large strains, high strain rates, and high temperatures. The flow stress can be expressed as:

$$\sigma = (A + B\varepsilon^n)\left[1 + C\ln\left(\frac{\dot{\varepsilon}}{\dot{\varepsilon_o}}\right)\right]\left[1 - \left(\frac{T-T_R}{T_M-T_R}\right)^m\right] \qquad (5.21)$$

where,

ε = equivalent plastic strain

$\dot{\varepsilon}$ = strain rate normalized with a reference strain rate $\dot{\varepsilon}_o$

T = instantaneous temperature

T_M = melting temperature

T_R = reference temperature

Here, the first bracketed term called elasto-plastic term represents strain hardening of the yield stress that is given the stress as a function of strain. Next term (visco-plasticity term) models the increase in the yield stress at elevated strain rates and final term is softening of the yield stress due to local thermal effects. The above yield strength portion of the J-C model has five material constants. A is the yield stress, B and n represent the effect of strain hardening determine at $\dot{\varepsilon}_o$. C is the strain rate constant. A, B, C, n and m are measured at T_R or below T_R.

5.3   Damage Criterion

J-C expanded the model with the inclusion of fracture model based on cumulative damage. The J-C damage model is suitable for progressive damage to high strain rate deformation such as high speed machining. According to J-C damage criterion the expression for fracture strain is:

$$\varepsilon^f = \left(D_1 + D_2 exp D_3 \frac{\sigma_m}{\bar{\sigma}}\right)(1 + D_4 ln \frac{\dot{\varepsilon}}{\dot{\varepsilon}_o})(1 + D_5 \frac{T - T_R}{T_M - T_R}) \qquad (5.22)$$

where,

D_1= Initial fracture strain

D_2= Exponential factor

D_3= Triaxiality factor

D_4= Strain rate factor

D_5= Temperature factor

σ_m = Average of the three normal stress

$\bar{\sigma}$= Von-Mises equivalent stress

Here the first, mid and last bracketed term in J-C damage model includes the effect of stress triaxiality, strain rate and local heating respectively. Damage initiation begin according to standard damage law,

$$W = \sum \frac{\Delta\varepsilon}{\varepsilon^f} \qquad (5.23)$$

where, W is the damage parameter and $\Delta\varepsilon$ is the accumulated increment of equivalent plastic strain during an increment step. According to this model, damage initiation is followed by damage evolution criterion which governs the propagation of plastic strain until an ultimate failure happens. The criterion for damage ignition is met when the following criterion is satisfied.

$$W = \int \frac{d\varepsilon}{\varepsilon^f\left(\frac{\sigma_m}{\bar{\sigma}}, \dot{\varepsilon}\right)} = 1 \qquad (5.24)$$

Each damage initiation criterion have an associated damage evolution law. The law defines how the material degrades after the damage initiation criteria are met. The characteristic stress-strain behavior of a ductile material undergoing damage is shown in Fig.5.6. The solid curve in the Fig.5.6 represents the damaged stress-strain response, while the dashed curve is the response in the absence of damage. In the Fig. σ_{y0} and $\bar{\varepsilon}_0^{pl}$ are the yield stress and equivalent plastic strain at the onset of damage, and $\bar{\varepsilon}_f^{pl}$ is the equivalent plastic strain at failure; that is, when the overall damage variable D reaches the value 1. The value of the equivalent plastic strain at failure, $\bar{\varepsilon}_f^{pl}$, depends on the characteristic length of the element and cannot be used as a material parameter for the specification of the damage evolution law.
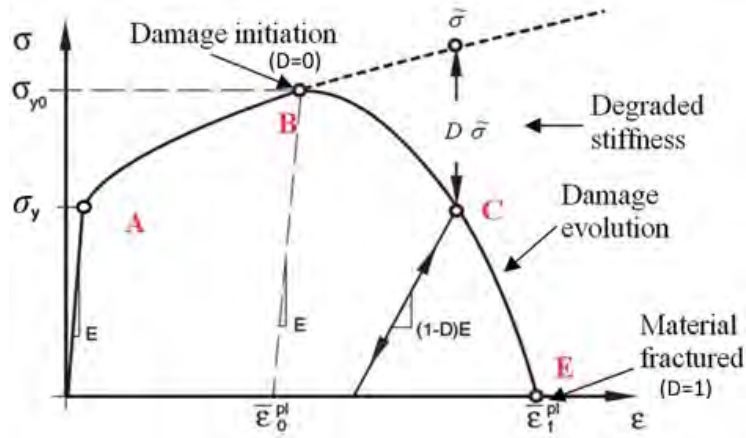
Fig.5.6 Stress-strain curve with progressive damage degradation [**ABAQUS Analysis User's Manual, 2014**]

The damage evolution law can be specified in terms of equivalent plastic displacement, $\bar{u}^{pl}$, or in terms of fracture energy dissipation, G_f. Before damage initiation, the equivalent plastic displacement is $\bar{u}^{pl} = 0$. Once a particular initiation criterion is satisfied, the material stiffness is degraded according to the specified damage evolution law, and the equivalent plastic displacement becomes $\bar{u}^{pl} = L\bar{\varepsilon}$. Here L is the characteristic length of the mesh element near cutting edge. This damage evolution law describes the degradation rate of the material stiffness once the corresponding initiation criterion has been reached. The damage parameter is expressed as,

$$D = \frac{L\bar{\varepsilon}}{\bar{u}^f} = \frac{\bar{u}^{pl}}{\bar{u}^f}$$

(5.25)

where the equivalent plastic displacement at failure, $\bar{u}^f$, was computed as

$$\bar{u}^f = \frac{2G_f}{\sigma_y}$$

(5.26)

The formulation of the model ensures that the energy dissipated during the damage evolution process is equal to G_f. When $\bar{u}^{pl} = \bar{u}^f$, the material stiffness fully degraded (D=1), that is the material fails and will be removed from the calculation. To mitigate the mesh dependency, damage evolution model based on fracture energy proposed by Hillerborg et al.[**1976**] is used in this study. The authors defined the energy required to open a unit area of crack G_f as a material parameter. With this approach, the softening

(5.27)

response after damage initiation is characterized by a stress–displacement response rather than a stress–strain response. The fracture energy is then given as

$$G_f = \int_{\bar{\varepsilon}_0^{pl}}^{\bar{\varepsilon}_f^{pl}} L\sigma_y \, d\bar{\varepsilon}^{pl} = \int_0^{u_f^{pl}} \sigma_y \, d\bar{u}^{pl}$$

This expression of G_f introduces the definition of the equivalent plastic displacement $\bar{u}^{pl}$, as the fracture work conjugate of the yield stress after the onset of damage. In this study G_f is provided as an input parameter and theoretically it is a function of fracture toughnessK_c, Young's modulus E, and Poisson's ratio υ. The fracture energy required for the damage evolution can be determined by the following Eq. (5.28)

$$G_f = K_c^2 \left(\frac{1-v^2}{E}\right) \tag{5.28}$$

The experimental evidence shows that the fracture toughness of metals is dependent on the size of the specimen during the test [**Sisto et al. 1964**]. But the fact is, when chip formation is considered, the chip size is relatively small where the fracture initiated and propagated. So it is not realistic to use K_c values measured at nominal test specimen size, which is relatively higher than required for chip formation. Mabrouki et al. [**2008**] employed fracture energy method into the FEM model by using K_c values measured at a nominal size to estimate the fracture energy. They used the K_c values of 37 MPa$\sqrt{m}$ for the opening mode of fracture (tensile mode) and 26 MPa$\sqrt{m}$ for the shearing mode of fracture (sliding mode). On the contrary, Opoz and Chen [**2016**] did not determine the K_c values for damage evaluation. They directlyused the range of G_f values (250 N/m to 20000 N/m) to investigate the influence of fracture energy on chip shape and morphology. According to them, K_c varies depending on the fracture mode of material including the micro-crack formation, element dislocation, and subsequent crack growth. In this study for different hardness level of workpiece the K_c values were used by following the investigation of Ripling and Corsley [**1981**] for 4140 steel. Their experiment for toughness value was based on the specimen size and yield strength of material.

5.4   FE Modeling of Heat Generation in Metal Cutting

There are two main sources of heat production in metal cutting: material plastic deformation and friction. In high-speed machining, heat produced due to local energy dissipation may not have adequate time to diffuse away, and local heating will take place in the active plastic zones and sliding frictional interface. Thus, the temperature rise in the chip can be estimated with the adiabatic heating condition. The temperature increase is calculated directly at the material integration points according to the adiabatic thermal energy increases caused by inelastic deformation. The rate of heat generation by plastic deformation $\dot{q}_p$ is given by Eq. (5.29),

$$\dot{q}_p = \eta \dot{\sigma} \varepsilon \tag{5.29}$$

where, η is the fraction of plastic deformation energy is converted into heat, $\dot{\sigma}$ is the material flow stress tensor, and is ε is the plastic strain rate tensor. η is usually between 0.85 and 0.95 [**Shet and Deng, 2000**]. The heat equation solved at each point is given in eq. (5.30).

$$\rho C_p \frac{\Delta T_p}{\Delta t} = \dot{q}_p \tag{5.30}$$

where, ρ is the material density and C_p is the specific heat. Considering Eq. (5.29) and (5.30) local temperature rise due to plastic deformation can be given by,

$$\Delta T_p = \eta \frac{\dot{\sigma} \varepsilon \Delta T_p}{\rho C_p} \tag{5.31}$$

Similarly, heat generated by friction forces $\dot{q}_f$ lead to a rise in temperature ΔT_f.

$$\dot{q}_f = \eta_f J \tau \dot{\gamma} = \rho C_p \frac{\Delta T_f}{\Delta t} \tag{5.32}$$

Then temperature rise due to sliding friction in tool-chip interface is determined by,

$$\Delta T_f = \eta_f \frac{J \tau \dot{\gamma} \Delta t}{\rho C_p}$$

where, η_f is the fraction of dissipated energy caused by friction and assumed as 0.9 to 1.0 [**Courbon, 2011;Opoz and Chen , 2016**]. J the equivalent heat conversion factor, τ shear stress computed by Coulomb's law and $\dot{\gamma}$ is slip strain rate.

Frictional heat going into the workpiece β is given by Eq. (5.34)[**Jacobus et al. 2000**] and depends on the effusivity, Ef which is also known as heat absorption coefficient of the workpiece Ef_{wp} and the tool Ef_t; where k is the thermal conductivity.

$$\beta = \frac{Ef_{wp}}{Ef_{wp}+Ef_t}, \quad \text{where,} Ef = \sqrt{(k\rho\ _p)} \tag{5.34}$$

5.5   Present Finite Element Model Development of Metal Cutting

In this study, a 2D ALE FE model is built using Abaqus/Explicit version 6.14 to simulate the previously performed turning process of 42CrMo4 by coated carbide insert under dry and HPC condition. To simulate a 3D process in 2D it is essential to define a projection of the 3D case to 2D. The turning process is simplified by considering only a small segment from the workpiece. Since the depth of cut, feed rate and the simulated workpiece arc is negligibly small compared to the radius of the workpiece, the segment is
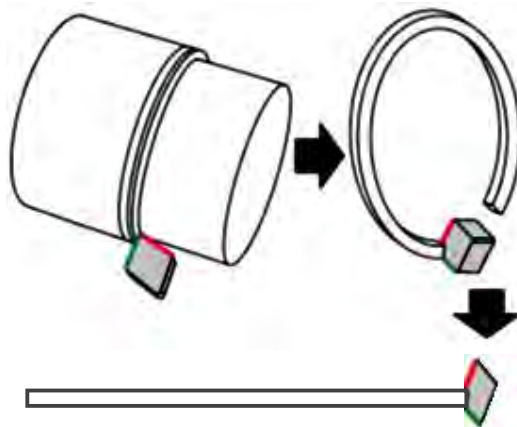
Fig.5.7 Illustration of the 3D-2D projection

considered to be straight. The illustration of the 3D-2D projection is given in Fig.5.7.

5.5.1 Workpiece and Tool Modeling

According to this projection illustrated in Fig.5.7, the position of tooltip and the top edge of the workpiece corresponds to the feed rate from the measurement data, not to the depth of cut. The Fig.5.8 shows the basic geometry of the used FE model with the applied boundary conditions, where cutting takes place in the XY plane under plane strain condition. The length and width of the workpiece is set to 3 mm and 1 mm respectively. A parting line AB has created at the workpiece. This line indicates the uncut chip thickness which is feed for the 2D simulation modeling. The tool tip was placed exactly at the level of parting line AB. In this particular machining process, two edges of the tool are involved in cutting - rake face and clearance face. At the two face negative rake angle of 6° and clearance angle of 6° was drawn as real geometry of cutting tool. Nose radius is assumed to be very small 0.06 mm, as in 2D it has no effect on metal cutting.
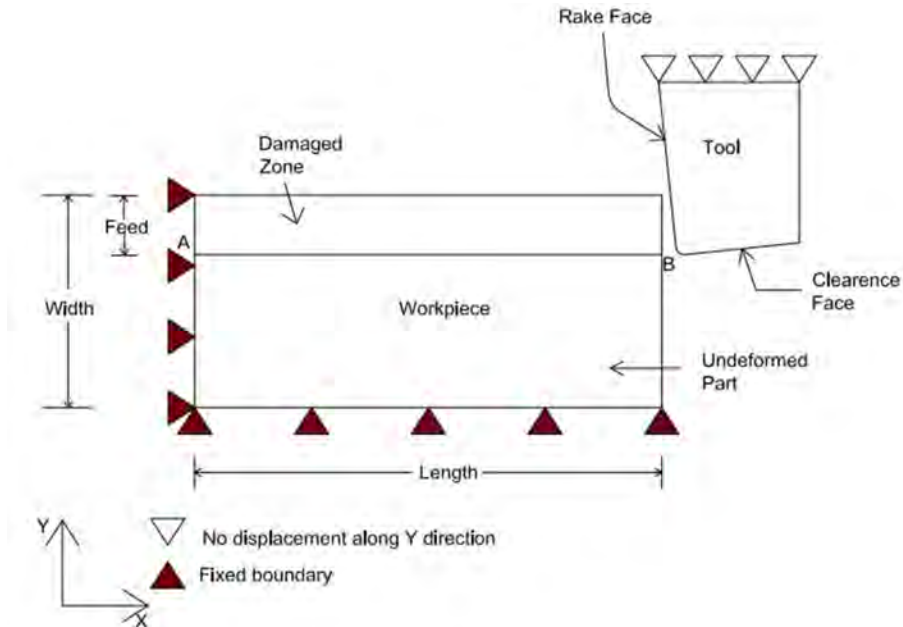
Fig.5.8 The basicFE model for the 2D simulation

In the current study the material plastic behavior was modelled using J-C constitutive material model and J-C damage model was used for initializing the chip separation. For crack initiation the fracture energy was used as damage evolution and calculated by Eq. 5.7. The materials properties of 42CrMo4 and coated carbide tool adopted in the numerical models are given in Table 5.1.

Table 5.1 Workpiece and cutting tool material properties

Property Type	Parameters	Workpiece	Tool
Physical Properties [**MatWeb, LLC, 2018**]	Density ρ (Kg/m^3)	7850	14450
	Elastic modulus E (GPa)	210	630
	Poisson's ratio ν	0.29	0.22
	Specific heat Cp (J/kg/°C)	473	226
	Thermal conductivity λ (W/m/°C)	42.6	44.6
	Thermal Expansion Co-efficient (/°C)	1.37e-5	7.7e-6
	Inelastic Heat Fraction (β)	0.9	
	T_{room} (°C)	25	
	T_{melt} (°C)	1520	
J-C Parameters [**Pantale et al. 2004**]	A (MPa)	595	
	B (MPa)	580	
	C	0.023	
	n	0.1333	
	m	1.03	
Damage law parameters [**Pantale et al. 2004**]	D_1	1.5	
	D_2	3.44	
	D_3	2.12	
	D_4	0.0002	
	D_5	0.1	
Damage Evolution	Fracture Toughness K_c (MPa√m) [**Ripling and Corsley, 1981**]	119.44 for 42 HRC 94.72 for 43 HRC 117.35 for 45 HRC 107.35 for 48 HRC 77.68 for 49 HRC 67.57 for 51 HRC	

After the creation of the two parts (workpiece and tool) and assignment of material properties, the geometry of the assembly was defined by creating instances of a part and then positioned the instances relative to each other in a global coordinate system. Then instances were merged to create total metal cutting model. Fig.5.9 shows the assembly model of workpiece-tool.
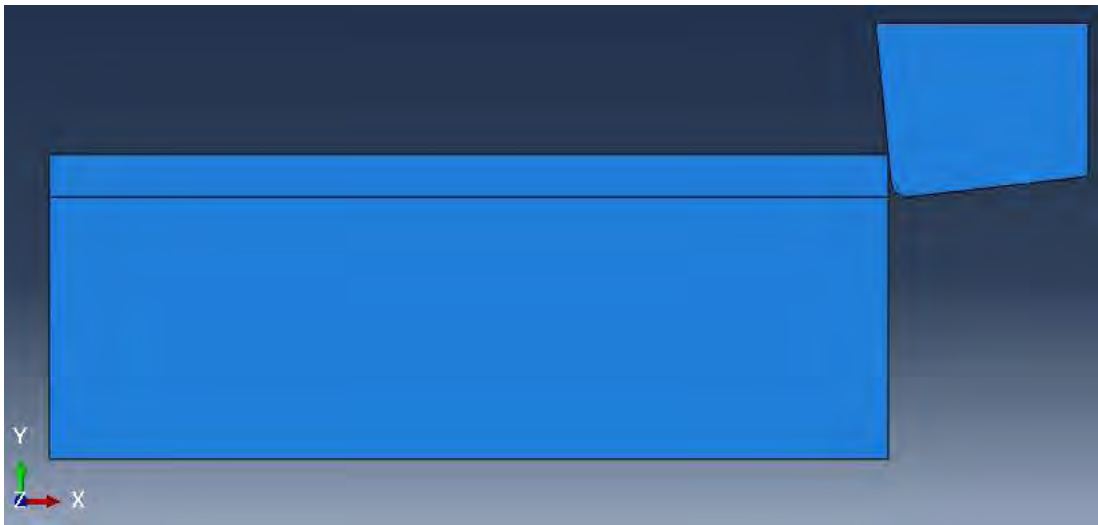
Fig.5.9 Assembly model of workpiece-tool

The applied mesh consisted of CPE4RT elements with plane strain condition. CPE4RT means 4 node bilinear displacement and temperature, reduced integration with hourglass control. The mesh is composed of 2D 4-node elements with a 12 μm x 5 μm rectangular face in the workpiece. The tool is composed of the CPE4RT and some triangular elements, but of variable length. The mesh distribution of the assembly is shown in Fig. 5.10, where the different densities can be seen. The model has total 64,206 elements and 64,669 nodes (50,000 elements and 50,451 nodes for the workpiece).
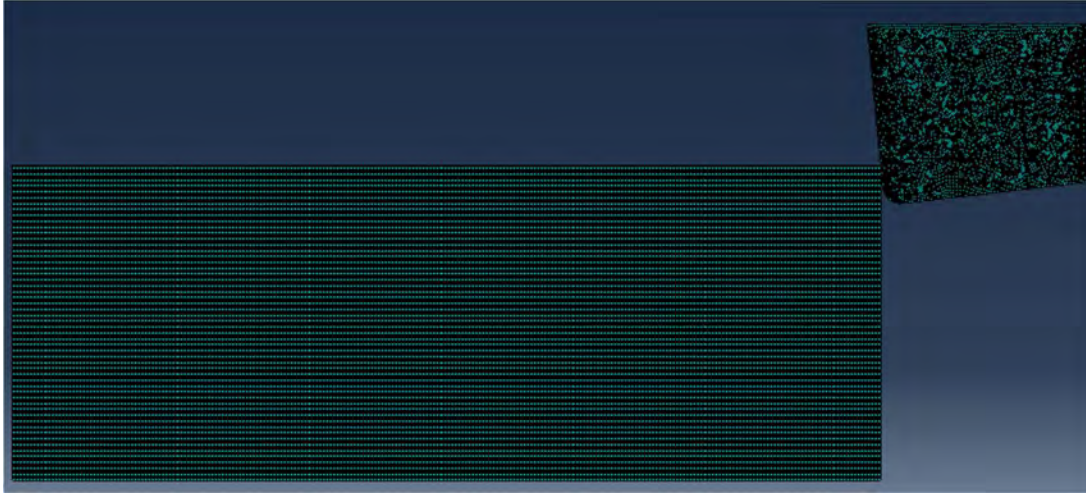
Fig.5.10: Mesh structure of workpiece and tool

5.5.2   Interaction Modeling

The contact of the tool and workpiece was modelled with a surface-to-node interaction. It consists of two surfaces expected to come into contact during the tool-workpiece interaction. These contact surfaces are designated by the master surface (edges of tool) and slave nodes (node region of top portion of workpiece). Further, a self-contact was assigned to the top edge of the workpiece due to considering the possibility of the chips can be folded onto itself during high deformation. Both type of contacts areshown in Fig.5.11.
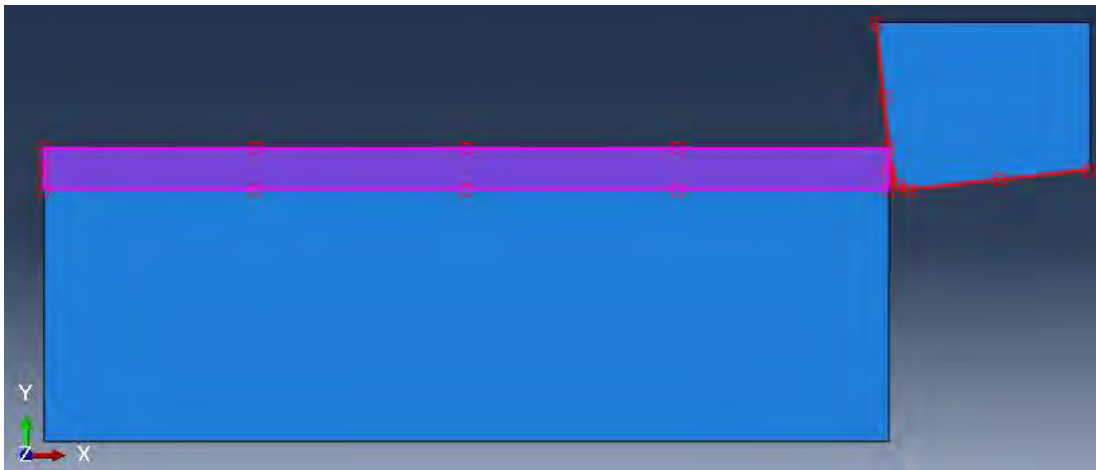
(a) Surface to surface contact
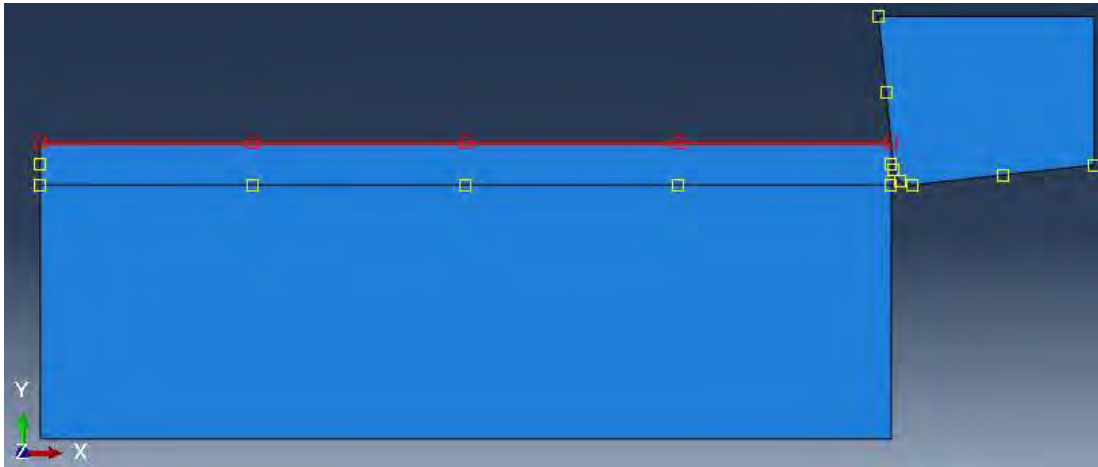
(b) Self- contact

Fig.5.11 Contact model of workpiece and tool

In this study, the multi-faceted geometry was defined by assigning a kinematic contact property model based on Coulomb's friction law. Although it is a simple model, it has been widely used in metal cutting simulations by researchers namely a few of them Nasr [**2008**], Arrazola [**2010**], Proudian [**2012**], Krishnakumar [**2013**]. Moreover, one of the studies on friction modeling in orthogonal machining by Felice et al. [**2007**] concluded that the main mechanical results as in forces, contact length, etc. are practically not sensitive to friction model, only by small differences. In this present model, based on the experiences of many previous authors [**Nasr, 2008; Opoz and Chen, 2016**] the friction coefficient was set to 0.2 for dry cutting and 0.07 for cutting under HPC condition as mentioned in the research paper of Gariani et al. [**2017**].

Heat radiation and convection were neglected in the cutting model, as they are negligible compared to conduction. High speeds allow no time for heat transfer between integration points with which the process treated as adiabatic process. Based on the material properties, fraction of heat absorbed by the workpiece was calculated by Eq. 5.34. 100% of the frictional energy has been supposed transformed into heat. The coefficient of heat conduction between the tool and workpiece was assumed to be 10^8 W/m^2/^{o}C, which was similar to that used in [**Saez-de-Buruaga et al. 2017; Imbrogno et al. 2017; Klocke et al. 2017**]. This conductance was imposed for the distance in contact pair is less than 10^{-7} m.

In case of HPC the cooling effect of the jet has been integrated in the model by a convective heat-transfer coefficient. The traditional correlations for forced convection use a heat transfer co-efficient (film coefficient, h) of the form:

$$h = f(Nu) = f(Re, Pr, geometry)$$

For cylindrical workpieces, the Nusselt number (Nu), Reynolds number (Re) and Prandlt number (Pr) are given below:

$$Nu = \frac{hD}{k} \tag{5.35}$$

$$Re = \frac{\rho V_f D}{\mu} \tag{5.36}$$

$$Pr = \frac{\mu C_p}{k} \tag{5.37}$$

Pr depends only on the dynamic viscosity (μ), specific heat (Cp) and thermal conductivity (k) of fluid. Re depends on fluid density (ρ), dynamic viscosity (μ), fluid velocity (V_f), and workpiece diameter (D). For a jet application of cutting fluid on the workpiece an appropriate correlation for the average Nu [**Martin, 1977**] is given by Eq. 5.38.

$$\frac{\overline{Nu}}{Pr^{0.42}} = 2G Re^{0.5}(1 + 0.005 Re^{0.55})^{0.5} \tag{5.38}$$

Where, G is given by

$$G = \frac{D_n}{R}\left(\frac{1 - 1.1\,{D_n}/{R}}{1 + 0.1(^H/_{D_n} - 6)\,{D_n}/{R}}\right) \tag{5.39}$$

here,

Dn = Jet nozzle diameter

R = Radial distance from jet stagnation point

$^H/_{D_n}$ = Jet to plate vertical non-dimensional distance

The VG 68 cutting oil was used as coolant in this study. The necessary parameters to calculate the film coefficient are tabulated in the Table 5.2. The HPC effect was modeled by setting surface film condition at tool rake face. The local temperature inside was set equal to 25 °C. The film coefficient was computed using Eq. 5.35 to 5.39.

Table 5.2 Fluid property and HPC application parameters

Parameters	Corresponding Value
Density ρ (kg/m3)	864.12
Dynamic Viscosity μ (N-s/m2)	$3.53*10^{-8}$
Thermal conductivity λ (W/m/°C)	0.163
Prandtl number (Pr)	754
Diameter of the nozzle injector (mm)	1
Diameter of outlet nozzle (mm)	0.5
Pressure inside nozzle (bar)	80
Angle of the spray pattern	20°
Flow rate of cutting fluid (l/min)	12

In the stress relaxation model, where the workpiece was left to cool down to room temperature of 25°C. Both the parts were set to exchange heat to air by setting a convection coefficient equal to 20 W/m^2/°C, which is considered the standard value for free-air convection in the research of Imbrogno et al. [**2017**].

5.5.3   Simulation Environment and Boundary Conditions

The workpiece was modelled as elastic–plastic body with strain hardening properties, while the tool was modelled as an elastic body. In this work, an FEM simulation model with ALE scheme with pure Lagrangian boundaries is designed and kinematic penalty contact conditions between tool and the workpiece are defined as shown in Fig.5.12. This model allows a FEM simulation scheme to simulate the chip formation from the incipient to steady-state as it was proposed by the authors in reference [**Ozel and Zeren, 2005**].
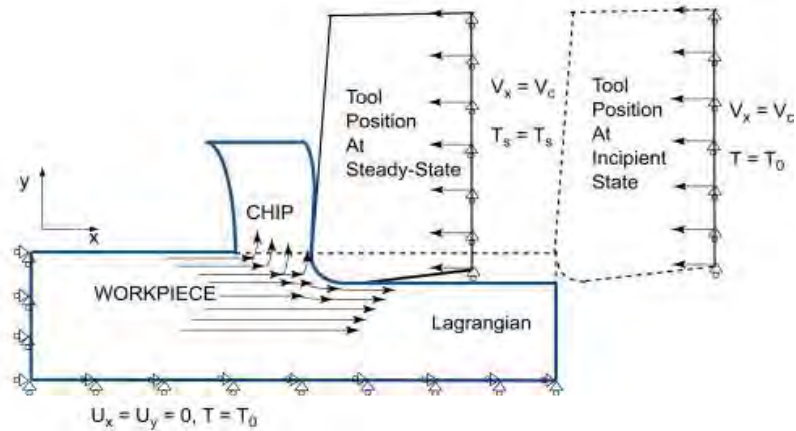
Fig.5.12 ALE formulation with pure Lagrangian boundary conditions

The boundary conditions for the 2D ALE Lagrangian base model along with geometry of the system is shown in Fig.5.13. For the boundary conditions, ENCASTRE (fully built-in) applied to the workpiece at its left and bottom surfaces, restricting the workpiece in the X and Y direction, respectively. The tool is moved against the workpiece by applying constant cutting velocity. The tool moves in the –X direction. Element deletion technique is used to allow element separation to form a chip. The applied boundary conditions are shown in the Fig. 5.13. Then at unloading step the tool was detached from the chip and workpiece by moving it to +X and +Y direction. And then the stress relaxation process of workpiece was initiated.

Fig.5.13 Boundary conditions of workpiece and tool

The ALE adaptive meshing technique is used to reduce element distortion in cases of extreme deformation and applied at top portion of workpiece. So that, in this region the associated nodes move with the material in the direction normal to the material's surface

and nodes are allowed to adapt (adjust their position) tangent to the free surface. The ALE remesh was used with frequency of 2 and 1 remeshing sweeps per increment. The adaptive mesh was controlled by volume based smoothing algorithm and the mesh motion was constrained to follow the underlying material.

5.5.4   Cutting Conditions and Data Collection for Simulation

Several simulations are tested with varying cutting conditions, in order to study the effect of each on the RS induced in the machined component after machining and for the verification of the model. The simulation of RS evaluation for HPC condition was designed for the optimal process parameters obtained in previous chapter. Total 15 set of parameters was generated after performing the optimization procedure. Considering every feed and low-to high speed and workpiece hardness total 8 of the generated combinations was selected for RSmodeling. In the purpose of verification, temperature distribution was checked for both of the cutting environment comparing to the experimental result. The simulated combination of cutting process parameters are listed in Table 5.3.

Table 5.3 Selected combination of parameters for simulation

Purpose		Cutting Velocity, V (m/min)	Feed, f (mm)	Hardness (HRC)
Temperature modeling and Verification		Dry		
		165	0.16	48
		165	0.14	48
		HPC		
		165	0.16	48
		82	0.12	48
Residual stress Comparison		Dry		
		165	0.16	48
		HPC		
		165	0.16	48
Residual stress modeling	Test no.	HPC		
	1.	55	0.12	51
	2.	56	0.13	42
	3.	68	0.12	45
	4.	91	0.12	43
	5.	127	0.12	49
	6.	146	0.12	49
	7.	150	0.12	45
	8.	152	0.12	42

Mechanical and thermal parameters of the machining process; RS and temperature are calculated along the workpiece in the simulation. Temperature values are collected by selecting the tool-chip interface nodes at three different time of machining. The data was averaged and then compared to the corresponding experimental one. Fig.5.14 represents the data collection procedure for RS. The data collection was performed by dividing the area of machined surface into 5 points and for each point the data is collected for newly generated surface to the depth reaching upto bottom surface. RS values were captured in two directions: circumferential (S11) and axial (S22). Collected data is then averaged and graphed. This data collection process is repeated throughout the study for all cutting
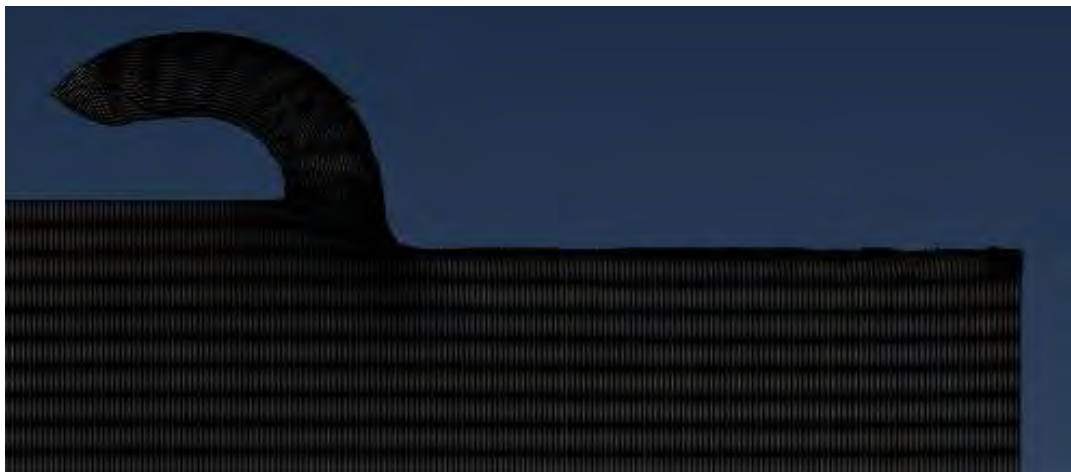
conditions.

Fig.5.14: Data collection way for RS profile generation

5.6   Simulation Results

5.6.1   Evaluation of Simulation

The von Mises stress distribution is shown in the Fig.5.15a-f. As an illustration the chip formation simulation procedure and the consequence steps of relaxation way can be seen on these figures. This figure is depicted for 48 HRC workpiece hardness with one specific simulation cutting condition of 165 m/min cutting speed, 0.12 mm feed and the environment is with coolant effect.

(a) Machining simulation at time 0.00007s

(b) Machining simulation at time 0.00017s

(c) Machining simulation at time 0.00027s

(d) Machining simulation at time 0.00037s

(e) Tool unloading

(f) Convection to ambient
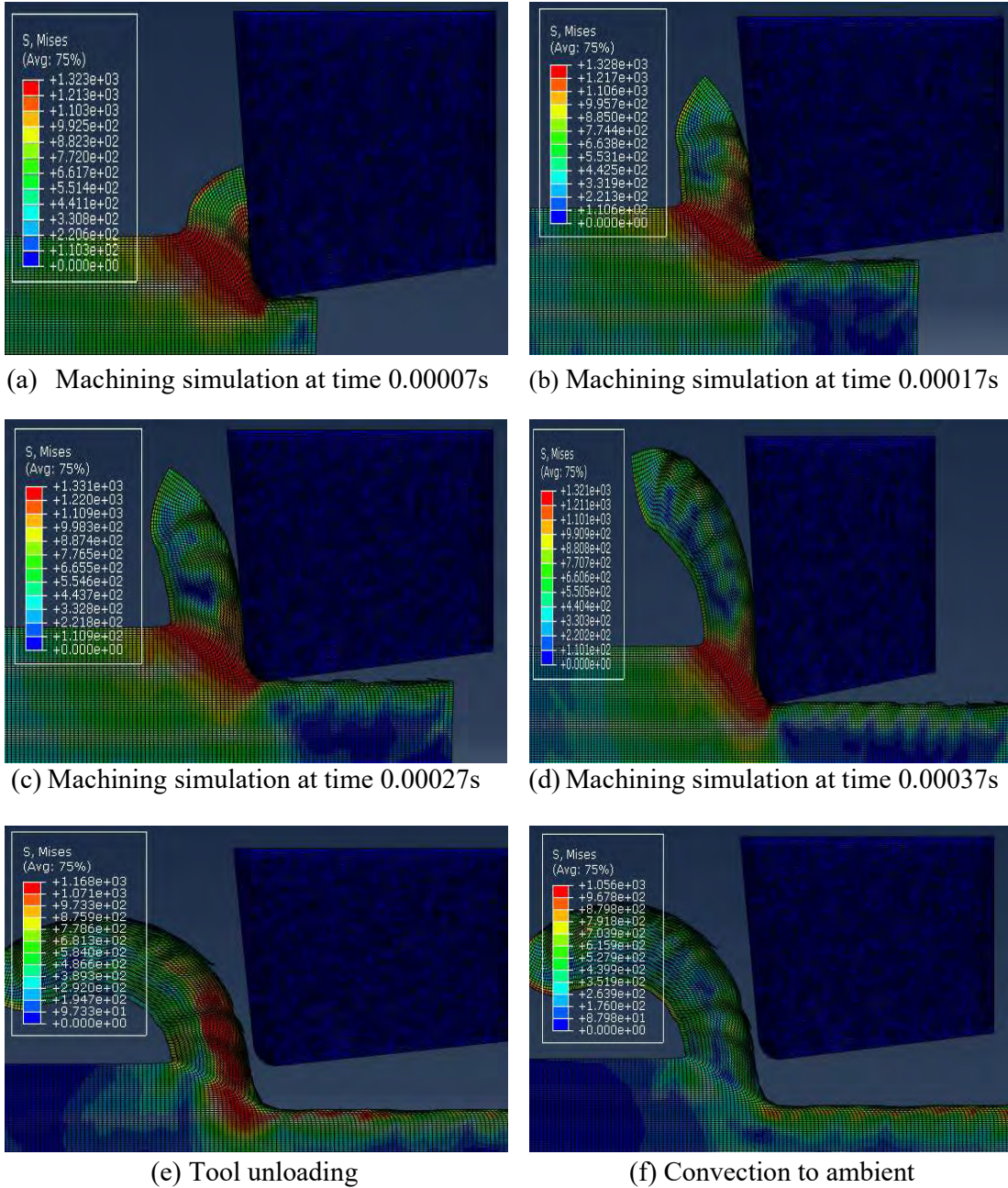
Fig.5.15 Development of the von Mises stress for a cutting speed of 165m/min, feed of 0.12mm (workpiece hardness 48 HRC)

The instant represented by the Fig.5.15a shows a state where shear band is nearly to develop and the deformation occurs mainly along the curved band. In the instant depicted by the Fig. 5.15b the deformation occurs in this band, but there is also some deformation in the region under this shear band, leading to a dam the material. Generally, the concentration of the deformation begins at the tool tip, but a second deformation

concentration starts at the free surface, close to the tool rake face (Fig.5.15c). During this cutting phase, the von Mises stress inside the zone where deformation concentrates is larger than in the adjacent zones. The instance depicted in Fig.5.15d, strain localization has begun near the tool tip as the von Mises stress experiences a decrement there. At the tool unloading phase (Fig.5.15e) the deformation concentrates at the free surface, which is not a localized deformed area because the von Mises stress is larger here than in the adjacent zones. This happens also due to the self-contact effect for which the chips tend to bend for self-weight and strain has localized at the inner and outer corner of the chips. At the instance Fig.5.15f the convection to ambient gives lower stress distribution to the machined surface compared to other instances. This also happens to the other area of chips where the strain localization was continued and consequently decreases the stress intensity.

5.6.2   Cutting Temperature Modeling and Validation

Initially the orthogonal cutting process simulations are validated with measured cutting temperature. This is the main output parameter in this study that can be compared with experimental results. The temperature distributions in a workpiece before relaxing of the machined component was observed. Fig.5.16 depicts the temperature distribution at 165 m/min cutting speed and feed 0.16 mm feed. It is noticed from the Fig.5.14 that the temperature intensity in machined surface for HPC condition is lower and affected area is smaller than the dry cut.
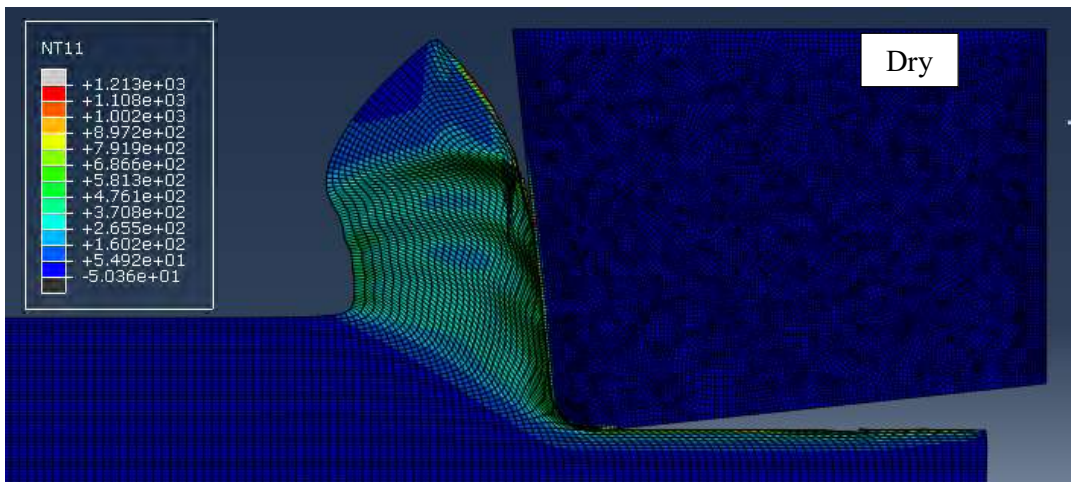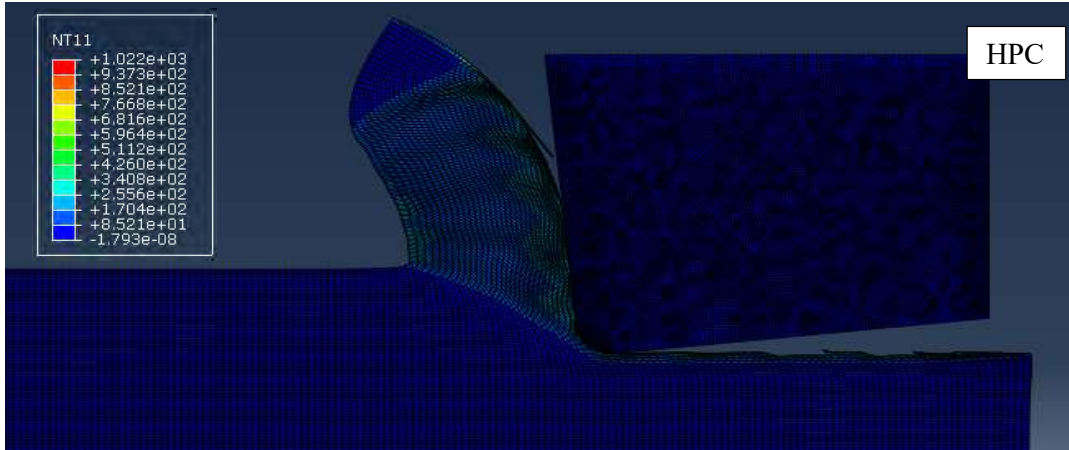
Fig.5.16 Temperature Distribution at cutting speed 165m/min and feed 0.16 mm
(workpiece hardness 48 HRC)

The temperature values were collected at the instant of 0.0001s, 0.0002s and 0.0003s simulation for dry condition and for HPC the time of data gathering was at 0.000408s, 0.000507s and 0.000608s of cutting simulation. Fig. 5.17displaysa sample of the graph of temperature distribution at the tool-chip interface with average oneand experimental value for dry environment. Following this method average temperature values were calculated for the cutting conditions stated for validity test.
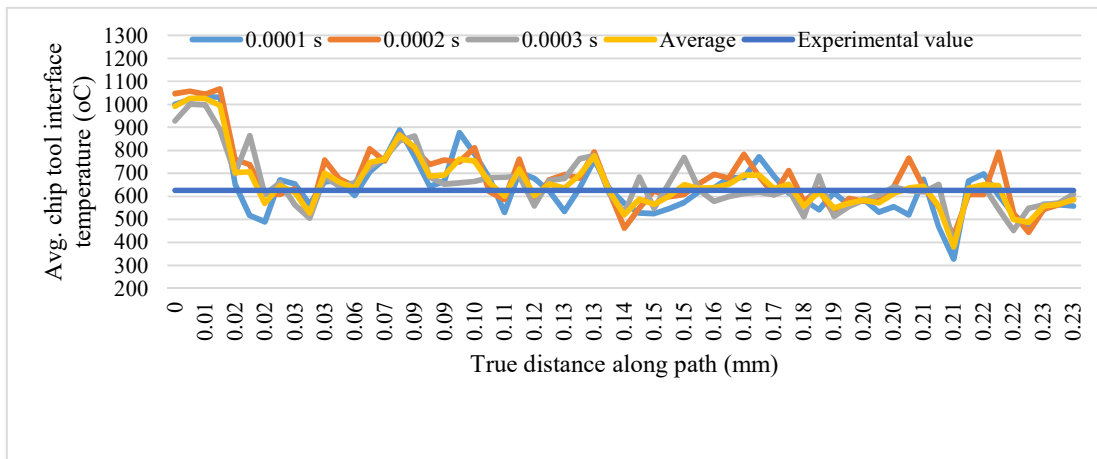
Fig.5.17 Cutting temperature distribution for different machining time (Dry cut, cutting speed 165 m/min and feed 0.16 mm)

Table 5.4 shows the difference between simulated value and experimentally measured value. The relative error was also calculated and found less than 10% discrepancy for all of the cutting condition.

Table 5.4 Comparison of experimental and simulated values in terms of cutting temperature

Cutting Environment	Cutting Velocity, V (m/min)	Feed, f (mm)	Hardness (HRC)	Experimental Value	Simulated Value	Error
Dry	165	0.16	48	626 °C	660 °C	+5.53%
	165	0.14	48	550 °C	590 °C	+7.27%
HPC	165	0.16	48	314 °C	299 °C	-4.63%
	82	0.12	48	130 °C	123 °C	-5.04%

5.6.3 Residual Stress Profiles

Circumferential and Axial residual stress analysis: Fig.5.18 presents a sample of the scattered circumferential residual stresses for 5 selected points in the newly machined surface with average one. All of the simulated RS data were compiled in this way and are shown in Fig.5.19 for different cutting conditions. All of the combinations show the machining induced RS profiles with respect to the depth beneath the newly machined surface for stress components along cutting direction or circumferential direction (S11) and axial direction (S22) which are computed from the simulated stress fields by the stated procedure. It is notable that the shape of the RS profile is coherent to the typical stress profile (Fig.1.2). From Figs.5.19 it is apparent that the circumferential residual stress is larger than the axial residual stress for maximum test conditions.
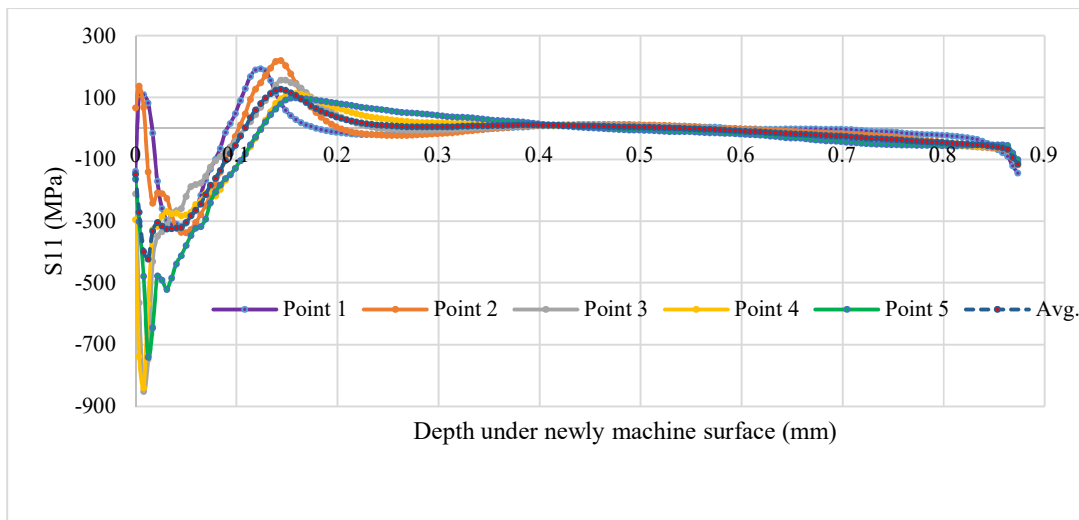
Fig. 5.18: Scattered data collection of S11 in cutting speed 54 m/min and feed 0.12mm (workpiece hardness 48 HRC)

Test Condition 1
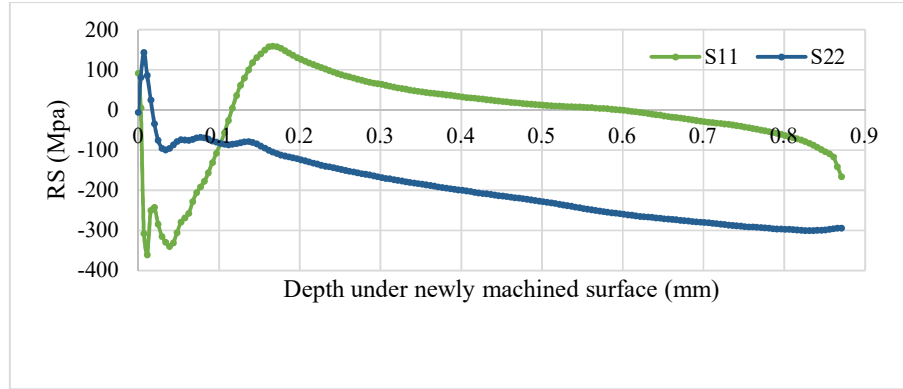
Test Condition 2
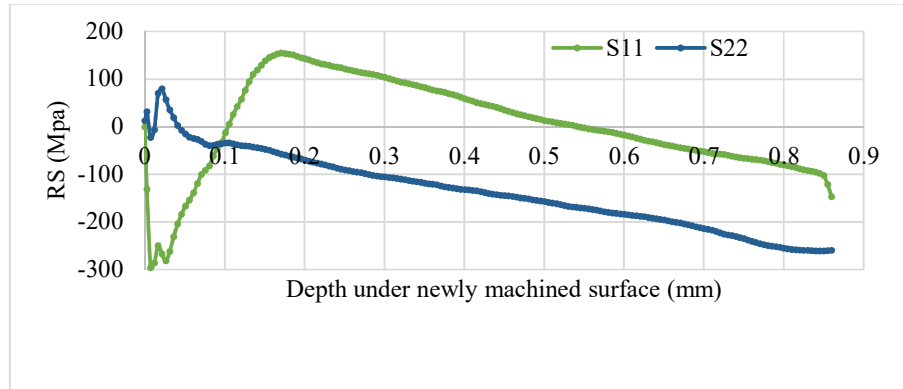
Test Condition 3

Test Condition 4

Test Condition 5

Test Condition 6
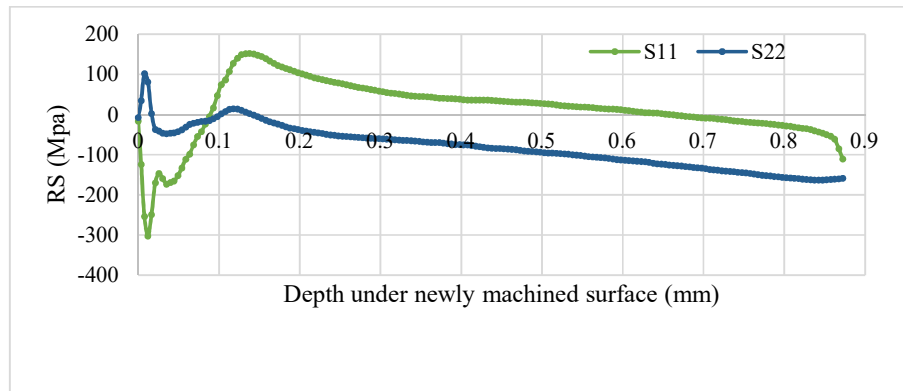
Test Condition 7
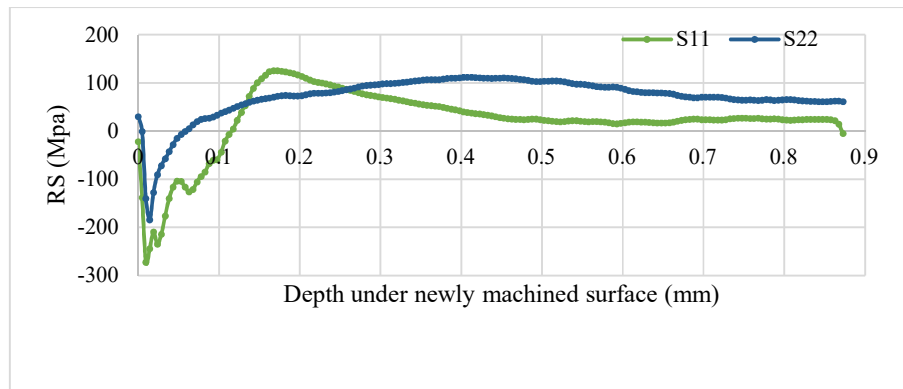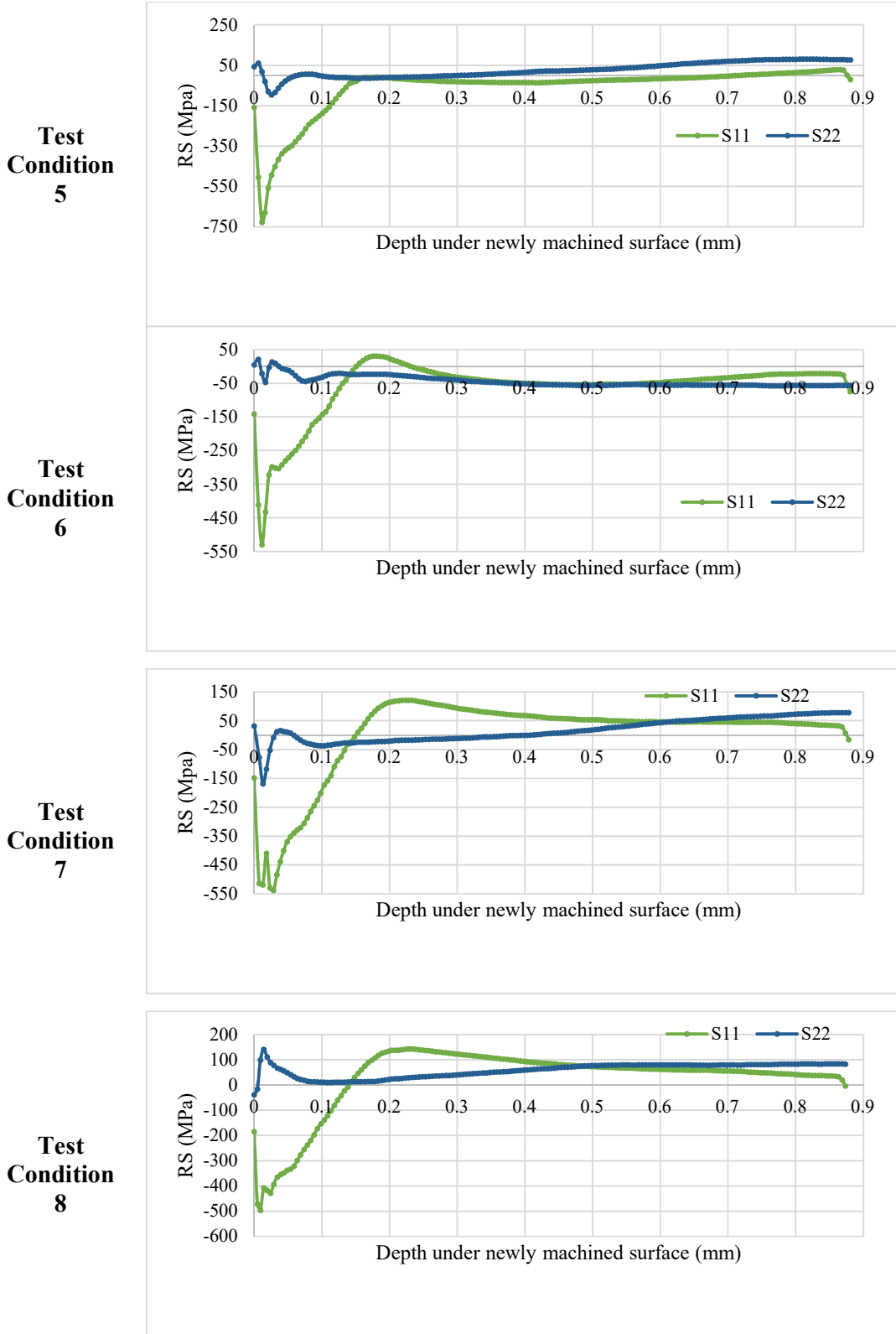
Test Condition 8

Fig.5.19: Residual stress profile after relaxation at test condition 1 to 8

Influence of Cutting Environment: Residual stress profiles for dry and HPC cutting conditions are evaluated for an identical speed-feed combination.The Fig.5.20 and Fig.5.21 presents the RS profile for S11 and S22 direction respectively for a specific machining parameter (cutting speed 165 m/min, feed 0.16 mm and workpiece hardness 48 HRC). Both of the figures show that compressive RS is higher at surface for HPC cutting condition compared to dry cut. At circumferential direction the compressive behavior remains at far depth under the surface in HPC than the dry cut.
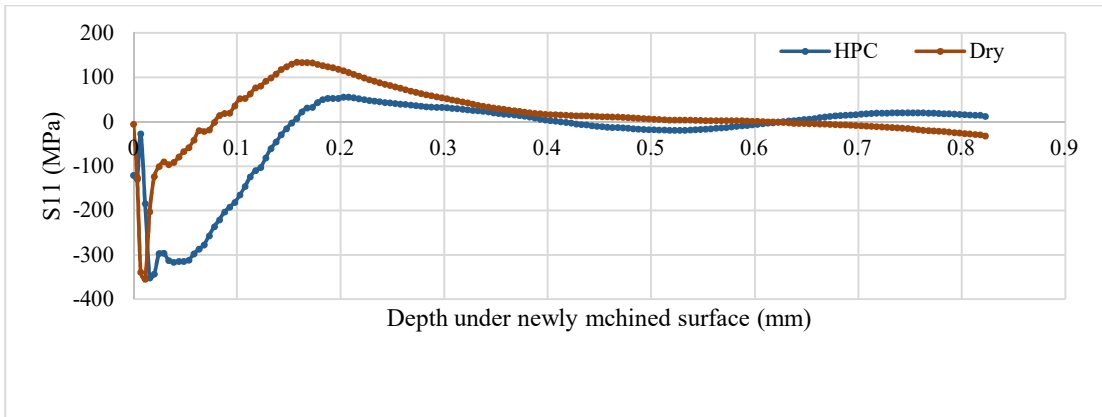
Fig.5.20 S11 in cutting environment simulations at speed 165 m/min and feed 0.16 mm
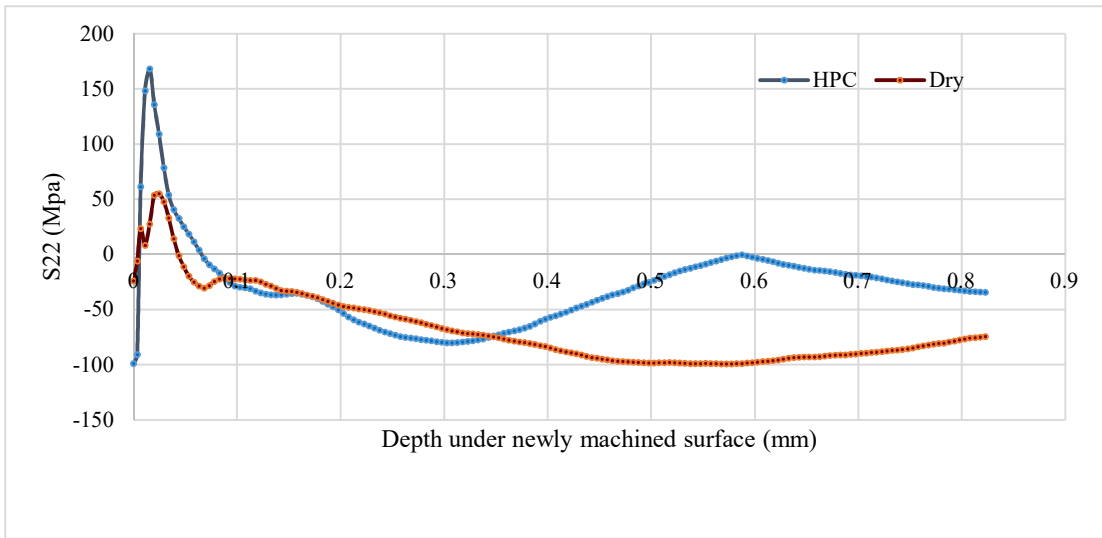
Fig.5.21 S22 in cutting environment simulations at speed 165 m/min and feed 0.16 mm

Influence of Cutting Speed: The influence of the cutting speed on the RS induced in a machined component is analyzed for 48 HRC hardened steel by keeping the feed rate constant at 0.12 mm/rev. The tests were run at four different cutting speeds; 55 m/min, 91 m/min, 127 m/min and 152 m/min. Fig.5.22presents the circumferential RS distribution graph of the cutting speed simulations compared to each other. As seen in this figure, S11 at the surface has higher tensileRS as the cutting speed increase. Afterwards it continues to decrease at lower depths in the work piece and then go for steady state. The peak compressive RS is also maximum for higher cutting speed. This type of trend is also observed in the Fig.5.23for axial (S22) stress distribution.
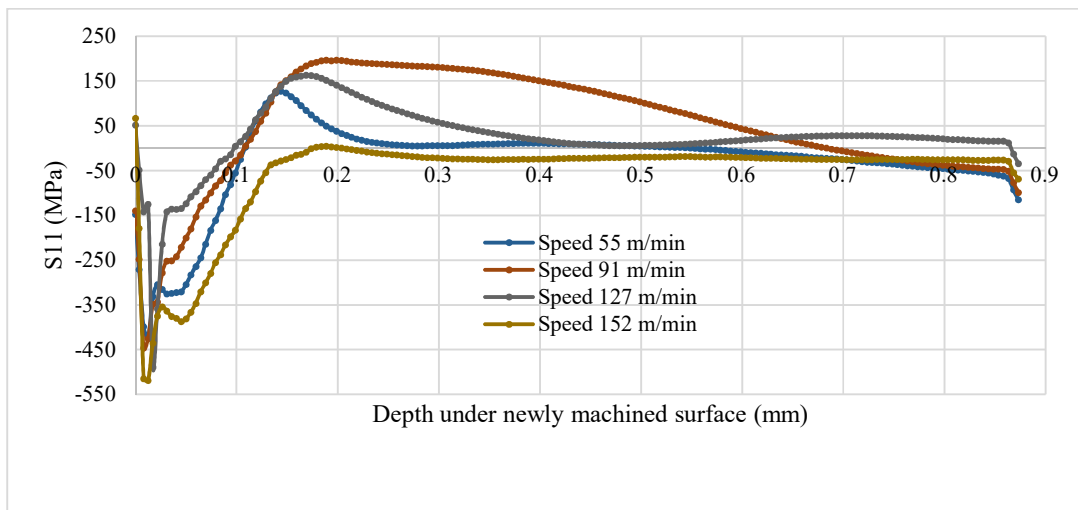
Fig.5.22 S11 in cutting speed simulation at feed 0.12 mm (workpiece hardness 48 HRC)
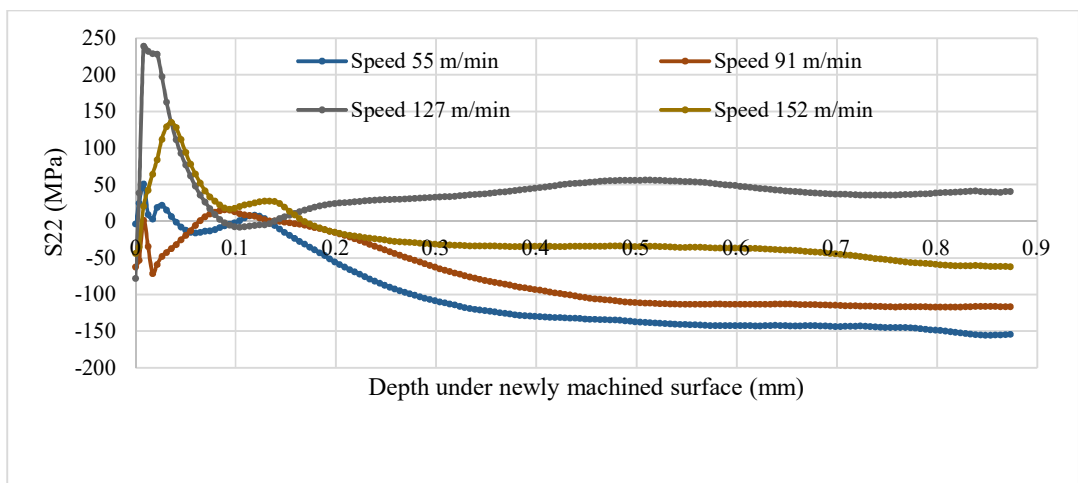
Fig.5.23 S22 in cutting speed simulation at feed 0.12 mm (workpiece hardness 48 HRC)

99

The maximum circumferential RS values at surface and subsurface of job at the stated speed ranges is showed in the following bar chart. Fig.5.24 represents the increasing trend of compressive to tensile S11 RS values at surface while moving from low to high speed. However, the trend is fully opposite for subsurface RS values. On the contrary, there does not show any specific trend for axial stress distribution depicted in Fig.5.25.
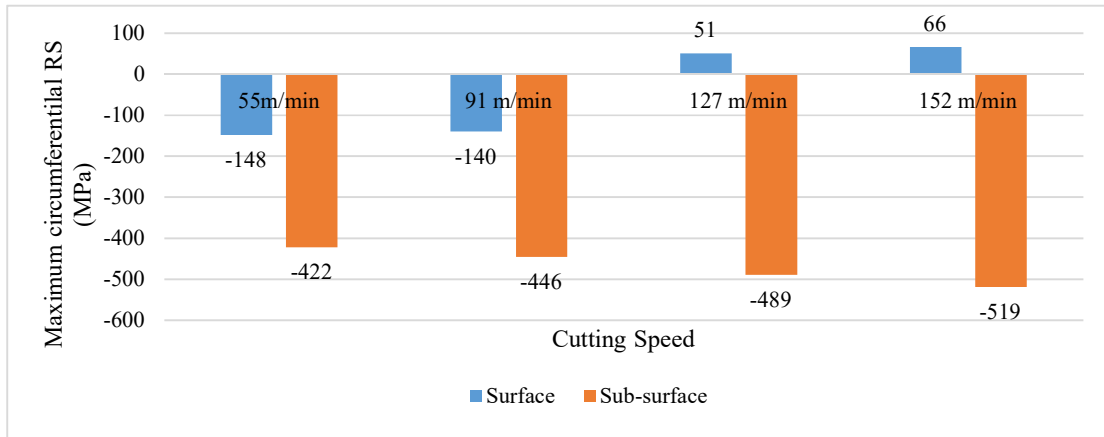
Fig.5.24: Maximum circumferential RS distribution for different cutting speed at feed 0.12 mm
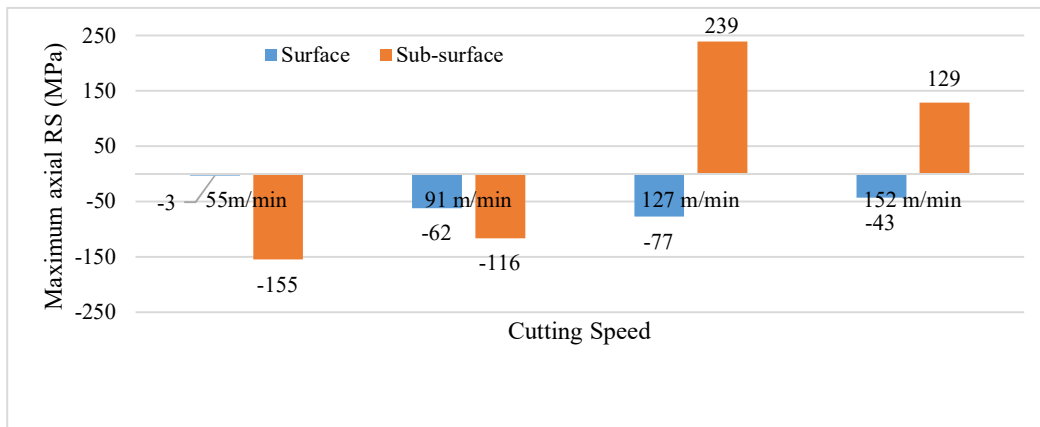
Fig. 5.25: Maximum axial RS distribution for different cutting speed at feed 0.12 mm

Influence of feed: In this part of the study, three feed rates are tested: 0.12mm, 0.13 mm and 0.14 mm at constant speed 140 m/min for machining 48 HRC hardened steel. The results for each test are presented and then the tests are compared to each other in order to find a trend in the results. Fig.5.26 and Fig.5.27 presents the graph of the

circumferential RS and axial RS at different feed respectively. It is apparent from the figures that the S11 and S22 did not follow any particular trend by feed changing.
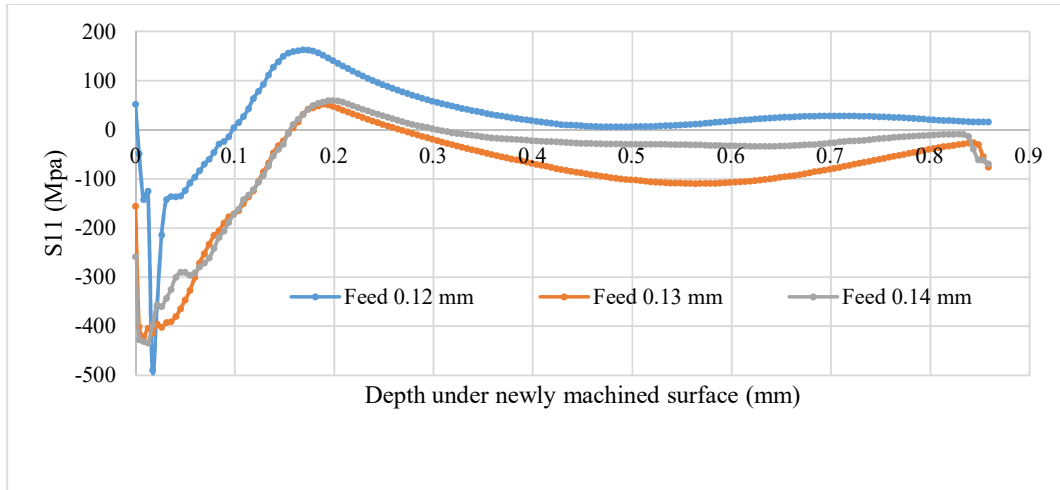
Fig.5.26: S11 in feed simulations at speed 140m/min (workpiece hardness 48 HRC)
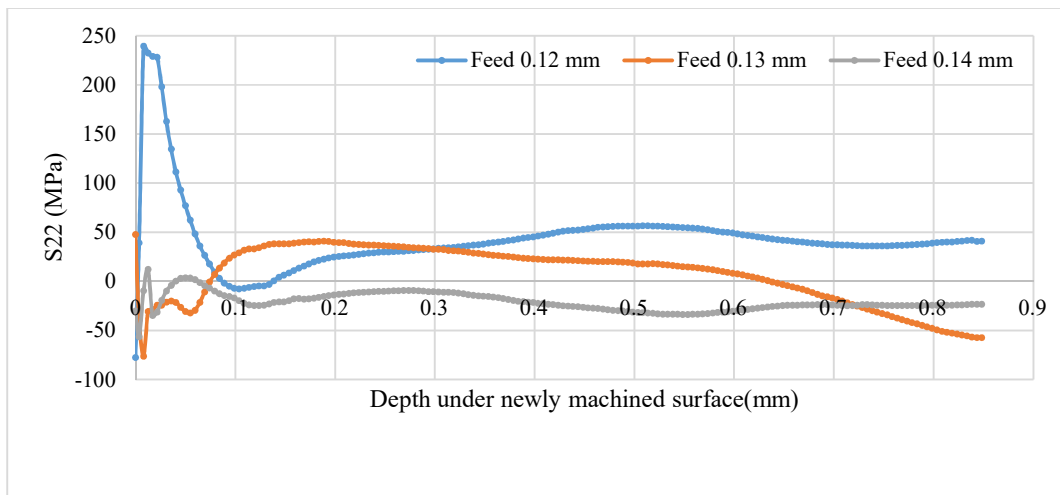
Fig.5.27: S22 in feed simulations at speed 140 m/min (workpiece hardness 48 HRC)

Influence of workpiece hardness: The effect of workpiece hardnesson the RS induced in themachined part is analyzed by keeping the cutting speed and feed rate constant at 150 m/min and 0.12 mm respectively. The tests were run at four workpiece hardness; 42 HRC, 45 HRC, 49 HRC and 51 HRC. Fig.5.28 and Fig.5.29 presents the graph of the circumferential RS and axial RS at different feed respectively. As seen in this Fig.5.28, S11 at the surface has higher compressive RS as the hardnessincrease. It is also apparent from the Fig.5.29 that S22 did not follow any particular trend by hardness changing.
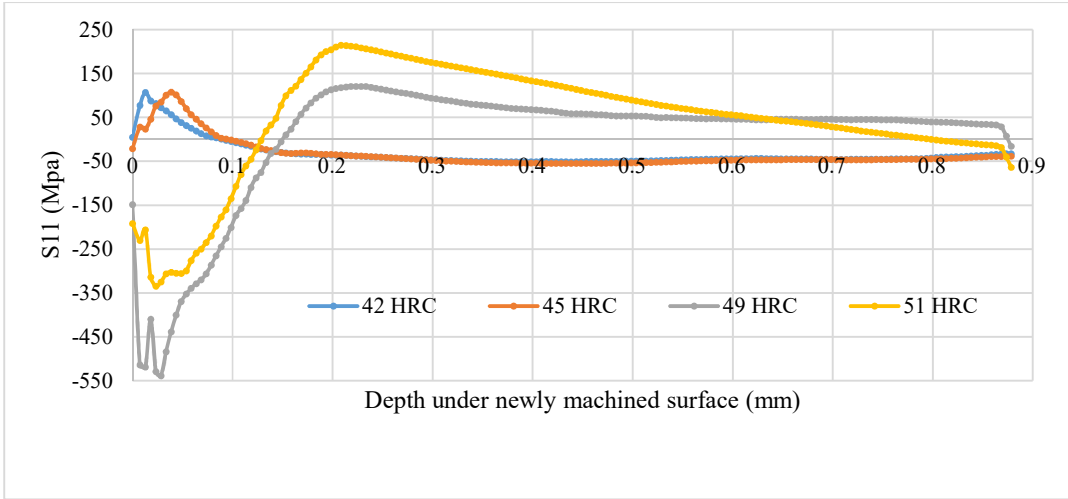
Fig.5.28: S11 in workpiece hardness simulations at speed 150 m/min, feed 0.12 mm
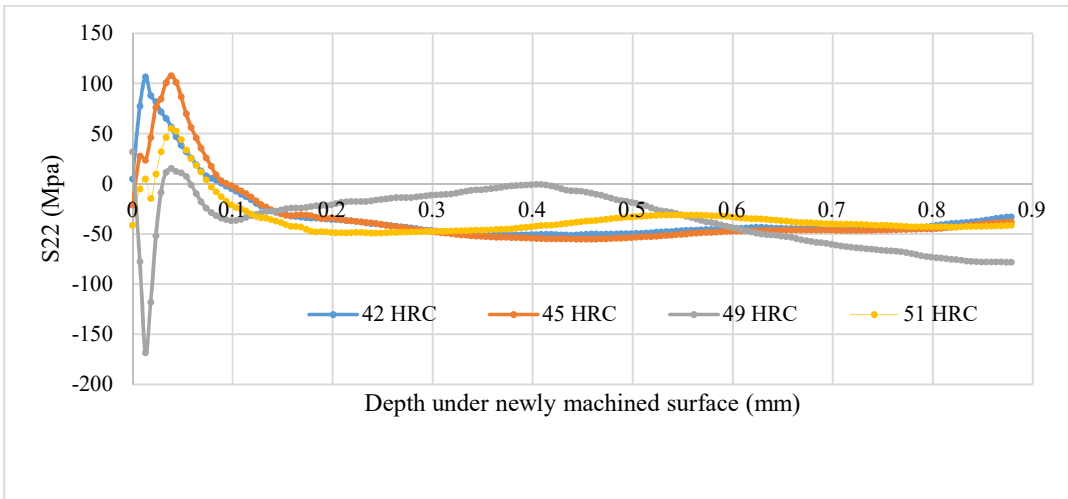
Fig.5.29: S22 in workpiece hardness simulations at speed 150 m/min, feed 0.12 mm

Chapter-6

DISCUSSION ON RESULTS

6.1   Machining Chips

In the present study chips generated from machining alloy steel with SNMM insert is investigated based on the cutting speed, feed, and environmental condition. This study is performed considering the shape and colour of the chip, and chip reduction coefficient as well. Table 2.2, Table 2.3 and Table 2.4 show the shape and color of chips are noticeably different while machining was done under two different environment for all hardness variation. Ribbon type snarled chips was generated under dry condition while under HPC the chip shape was helical. The jet of HPC penetrated to the cutting edge providing a short shear zone resulted in thin chips that readily broke into small piece. Under HPC condition the color of the chips appeared lighter that is blue to metallic due to a reduction in cutting temperature. On the other hand, under dry condition, the energy consumption is relatively higher than HPC. Friction between tool and work material increases and high temperature is reached which causes the blue color chips in dry machining.

In machining ductile metals and alloys, the value of the chip thickness usually becomes larger than the uncut chip thickness. The reason is associated with compression of the chip ahead of the tool and the frictional resistance to chip flow. A larger value of ξ means larger cutting forces and friction and is hence undesirable. Fig.2.3 shows the variation of chip reduction coefficient with speed at different feed rate for three level of hardened steel. In this study, it shows the value of the chip reduction coefficient decreases with the increase of cutting speed and feed rate under both dry and HPC condition. Thus is due to the increase in sliding velocity with the increase of cutting speed results reduction in friction and built-up edge formation which ultimately shrink the shear zone and decrease

the chip reduction coefficient. With the increase in feed (i.e. uncut chip thickness) also the value of ξ decreases due to increase in effective rake angle of the tool with edge beveling. Again the lower values of chip reduction coefficient is noticed for HPC as compared to dry cutting for all three workpiece hardness value. HPC transports heat from the job and reduces friction at chip-tool interface. And thus, by high-pressure jet application, chip reduction coefficient is reasonably expected to decrease for its lubricating and cooling effect.

6.2   Cutting Temperature

In this research work the role of HPC was examined on average chip-tool interface temperature. Fig.2.4 indicates the variation of cutting temperature at different *V-f* combinations under dry and HPC machining for specified hardness of workpieces. It is apparent that, with the increase in cutting speed and feed, the cutting temperature increases for both dry and HPC conditions. But in magnitude the temperature is always found lower in HPC machining as expectation compared to dry cutting.

The reduction in temperature by HPC for different cutting speed and feed rate have calculated shown in following Table 6.1. The table shows, the temperature is significantly reduced at HPC condition and the most notable point is the reduction is more than 41% for all *V-f-H* combinations. The maximum percentage reduction amount is around 71%. Another remarkable fact is that under high speed condition the reduction amount becomes small than low speed. The reason is that, at high cutting speed, plastic contact is increased and made the jet less effective to enter into the interface. It is also obvious that with the increase of workpiece hardness, the cuttingtemperature also increases and it reaches around 700^0C then the application of HPC reduces it below 500^0C. However, the effect of HPC jet on machining performance is always dominant over dry machining. The HPC jet makes it possible to penetrate in the chip-tool interface zone thus reducing chip-tool contact length resulting lower values of frictional co-efficient due to less sliding contact.

Table 6.1 Percentage reduction in cutting temperature in turning 42CrMo4 steel

Hardness (HRC)	Feed (mm/rev)	Cutting Speed (m/min)	Percentage Reduction in Temperature
42	0.12	54	67.38
		82	67.87
		118	68.51
		165	63.25
	0.14	54	68.17
		82	66.50
		118	66.36
		165	66.15
	0.16	54	65.93
		82	65.70
		118	63.86
		165	59.51
48	0.12	54	70.78
		82	67.42
		118	60.71
		165	54.46
	0.14	54	67.24
		82	64.84
		118	62.20
		165	50.09
	0.16	54	66.43
		82	61.87
		118	56.17
		165	44.88
56	0.12	54	68.43
		82	66.13
		118	65.41
		165	58.79
	0.14	54	65.96
		82	63.41
		118	58.02
		165	49.83
	0.16	54	66.46
		82	65.75
		118	62.40
		165	41.86

The temperature model based on FEM using ABAQUS is found to be a successful technique to estimate cutting temperatures with respect to various combinations of variables. The cooling effect of HPC was modelled by convective heat-transfer coefficient for forced convection. The friction coefficient was also reduced to some extent than dry modeling as mentioned by Gariani et al. [**2017**]. In consequence, the maximum and average temperature was found lower in HPC than dry condition for all test run. It is also noticed from the temperature distributions plots (Fig.5.17) that, the maximum interface temperature exists in the vicinity of the cutting edge i.e. at the tool-chip contact. The reason is the normal stress is greatest at the tool tip and gradually decreases at the point where the chip separates from the rake face. This also supports that Coulomb friction model can give the exact trend of temperature through tool-tip to chip separation point. Another observation from Fig.5.16 is that temperature decreases at lower surfaces in the machined component and is mainly centered in the chip (i.e. material being removed). The Table 5.4 shows the error of simulated temperature value for both cutting environment. It is revealed from this table that, the model considering cooling effect results the temperature lower than the experimental one. The reason of this can be described with logical interpretation. In real-world the machining is associated with loss in fluid results in heat loss which was not considered in this model. Again, the 2D model cannot describe the heat effect in z direction. So, of course there is possibility of temperature reduction compared to real scenario. Thereafter, this is reflected in the present simulation model. However, the error quantity lower than 10%, is a major achievement of this study as a first attempt of modeling orthogonal cutting while allowing some hypothesis on friction coefficient, thermal conductance and convective coefficient.

6.3   Surface Roughness

The surface roughness attained after machining of the hardened steels at various cutting *V-f* combinations under dry and HPC conditions are shown in Fig.2.5. It is clearly visible that there is gradual decrease of surface roughness with increase in cutting velocity and increase with decrease in feed. The level of feed directly and almost proportionally governs the surface roughness in machining by single point tools. The surface roughness (h) geometrically caused by feed marks only depends upon the value of feed rate and cutting tool nose radius r [**Bhattacharyya, 1984**], as

$$h = f^2/8r$$

where, h is the peak value of roughness caused due to feed marks. But, the value of cutting velocity also affects the pattern and extent of surface finish, though indirectly through deformation of the tool nose profile, built up edge formation and vibration. The surface roughness values for the present insert having 0.8 mm nose radius have been evaluated and found to be around 2.25μm, 3.06μm and 4.0μm for feed 0.12, 0.14 and 0.16 mm/rev respectively. But the actual values of roughness have been much less than those values. This might be due to the deformation of the tool nose in such a way that initially the tool nose radius effectively increased and then decreased sharply for irregular deformation of the cutting edge. Reduction in surface roughness with the increase in speed may be attributed to smoother chip-tool interface with lesser chance of built-up edge formation. In addition, there might be truncation of the feed marks and slight flattening of the tool-tip.

Another visible point is that application of HPC reduces surface roughness significantly compared to dry cutting. This might be due to the HPC jet assist in lifting the chips so as to prevent rubbing of tool and chip on surface. The incident of welding hot chips is also impeded by pressurized HPC jet eventually reduces the surface roughness.

6.4   Tool Wear

In this research work the role of HPC was examined on average flank wear. Fig.2.6 indicates the variation of flank wear at different machining time varying from 0.40 min. to 15 min. under both dry and HPC machining. It is apparent that, with the time passes, the tool wear increases for both dry and HPC conditions. But in magnitude the tool wear is always found lower in HPC machining as expectation compared to dry machining. Fig. 2.7 shows the growth of average principal flank wear with time for dry and HPC environments with SNMM inserts for three workpiece with hardness HRC42, HRC48 and HRC56. It is noticeable that there is gradual increase of tool wear with increase in cutting speed and feed.

6.5   Residual Stress

In this work, the machining induced RS of 42CrMo4 studied using FEM. Besides the RS model the chip formation process and temperature distribution were also analyzed for the study purpose.

The Fig.5.15 shows the chip formation process in cutting. The evolution of the cutting is shown in four different time instants, going from Fig5.15a-d in all of them the von Mises stress is depicted. The shear band depicted in these figures occurs due to strain localization. The local plastic shear instability arises from the tendency of the material to soften if the local heating due to this plastic work is large enough. Local inelastic deformation causes thermal softening, results in formation of adiabatic shear band and contributes to the decrease of yield stress which instigates a significant upward movement of the portion of the chip above the shear band.

The RS profile found from the simulation in Figs.5.19 shows the stress component in cutting speed direction S11 is higher than that in axial direction S22. In fact, the trend is same for maximum cutting conditions. This trend can also be found in the study of RS in machining byMohammadpouretal. [2010], Umbrello et al. [2007] and Huang and Yang [2016]in the. The relationship of S11 and S22 in residual stress can be determined by their source, i.e., the stress during cutting. As the cutting force is higher than axial force during cutting, the stress component in cutting speed direction is higher than that of in axial direction correspondingly. However, the curve shape was found better for the S11 than S22 for all tests. So, it would be better to evaluate the effect of cutting parameters on RS based on S11 result.

The process induced stress profiles in Figs.5.19 depict that there exist both compressive and tensile stress regions at the surface and beneath the surface. The curves reveal a tensile stress at the top surface of the workpiece. From the top surface the residual stress profile go to the peak tensile or compressive RS and then decreases or increases until it reaches the initial stress state of the material. The tensile surface layer is due to the thermal effect associated with cutting whereas the in-depth compressive stress are mainly generated by plastic deformation. Hence, the degree of thermal–mechanical work is influential of these RS characteristics. Therefore, in case of the higher cutting speed higher temperatures reached and more thermal loads generate higher RS. Outeiro et al. [2006] and Wang et al. [2006] found their study in this similar consequence and concluded that RS

increase with cutting speed. Also, the RS beneath the surface varies with the cutting speeds. The predicted results are in agreement concerning the lower compressive stresses and higher tensile stresses for higher cutting speeds with findings in literature [**Mohammadpour et al. 2010; M'Saoubi et al. 1999**]. Simulation of RS result in machining 48 HRC 42CrMo4 alloy at feed 0.12 mmindicates that circumferential RS at the surface increased (-148 MPa to 66 MPa) with increasing cutting speed (Fig.5.24).The simulated speed value was 55 m/min, 91 m/min, 127 m/min and 152 m/min. From the Fig.5.24 peak compressive RS in circumferential direction were found around 0.12mm. This peak was found maximum (-519 MPa) at high cutting speed of 152 m/min.As a consequence, to suppress the crack initiation in fatigue failure, and improve the dimensional accuracy of the product of turning42CrMo4 steel, high cutting speed is recommended.However, it appears that feed does not affect significantly the residual stress profiles in the chosen range of cutting conditions.

Varying the workpiece hardness value by 42 HRC, 45 HRC, 49 HRC and 51 HRC the RS distribution is depicted in Fig.28 and Fig.29 for S11 and S22 respectively. With the increase of workpiece hardness the circumferential RS becomes more compressive (5 MPa to -191 MPa) at machined surface (Fig.28). On the other hand, tensile to compressive surface axial RS occurs for HRC 42 to HRC 45 and HRC 49 to HRC 51 (Fig.29). Here the maximum compressive axial RS (-41 MPa) also found at higher hardness workpiece (HRC 51). The reason behind this can be discussed by considering the shear angle effect on the deformation. From the experiment the chip thickness is always found less with the increase of material hardness for all cutting condition. This results lower chip reduction coefficient (ξ) that means higher chip thickness ratio (r) and finally gives the higher value of shear angle. The shear angle, $\beta$is expressed as [**Bhattacharyya, 1984**],

$$\beta = \tan^{-1}\frac{r\cos\gamma_0}{1 - r\sin\gamma_0} \qquad (6.1)$$

Here, γ_0 = rake angle. The shear angle values for the present insert having 6^0rake angle have been calculated by Eq. 6.1 for different randomly selected experimental cutting conditions given in Table 6.2 and found increasing with the increase of material hardness.This increasing nature of shear angle with material hardness results compressive RS on the machined surface. This change in surface RS from tension to compression in

harder materials was explained through shear angle effect by the authors WU and Matsumoto [**1990**]. From their analysis it was found that the effect of hardness on RS pattern mainly responsible for shear angle where the shear angle remarkably increased with higher material hardness results tensile to compressive RS.

Table 6.2 Shear angle for HPC cutting condition for different workpiece hardness

Process parameters		Chip thickness ratio (r)			Shear Angle (β)		
Feed (mm/rev)	Cutting Speed (m/min)	HRC 42	HRC 48	HRC 56	HRC 42	HRC 48	HRC 56
0.12	54	0.529	0.535	0.562	29.11^0	29.39^0	30.69^0
	82	0.549	0.552	0.588	30.10^0	30.24^0	31.93^0
0.14	118	0.588	0.645	0.654	31.94^0	34.53^0	34.90^0
	165	0.617	0.689	0.709	33.27^0	36.47^0	37.30^0
0.16	82	0.584	0.629	0.667	31.78^0	33.80^0	35.48^0
	165	0.633	0.730	0.752	33.98^0	38.16^0	39.06^0

Inthepurposeof finding the optimum cutting conditions for controlling the cutting temperature, surface roughness, tool wear and residual stress in turning 42CrMo4 alloy steel the technique combining the statistical method, artificial intelligence and FEM was performed. The input parameter combinationsgenerated by the GA method was mainly adjusted to the low feed and speed and hardness ranging low to high in purpose of minimizing cutting temperature, surface roughness and tool wear. The multi-objective problems require a decision maker to make a choice of preferred solutions. The selection is essentially a tradeoff of one complete solution over another in multi-objective space. As the performed optimization results was Pareto optimal so there is no other solution that performs at least as well on every criteria and strictly better on at least one criteria. Thus, the non-dominated solutions cannot be improved upon without hurting at least one of the criteria. The resulting optimum combination was fed for RS modeling. On the contrary, the evolution of simulated RS profile prefers the large cutting speed and harder material for machining to minimize the possibility of crack initiation by controlling the tensile and compressive RS.

Chapter-7

CONCLUSION AND RECOMMENDATION

7.1   Conclusion

The aim of the present research work was to optimize the process parameters for residual stress analysis while turning 42CrMo4 alloy steel by coated carbide insert(SNMM 120408) under HPC condition. This research work justifies the significance of machining induced RS investigation for the product under HPC condition. The analysis was started with the evaluation of the effects of HPC on the chip thickness, cutting temperature, surface roughness and tool wear. Predictive model was developed for the latter three responses and the GA based optimization was performed concerning the cutting speed, feed and workpiece hardness to minimize all of these responses. Modeling of the RS wasdone by FEM.The following conclusions can be drawn from the research work.

i.   The two jet coolant application at high pressure enabled the substantial reduction in chip reduction coefficient, average chip-tool interface temperature and surface roughness up to significant level for all experimental run compared to the dry cut. The produced chip shape and color also indicates the reduction of temperature due to HPC jet which ensuredfavorable chip-tool interaction and friction elimination.

ii.   Cutting temperature is found to be proportional with cutting speed and feed rate. HPC application extensively reduces this temperature compared to dry cutting. The reduction is over 41% to 70% for all of the *V-f-H* combinations. Such apparent reduction in the cutting temperature is expected to have some favorable influence on other machinability indices.

iii. With the application of HPC jet the surface finish obtained is much better than the situation of dry cut. Under certain condition the surface finish found as satisfactory as grinding operation. The attained minimum roughness is about 0.72 μm and maximum is 1.32 μm for HPC condition. This favorable formation of surface indicates improvement in surface quality.

iv.   Application of HPC jet produced reduced flank wear compared to dry cut. This would enable either remarkable improvement in tool life or enhancement of productivity allowing high cutting speed and feed rate. Such reduction in tool wear might have been possible for retardation of abrasion and notching, decrease prevention of adhesion and diffusion type tool wear at flanks.

v.   The empirical modeling by RSM provides quadratic model for cutting temperature, surface roughness and tool wear. The results of ANOVA have proved that the proposed threemathematical models could adequately describe the performance indicators. The analysis of models shows that speed, feed and the quadratic effect of speed and hardness mostly influence all of the responses. Again, the cutting temperature and surface roughnessalso influenced by hardness where the interaction of speed-feed and speed-hardness are also importantto affect the cutting temperature.

vi.   The optimization was subjected to satisfying the constraints of present experimental speed (54 m/min to 165 m/min), feed (0.12mm/rev to 0.16 mm/rev) and workpiece hardness (42 HRC to 56 HRC) range.The objective of minimizing cutting temperature, surface roughnessand tool wear are formulated as non-linear optimization problem. The Pareto based method provides non-dominated solutions from problems coupled with GA. The solution set gives the results of input are in range of 54m/min to 152 m/min

speed, 0.12mm/rev. to 0.13mm/rev feed and HRC 42 to HRC 51 workpiece hardness.Since none of the solutions in the Pareto optimal set is absolutely better than any other, any one of them is an acceptable solution. The choice of one solution over the other depends on the requirement of the process engineer. It should be noted that any set of input parameters can be taken to achieve the corresponding response values depending upon manufacturer's requirement.

vii.   The temperature distribution and RS modeling by FEM was carried out with the ALE and element deletion technique in2D.The model was developed for both dry and HPC environment. It was found that, high-temperature region is confined to the tool–chip contact area and found to be decreased as chip moves away from the tool rake face. Error in temperature prediction was found less than 10% which gives the sufficient consistency to use this FEM model for further analysis.

viii.   The prediction of the machining induced RS in the S11 and S22were the main focus point of numerical modeling. As no experimental RS value was found for the 42CrMo4 machining under cooling effect, measured temperature values were used to verify the developed model. The experimental and numerical researches of RS in previous literatures show that the RS in cutting speed direction is higher than that of in axial direction for different cutting conditions and workpiece materials. FEM of stresses is performed on the *V-f-H* combination resulted from optimization method. The computed results of the proposed model are consistent with these previous researches. Process induced stress profiles depict that there exist both compressive and tensile stress regions beneath the surface. The results indicate that higher cutting speed (152m/min)and higher hardness (HRC 51) valueproportionallyaffects the compressive RS at subsurfaceand surface respectively. However, influence of feed was not found significant to mention.

7.2   Recommendations

i.   For the experimental part, depth of cut was kept constant while changing the cutting velocity and feed rate. This research work can be extended by varying the depth of cut to study its influence on the machining responses. Again, variables related to HPC application system can be considered by differing the pressure and flow rate of the jet.

ii. Another area that needs significant attention is in tool design. All testing in this research work used identical tool geometry. Previous works have shown that this also significantly affects machining responses. The experimental and modelingwork should be used to identify the best tool geometry for different materials, cutting conditions and applications.

iii. At the step of optimization procedure incorporating other objectives like production cost, machining time and/or other constraints like machine power, material removal rate can make the result more realistic. Again, another algorithms beyond GA can be studied to observe that the range of resultswill vary or not.

iv. The mechanical effect of jet should be included in the FEM to get better results. The 3D FE-model is necessary to approach the kinematic energy of cutting fluid. So, the transformation of the model for orthogonal cutting 2D to 3D should be made.Again, the values of different modules of software such as mesh distribution, adaptive mesh domain, hourglass etc., can be changed to study the degree of influence on outputs.

References

ABAQUS Analysis User's Manual, version 6.14, Dassault Systèms Simulia Corp. 2014

Arrazola, P.J., Barbero, O., and Urresti I., "Influence of Material Parameters on Serrated Chip Prediction in Finite Element Modeling of Chip Formation Process", International Journal of Material Forming, Vol. 3(S1), pp. 519–522, 2010.

Attanasio, A., Ceretti, E., Rizzuti, S., Umbrello, D., and Micari, F., "3D Finite Element Analysis of Tool Wear in Machining", CIRP Manuf. Tech., Vol. 57, pp. 61-64, 2008

Bhattacharyya, A., "Metal Cutting-Theory and Practice", Central Book Publisher, India, 1984

Bogdan, A., and Gavrila, C., "The Economic Efficiency of Replacing Grinding with Hard Turning", Recent, Vol. 18(2), pp. 71-76, 2017

Brnic, J., Turkalj, G., Canadija, M., Lanc, D., and Brcic, M., "Study of the Effects of High Temperatures on the Engineering Properties of Steel 42CrMo4", High Temp. Mater. Proc. Vol. 34(1), pp. 27–34, 2015

Cao, Y.J. and Wu, Q.H., "Teaching Genetic Algorithm Using MATLAB", Int. J. Elect. Enging. Educ., Vol. 36, pp. 139–153, 1999

Capello, E., "Residual Stresses in Turning Part I: Influence of Process Parameters," J. ofMaterials Processing Technology; Vol. 160, pp. 221–228, 2005

Coto, B., Navas, V.G., Gonzalo, O., Aranzabe, A., and Sanz, C., "Influences of Turning Parameters in Surface Residual Stresses in AISI 4340 Steel", Int. J. Adv. Manuf. Tech. Vol.53(9-12) pp. 911–919, 2011

Courbon, C., Sajnb, V., Kramarb, D., Recha, J., Koselb, F., and Kopac, J., "Investigation of Machining Performance in High Pressure Jet Assisted Turning of Inconel 718: A Numerical Model", J. of Mat. Processing Tech., Vol. 211, pp. 1834– 1851, 2011

Dahlman, P., and Escursell, M. "High-Pressure Jet-Assisted Cooling: A New Possibility for Near Net Shape Turning of Decarburized Steel", Int. J. Machine Tools and Manuf. Vol. 44(1), pp. 109-115, 2004

Dahlman, P., Gunnberg, F., and Jacobson, M., "The Influence of Rake Angle, Cutting Feed and Cutting Depth on Residual Stresses in Hard Turning," Journal of Materials Processing Technology; Vol. 147, pp. 181-184, 2004.

Donea, J., Fasoli-Stella, P. and Giuliani, S., "Lagrangian and Eulerian Finite Element Techniques for Transient Fluid-Structure Interaction Problems", In Trans. 4th Int. Conf. on Structural Mechanics in Reactor Tech., Paper B1/2, San Francisco, 1977

Doriana, M., D'Addona, D.M., and Teti, R., "Genetic Algorithm-Based Optimization of Cutting Parameters in Turning Processes", Procedia CIRP 7, pp. 323 – 328, 2013

Das, S.R., Kumar, A., and Dhupal, D., "Effect of Cutting Parameters on Tool Wear, Surface Roughness and Material Removal Rate during Dry Turning of EN-31 Steel", J. of Current Engineering Research, Vol. 2(6), pp. 37-43, 2012

El-Axir, M.H., "A Method of Modeling Residual Stress Distribution in Turning for Different Materials," Int. J. of Machine Tools & Manuf., Vol. 42 (9), pp. 1055-1063, 2002

Ezugwu, E. O., "Key Improvements in the Machining of Difficult-to-Cut Aerospace Superalloys," Int. J. of Machine Tools and Manufacture; Vol. 45, pp. 1353-1367, 2005

Ezugwu, E.O. and Bonney, J., "Effect of High-Pressure Coolant Supply when Machining Nickel-Base, Inconel 718, Alloy with Coated Carbide Tools", J. of Mat. Processing Tech.; Vol. 153–154, pp. 1045–1050, 2004.

Filice, L., Micari, F., Rizzuti, S. and Umbrello, D., "A Critical Analysis on the Friction Modeling in Orthogonal Machining", International Journal of Machine Tools and Manufacture, Vol.47, Nos. 3–4, pp.709–714, 2007

Gardner, J.D., Vijayaraghavan, A, and Dornfeld, D.A., "Comparative Study of Finite Element Simulation Software", UC Berkeley: Laboratory for Manufacturing and Sustainability, 2005

Gariani S., Shyha, I., Fawad Inam, F., and Huo, D., "Evaluation of a Novel Controlled Cutting Fluid Impinging Supply System when Machining Titanium Alloys", Applied Sciences, Vol. 7(6), pp. 1-16, 2017

Globočki – Lakić, G., Sredanović, B., Kramar, D. and Kopač, J., "Machinability of C45e Steel - Application of Minimum Quantity Lubrication and High Pressure Jet Assisted Machining Techniques," Transections of FAMENA; Vol. 40 (2), pp. 45-58, 2016

Goldberg, D.E., "Genetic Algorithm in Search, Optimization and Machine Learning", Pearson Education, Singapore, pp. 1–21, 2001

Hadzley, A.B.M., Izamshah, R., Sarah, A. S. and Fatin, M. N., "Finite Element Model of Machining with High Pressure Coolant for Ti- 6Al-4V alloy," Procedia Engineering; Vol. 53 pp. 624 – 631, 2013

Hillerborg, A., Modeer, M., and Petersson, P.E., "Analysis of Crack Formation and Crack Growth in Concrete by Means of Fracture Mechanics and Finite Elements", Cement and Concrete Research Vol. 6, pp. 773–782, 1976

Huang, K., and Yang, W., "Analytical Modeling of Residual Stress Formation in Workpiece Material due to Cutting", Int. J. Mechanical Sciences, Vol. 114, pp. 21–34, 2016

Imbrogno, S., Sartori, S., Bordin, A., Bruschi, S., and Umbrello, D., "Machining Simulation of Ti6Al4V under Dry and Cryogenic Conditions", Procedia CIRP, Vol. 58, pp. 475 – 480, 2017

Jacobus, K., Devor, R.E., and Kapoor, S.G., "Machining-Induced Residual Stress: Experimentation and Modeling", J. Manuf. Sci. Eng. Trans. ASME, Vol., 22(1), pp. 20–31, 2000

Kaladhar, M., K.V. Subbaiah, And Rao, C.S., "Optimization of Surface Roughness and Tool Flank Wear in Turning of AISI 304 Austenitic Stainless Steel with CVD Coated Tool", J. of Engineering Science and Tech., Vol. 8(2), pp. 165 – 176, 2013

Kaminski J., and Alvelid B., "Temperature Reduction in the Cutting Zone in Water-Jet Assisted Turning", J. of Mat. Processing Technology, Volume 106(1), pp. 68-73, 2000

Kaminski, J., Ljungkrona, O., Crafoord, R. and Lagerberg, S.' "Control of Chip Flow Direction In High Pressure Water Jet Assisted Orthogonal Tube Turning", Proc. Instn Mech. Engrs, Part B, Journal of Engg. Manuf.,Vol. 214, (B7), pp. 529-534, 2000

Kamruzzaman, M., "Effects of High Pressure Coolant on Machinability of Steels", Doctoral dissertation, BUET, Dhaka, Bangladesh, 2009

Kaya, E. and Akyüz, B., "Effects of Cutting Parameters on Machinability Characteristics of Ni-Based Super Alloys: A Review", DE GRUYTER; Vol. 7, pp. 330–342, 2017

Khan, M.A., "Effect of High Pressure Coolant Jets in Turning Ti-6al-4v Alloy with Specialized Designed Nozzle", M.Sc. Engineering dissertation, BUET, Dhaka, Bangladesh, 2015

Klocke, F., Döbbeler, B., Peng, B., Lakner, T., "FE-Simulation of the Cutting Process under Consideration of Cutting Fluid", Procedia CIRP, Vol. 58, pp. 341 – 346, 2017

Konak, A., Coit, D.W., and Smith, A.E., "Multi-objective Optimization using Genetic Algorithms: A Tutorial", Reliability Engineering and System Safety", Vol. 91, pp. 992–1007, 2006

Kramar, D. and Kopac, J., "High Pressure Cooling in the Machining of Hard-to-Machine Materials," Journal of Mechanical Engineering, Vol. 55(11), pp. 685-694, 2009

Krishnakumar, P., Marimuthu, K.P., Rameshkumar, K., and Ramachandran, K.I., "Finite Element Simulation of Effect of Residual Stresses during Orthogonal Machining Using ALE Approach", Int. J. Machining and Machinability of Materials, Vol. 14(3) pp. 213-229, 2013

Lazoglu, I., Ulutan, D., Alaca, B.E., Engin, S. and Kaftanoglu, B., "An Enhanced Analytical Model for Residual Stress Prediction in Machining", CIRP Annals – Manuf. Tech., Vol. 57, pp. 81–84, 2008

Li, X., "Study of the Jet-flow Rate of Cooling in Machining Part 1 Theoretical Analysis", Journal of Materials Processing Technology, Vol. 62, pp.149-156, 1996

Liang S.Y. and Su J-C., "Residual Stress Modeling in Orthogonal Machining," Annals of the CIRP; Vol. 56(1), pp. 65-68, 2007

List, G., Nouari, M., G'ehin, D., Gomez, S., Manaud, J. P., and Petitcorps, Y. L., "Wear Behavior of Cemented Carbide Tools In Dry Machining of Aluminum Alloy," International Journal of Wear; Vol. 259, pp. 1177- 1189, 2005

Liu, C.R. and Guo, Y.B., "Finite Element Analysis of the Effect of Sequential Cuts and Tool-chip Friction on Residual Stresses in a Machined Layer", Int. J. Mech. Sci., Vol. 42, pp. 1069-86, 2000

M'Saoubi, R., Outeiro, J.C., Changeux, B., Lebrun, J.L., and Morao Dias, A., "Residual Stress Analysis in Orthogonal Machining of Standard and Resulfurized AISI 316L Steels," Journal of Materials Processing Technology, Vol. 96, pp. 225–233, 1999

Mabrouki, T., Girardin, F., Asad, M., and Rigal, J.F., "Numerical and Experimental Study of Dry Cutting for an Aeronautic Aluminum Alloy (A2024-T351)", International Journal of Machine Tools & Manufacture, Vol. 48, pp. 1187– 1197, 2008

Machado, A. R., Wallbank, J., Pashby, I. R. and Ezugwu, E. O., "Tool performance and Chip Control when Machining Ti-6Al-4V and Inconel 901 using High Pressure Coolant Supply", Machining Science and Technology; Vol. 2 (1), pp. 1-12, 1998

Makadia, A.J. and Nanavati, J.I., "Optimization of Machining Parameters for Turning Operations Based on Response Surface Methodology," Measurement, Vol. 46, pp. 1521-1529, 2013

Malhotra, R., Singh, N., and Singh, Y., "Genetic Algorithms: Concepts, Design for Optimization of Process Controllers", Computer and Information Science Vol. 4 (2), pp. 39-54, 2011

Manna, A. and Salodkar, S., "Optimization of Machining Conditions for Effective Turning of E0300 Alloy Steel," J. of Materials Processing Tech., Vol. 203, pp.147–153, 2008

Martin, H., "Heat and Mass Transfer between Impinging Gas Jets and Solid Surfaces, Advances in Heat Transfer, Vol. 13, 1977

Matsumoto, Y., Barash, M.M., and Liu, C.R., "Residual Stress in the Machined Surface of Hardened Steel," ASME, Prod. Eng. Div. Vol.12 pp. 193–204, 1984

Matsumoto, Y., Barash, M.M. and Liu, C.R., "Effect of Hardness on the Surface Integrity of AISI 4340 Steel", J. of Engg. for Industry, Vo. 108, pp. 169-175,1986

Matsumoto, Y., Hashimoto, F., and Lahoti, G., "Surface Integrity Generated by Precision Hard Turning", CIRP Annals - Manufacturing Technology, Vol 48(1), pp. 59-62, 1999

MatWeb, LLC, Material Property Data, www. matweb.com, Retrieved on: January 18, 2018

Metelski, A. et al., "Taguchi Design of Experiment versus Dynamic Programming Approach in the Optimization of Turning Process", Applied Mechanics and Materials, Vol. 808, pp. 66-71, 2015

Mia, M. and Dhar, N.R., "Effect of High Pressure Coolant Jet on Cutting Temperature, Tool Wear and Surface Finish in Turning Hardened (HRC 48) Steel," J. of Mech. Engg.; Vol. ME 45(1), pp. 1-6, 2015

Mia, M. and Dhar, N.R., "Response Surface and Neural Network Based Predictive Models of Cutting Temperature in Hard Turning", Journal of Advanced Research, Vol. 7, pp. 1035–1044, 2016

Mia, M., Khan, M. A., and Dhar, N.R., "High-Pressure Coolant on Flank and Rake Surfaces of Tool in Turning of Ti-6Al-4V: Investigations on Surface Roughness and Tool Wear," The Int. J. of Adv. Manuf. Technol.; Vol. 90, (5-8) pp. 1825–1834, 2017

Miguélez, H., Zaera, R., Molinari, A., Cheriguene, R., and Rusinek, A., "Residual Stresses in Orthogonal Cutting of Metals: the Effect of Thermomechanical Coupling Parameters and of Friction," J. Therm. Stresses; Vol. 32, pp. 1–20, 2009

Mohammadpour, M., Razfar, M.R. and Saffar R.J., "Numerical Investigation the Effect of Machining Parameters on Residual Stresses in Orthogonal Cutting," Simulation Modeling and Theory; Vol. 18, pp. 378-379, 2010

Montgomery, D.C., "Design and Analysis of Experiments: Response Surface Method and Designs", New Jersey: John Wiley and Sons, Inc., 2005

Nasr, M.N.A., Ng, E.-G., and Elbestawi, M.A., "A Modified Time-Efficient FE Approach for Predicting Machining-Induced Residual Stresses," Finite Elements in Analysis and Design, Vol. 44, pp. 149 – 161, 2008

Öpöz, T.T., Chen, X., "Chip Formation Mechanism Using Finite Element Simulation", Journal of Mechanical Engineering Vol. 62(11), pp. 636-646, 2016

Outeiro, J.C., Pina, J.C., M'Saoubi, R., Pusavec, F., and Jawahir, I.S., "Analysis of Residual Stresses Induced by Dry Turning of Difficult-to-Machine Materials," CIRP Annals—Manufacturing Technology; Vol. 57, pp. 77–80, 2008

Outerio, J.C., Umbrello, D. and Saoubi, R.M., "Experimental and Numerical Modeling of the Residual Stresses Induced in Orthogonal Cutting of AISI 316L Steel," International Journal of Machine Tools & Manufacture; Vol. 46, pp. 1786-1,794, 2006

Özel, T. and Zeren, E., "Finite Element Method Simulation of Machining of AISI 1045 Steel with a Round Edge Cutting Tool," Proc. of the 8th CIRP Int. Workshop on Modeling of Machining Operations, Chemnitz, Germany, pp. 533-542, 2005

Özel, T., "Computational Modeling of 3D Turning: Influence of Edge Micro-Geometry on Forces, Stresses, Friction and Tool Wear in PCBN Tooling", J. of Mat. Processing Technology Vol. 209 pp. 5167–5177, 2009

Özel, T., and Karpat, Y., "Prediction of Surface Roughness and Tool Wear in Finish Dry Hard Turning Using Back Propagation Neural Networks" 17th Int. Conference on Production Research, Virginia, pp. 1-10, 2005

Ozel, T., and Ulutan, D., "Prediction of Machining Induced Residual Stresses in Turning of Titanium and Nickel Based Alloys with Experiments and Finite Element Simulations", CIRP Annals – Manuf. Tech., Vol. 61, pp. 547–550, 2012

Ozel, T., Karpat, Y., Figueira, L., and Davim, P., "Modeling of Surface Finish and Tool Flank Wear in Turning of AISI D2 Steel with Ceramic Wiper Inserts" Journal of Materials Processing Technology, Vol. 189, pp. 192–198, 2007

Pantale, O., Bacaria, J.-L., Dalverny, O., Rakotomalala, R., and Caperaa, S., "2D and 3D Numerical Models of Metal Cuttingwith Damage Effects", Comput. Methods Appl. Mech. Engrg. Vol., 193, pp. 4383–4399, 2004

Patil, D.H. and Sadiah, M., "Investigations on Finish Turning of AISI 4340 Steel in Different Cutting Environments By CBN Insert," Int. J. of Engineering Sci. and Tech., Vol. 3(10), pp. 7690-7706, 2011

Pencheva, T., Atanassov, and Shannon, A., "Modeling of A Roulette Wheel Selection Operator in Genetic Algorithms Using Generalized Nets," Bioautomation, Vol. 13(4), pp. 257–264, 2009

Proudian. J., "Simulating Residual Stress in Machining; from Post Process Measurement to Pre-Process Predictions", M.Sc. thesis, Royal Institute of Technology, 2012

Response Surface Methodology, Retrieved from: https://en.wikipedia.org/wiki/Response_surface_methodology, 2017

Ripling, E.J. and Crosley, P.B., "Crack Arrest Toughness of 4140, 1340 And 4340 Steel", Materials Research Laboratory Inc., 1981

Saez-de-Buruaga, M., Esnaola, J.A., Aristimuno, P., Soler, D., Björk, T., and Arrazola, P.J., "A coupled Eulerian Lagrangian Model to Predict Fundamental Process Variables and Wear Rate on Ferrite-Pearlite Steels", Procedia CIRP 58, pp. 251 – 256, 2017

Schwach, D.W. and Guo, Y.B., 'A Fundamental Study on the Impact of Surface Integrity by Hard Turning on Rolling Contact Fatigue," Int. J. Fatigue, Vol. 28, pp. 1838–1844, 2006

Senthil, A. K., Rahman, M. and Ng, S. L., "Effect of High-Pressure Coolant on Machining Performance," The Int. J. of Adv. Manuf. Technol.; Vol. 20 (2), pp. 83-91, 2002

Sharman, R.C., Hughes, J.I., and Ridgway, K., "The effect of tool nose radius on surface integrity and residual stresses when turning Inconel 718", Journal of Materials Processing Technology, Vol. 216, pp. 123–132, 2015

Shet C, and Deng X., "Residual Stresses and Strains in Orthogonal Metal Cutting," International Journal of Machine Tools & Manufacture; Vol. 43, pp. 573–87, 2003

Shet, C. and Deng, X., "Finite Element Analysis of the Orthogonal Metal Cutting Process", J. Mater. Process. Technol. Vol. 105, pp. 95–109, 2000

Sisto, T.S.D., Carr, F.L., and Larson, F.R., "The Influence of Section Size on the Mechanical Properties and Fracture Toughness of 7075-T6 Aluminum, 6AI-6V-2Sn Titanium, and AISI 4340 steel", Material Testing Laboratory U.S. Army Materials Research Agency Watertown, Massachusetts, 1964

Swamy, M.K., Raju, B.P., and Teja, B.R., "Modeling and Simulation of Turning Operation", IOSR-JMCE, Vol. 3(6), pp. 19-26, 2012

Thiele, J. D. and Melkote, S. N. "Effect of Cutting Edge Geometry and Workpiece Hardness on Surface Residual Stresses in Finish Hard Turning of AISI 52100 Steel". Trans. ASME, J. Mfg Sci. Engg., Vol. 122(4), 642–649, 2000

Totten G., Howes, M., and Inoue, T., (Eds.), "Handbook of Residual Stress and Deformation of Steel", Materials Park, Ohio: ASM International, 2002

Ulutan, D., Erdem Alaca, B. and Lazoglu, I., "Analytical Modeling of Residual Stresses in Machining," Journal of Materials Processing Technology; Vol. 183, pp. 77–87, 2007

Umbrello, D. and L. Filice, "Improving Surface Integrity in Orthogonal Machining of Hardened AISI 52100 Steel by Modeling White and Dark Layers Formation," CIRP Annals Manuf. Technol., Vol. 58 pp. 73-76, 2009

Umbrello, D., "Influence of Material Microstructure Changes on Surface Integrity in Hard Machining of AISI 52100 Steel" Int. J. Adv. Manuf. Tech., Vol. 54(9-12) pp. 887-898, 2011

Umbrello, D., M'Saoubi, R., and Outeiro, J.C., "The Influence of Johnson–Cook Material Constants on Finite Element Simulation of Machining of AISI316L Steel", Int. J. Mach. Tools Manuf., Vol. 47, pp. 462–70, 2007

Valiorgue, F., Rech, J., Hamdi, H., Gilles, P., and Bergheau, J.M., "A New Approach for the Modeling of Residual Stresses Induced by Turning of 316L", J. of Materials Processing Tech., Vol. 191, pp. 270–273, 2007

Wahde, M., "Biologically Inspired Optimization Methods", WIT Press, Southampton, UK, 2008

Wang, S.Y., Ai, X., Zhao, J., and Lv, Z.J., "FEM Simulation of the Residual Stress in the Machined Surface Layer for High-Speed Machining," Key Engineering Materials Vols. 315-316, pp. 140-144, 2006

Wang, X.-L. , Payzant, E. A., Taljat, B., Hubbard, C. R., Keiser, J. R., and Jirinec, M. J., "Experimental Determination of the Residual Stresses in a Spiral Weld Overlay Tube," Mater. Sci. Eng.; A232, pp. 31–38, 1997

Widia^{TM} Value, Retrieved from: www.widia.com, 2018, pp. F1-F21

Wiesner, C., "Residual Stresses after Orthogonal Machining of AISI 304: Numerical Calculation of the Thermal Component and Comparison with Experiment Results," Metall. Trans. A Vol. 23 pp. 989–996, 1992

Wrethim R., Rotberg J., and Ber A., "Influence of High Pressure Flushing, through the Rake Face Cutting Tool", Annals. of CIRP, Vol. 41 (1): pp. 101-106, 1992

Wu, D.W. and Matsumoto, Y., "The Effect of Hardness onResidual Stresses inOrthogonal Machining of AISI 4340 Steel", J. of Engg. for Industry, Vo. 112, pp. 245-252,1990

Yen, Y., Söhner, J., Lilly, B., and Altan, T., "Estimation of Tool Wear in Orthogonal Cutting Using the Finite Element Analysis", J. of Mat. Processing Tech., Vol. 146, pp. 82–91, 2004